A FINITE ELEMENT FORMULATION OF THE BOLTZMANN TRANSPORT EQUATION

by

Cheang Siew QUAH, M.Sc.,D.I.C.

A thesis submitted in fulfilment
of the requirement for the
degree of Doctor of Philosophy

Department of Mechanical Engineering,
Imperial College of Science and Technology,
London,
SW7 2BX.

1983

ABSTRACT

The finite element method has found ever increasing applications in the various branches of engineering and technology. In this instance it has been adopted to find solutions to the multigroup form of the Boltzmann transport equation.

A variational approach has been adopted in which a functional was derived from the second-order form of the Boltzmann equation. The solution of the integrals of the functional results in the discretization of both angle and space. In the former Spherical Harmonics expansions were used while finite elements were used for the spatial domain.

The main aim of this thesis was to develop a package to solve the discretised form of the functional. This package consists of two major parts. In the first instance CORFU was developed to handle the angular integrals arising from the angular discretization. It is interfaced with FELTRAN, the main program, in which the problem is solved. FELTRAN consists of data input, spatial integration, global assembly and solution of the resultant set of linear equations. The objective was to construct the package so that it would be modular in order that additional features can be built into the existing body with ease. Direct solution techniques were used in solving the global set of equations. An out-of-core solver, to overcome the problems of primary storage, was also incorporated.

In validating the package source and eigenvalue problems from various research work were used as the yardstick. Accurate solutions have confirmed that the technique has been correctly established and the potential lies in the fact that solutions have been obtained that can only be achieved by other established methods with difficulty and constraints on computing resources.

ACKNOWLEDGEMENTS

It has often been remarked that this is perhaps the most difficult page to write in any thesis. Certain people would be offended if they did not merit a mention or if they are not mentioned in glowing terms. On the other hand some people feel embarassed if they are heaped with honours and thanks but which they richly deserve. Nevertheless I would like to mention the following people who have been connected with my project in one way or another.

In the first instance I must acknowledge my gratitude to Dr. A.J.H. Goddard, without whose initiation, this project would never have taken place and for his enthusiasm and support throughout and after the duration of the project.

Professor R.T. Ackroyd, with whose work on variational principles, has helped to guide this project must be singled out for his often useful and helpful comments.

During the project I was fortunate enough to engage in discussion at fortuitous moments with two colleagues. In the first instance Dr. B.A. Splawski has helped with the creation of the CORFU concept (ref. Chapter 3), for checking the results and offering constructive criticisms. Then there is Dr. J.G. Issa with whom a lot of time was spent on discussing finite element and solution techniques. Without his often very helpful suggestions certain ideas would never have been attempted. Certainly, without their

collaboration, the volume and quality of the results would have been poorer.

Naturally over a period of three years a lot of contact is made with people who may or may not have direct involvement in the project but who have at one time or another rendered useful information. To Mr. K. Fletcher, Dr. S. Schofield, Mr. G. Stott, Dr. D.R. Tilley and Dr. A.K. Ziver I would like to acknowledge my thanks. Last but not least I must also acknowledge Mr. T. Sippel-Dau of the Imperial College Computer Advisory for invaluable help in using the AMDAHL 470/V8 computer.

The Science and Engineering Research Council and the National Nuclear Corporation have provided financial support for the project.

Finally I must thank Mrs. E. Noel for her efficient typing.

To

my

parents

CONTENTS

LIST OF FIGURES

LIST OF TABLES

CHAPTER 1

INTRODUCTION

1.1 The Importance of Numerical Methods

1.2 Finite Elements: A Historical Perspective

1.3 An Outline of the Finite Element Method

1.4 Practical Solution Methods

1.5 Current Status

"In brief, analytical methods are the foundation of the whole subject, and in practice they are the most accurate when they will work, but in the integration of partial equations, with reference to irregular-shaped boundaries, their field of application is very limited.

..... for engineering .... there is a demand for rapid methods, easy to be understood and applicable to unusual equations and irregular bodies".

L.F. Richardson [83]

CHAPTER 1

1.1 The Importance of Numerical Methods

Since high speed computing machines came into existence, numerical methods have been steadily developed to play the dominant role in the engineer's task of problem solving and analysis. Today it is inconceivable that solutions to engineering problems could be achieved without the aid of computers. The applications embrace all fields of engineering, be it iterative treatment of heat and mass balances such as in the analysis of flash distillation in chemical engineering or the prediction of flow and thermal patterns as in the analysis of the flow of fluids in various types of media. That numerical methods should assume such an important position in engineering analysis is due to several factors. Firstly, most natural phenomena can best be described by differential equations with varying boundary conditions whose solutions cannot be obtained by analytical means except in the simplest cases. Improvements in numerical techniques have made feasible at low cost precise solutions of problems significantly more complex than hitherto. As a consequence the stage has been reached where engineering tolerances can be tailored with a precision never dared before. This directly leads to an economic savings in terms of material and human resources. In the years before 1945 engineering analyses were lengthy, repetitive and time consuming because similar problems had to be performed from the beginning to the end with equally demanding efforts and care. Nowadays related problems

can be solved on a blackbox basis in a short space of time. This blackbox would comprise of a computer code with facilities for data input/output, modules for rendering the problem to be analysed numerically and the solution algorithm.

This potential of numerical analysis as seen in the light of present-day achievements contrasted with the cautious predictions when computers were just introduced in the 1940's. Then it was considered that only a dozen computers would suffice to perform all the envisaged numerical calculations [70].

Numerical methods, as a means for solving large scale engineering problems, saw their introduction in the paper delivered by L.F. Richardson [83] to the Royal Society in 1910. Later on, contributions by Liebmann [64] and Courant, Friedrichs and Lewy [23] laid the foundations of the finite-difference method. Progress in developing numerical methods before the 1940's was necessarily slow because of the absence of automatic computation. But since the arrival of the computer engineers and scientists have been quick to exploit numerical methods and its popularity has never declined since. The finite element method grew out of a number of intuitive procedures and associated mathematical techniques during the mid-1950's, in the way outlined in the next section. Before its conception the finite-difference method held the dominant position in the numerical solution of continuum problems. Today both

methods are equally important, each with its own advantages and disadvantages. However certain problems are more amenable to the finite element treatment than the finite difference method, and vice-versa. The choice of which method to use in solving a particular problem, although still subjected to the whims and fancies of the practitioner, is more or less dictated by the obvious advantages of one method over the other, although in certain applications there may be no clear cut advantages.

1.2 Finite Elements: A Historical Perspective

It was in the field of structural engineering that the finite element method (abbreviated to FEM from now on) had its origin. The early work of Hrennikoff [41] in 1941 and McHenry [68] in 1943 were probably the first attempts at discretizing a continuum into smaller regions or elements interconnected at only a finite number of nodal points. There was an inactive period following this early work which was finally broken in 1954 when Argyris [8, 9] and colleagues adapted the so-called matrix methods of structural analysis to solve problems in linear structural analysis. In particular, efficient solution techniques, well suited to automatic digital computation, were utilised for the first time. In 1956, Turner et al [96] of the Boeing Aircraft Co. introduced the direct stiffness matrix for triangular elements to solve plane stress problems. In 1960 Clough [21] coined the name "finite element" in a paper on plane elasticity. With the digital computer also becoming an ever more

effective tool for the engineer the FEM soon gained a firm footing.

After 1963 the foundations of the FEM were laid when Besseling [12], Melosh [69], Fraeijis de Veubecke [32] and Jones [47] recognised that the FEM was a form of the Ritz method in which variational principles can be used to handle the problems of elasticity.

In 1965 Zienkiewicz and Cheung [103] paved the way for the application of the FEM to problems other than structural engineering when they applied the FEM, using Variational Principles, to solve Poisson's Equation. This is usually referred to as the Rayleigh-Ritz Method and was a major milestone because the FEM was the exclusivity of the structural engineers prior to this period. Applications in other fields soon followed when Wilson and Nickell [101] and Doctors [27] applied the FEM to heat conduction and potential flow problems respectively.

In 1969 Szabo and Lee [93] utilised the weighted residuals approach in setting up a finite element analysis of a plane elasticity problem. This alternative approach is especially useful where no variational functional can be set up for a particular type of problem in order to apply the Rayleigh-Ritz Method.

During this interesting era in the formulation of the FEM, i.e. the 1960's, there was a concensus that the method might already have been formulated from a mathematician's point of view. The advocates were not to be

disappointed because the classic paper by Courant [22] in 1943 was soon recognised as the corner stone in the establishment of the FEM. In that paper Courant had used piecewise continuous functions over triangular domains and the principle of minimum potential energy in studying the St. Venant torsion problem. This view can be seen to be an extension of the Rayleigh-Ritz principle. Prager and Synge [80] in the late forties utilised the concept of function space, which resulted in the hypercircle method, to solve continuum problems in much the same manner as finite element techniques. The hypercircle method was applied to neutron transport problems by Ackroyd and Ball [4] in 1960 but the vogue in those days was to use finite difference techniques for such problems, and this method was not pursued by other researchers. Finally it was acknowledged that the work of Greenstadt [37], which appeared in 1959, contained many important and basic concepts that are essential in the mathematical formulation of the FEM.

1.3 An Outline of the Finite Element Method

The finite element method has been described in many excellent textbooks [10,20,42,45,76,91,92,95,102]. Besides, the number of papers published annually is of the order of thousands [102]. In the early days most of the contributions came from structural engineers but since Zienkiewicz and Cheung [103] reported the application of the finite element method to other types of problems contributions have come in from diverse fields of engineering and mathematics.

What is the finite element method? Since no single sentence can suffice to provide sufficient information to everyone it can briefly by described as the execution and compliance of the following stages:

(i) a continuum problem is divided into a number of parts, finite in number, called elements;

(ii) these elements are assumed to be connected at a number of points lying on the boundaries;

(iii) the values of the dependent variable at the nodal points constitute the set of unknowns whose solutions are desired;

(iv) a set of functions, known as the shape (or interpolation) functions, is chosen to represent the unknown variable within the element in terms of its nodal values;

(v) employment of the shape functions can be made by one of two available routes, i.e. either to use the method of weighted residuals or variational principles;

(vi) both procedures lead to sets of linear equations for the nodal values; the matrix of these equations is called the element stiffness matrix because of its first use in structural mechanics;

(vii) the load, or source, contributions of the problem are assumed to act at the nodes of the element;

(viii) the assembly of the whole system is achieved by collocating the individual element stiffness matrices and load vectors;

(ix) the solution of this global system of linear equations yields the values of the unknown nodal variables.

Items (i) to (ix) therefore constitute a short review of the finite element method.

At this juncture it would be best to elaborate on the method of weighted residuals and variational principles. In the first method the functions are substituted directly into the differential equation and this results in a residual owing to the approximate nature of the function. Then linearly independent weight functions are chosen to weight the residual by imposing the integral of the product of each weight function and the residual to be zero. The result is a set of algebraic equations. The three most commonly used weight functions are the Dirac delta functions, the interpolating functions (usually polynomials) defining the approximation, and the functions obtained by differentiating the residual with respect to each of the nodal values. The associated terms for these methods are the collocation, Galerkin. and least squares approaches to the method of weighted residuals. On the other hand, when variational principles are used the functions cannot be substituted directly into the differential equation. A functional has first to be obtained from variational considerations on the differential equation. The functions are then substituted and a set of algebraic equations result by requiring the first differential of the functional with respect to each nodal value to be zero.

The choice as to which approach to use is not always easy. To use the variational method a functional must first be found. Naturally in the situations where no variational functionals exist the method of weighted residuals is used. On the other hand the variational approach, and also the least squares approach, guarantee that the global matrix will be symmetric. This is important because only one-half of the matrix including the diagonal need to be stored.

No practical (or even a demonstration) finite element calculations can be accomplished without the aid of the digital computer. Consequently it should be borne in mind that the dependence on programming techniques, the ease of data input and the intermediate and post-processing of output, although not commented upon above, are important features.

In bringing continuum problems to a discretized form all numerical methods, and certainly the finite element method, involve an approximation which approaches the true continuum solution as the number of discrete components increases. Therefore one should be aware of the struggle between the different methods in achieving as accurate a solution as possible with the least number of discrete components. This can be realised from the point of view that computing effort and resources increase as the number of discrete components increases.

1.4 Practical Solution Methods

Just as the Navier-Stokes Equations govern the flow of fluids, the Boltzmann transport equation governs the behaviour of particles and their interaction with the bounded media in which they are diffusing. As will be seen in the next chapter, the equation, being of a differential-integral form, is complex. Therefore the problems are usually simplified by imposing certain assumptions. A host of methods exist for the solution of the Boltzmann transport equation and have been reviewed accordingly [5, 16,63,84]. However, the predominant methods for solving the Boltzmann equation are the discrete-ordinates method [18,58] and the Monte Carlo method [49,89].

In solving the Boltzmann equation one is also concerned with the angular variable owing to the scattering nature of the particles with the media in which they are diffusing. Therefore in the discrete-ordinates method, which was initially advanced by Carlson [17], the angular variable is discretized into a set of directions or rays while the spatial variables are treated by finite difference methods. Weights are assigned to the set of angular directions by means of quadrature sets. Incidentally, in the P_N method [29], the other major finite-difference based method, spherical harmonics are used to approximate the angular variable.

In the Monte Carlo method the histories of a significant number of particles are individually tracked. The course of each particle is followed from birth, through its various

interactions with the host media until its death which usually means an escape from the media under study or due to absorption. The book-keeping of all these particles enable one to draw up a macroscopic picture of the behaviour of the system.

Both these methods although popular, established and in general use, suffer from certain disadvantages. The discrete-ordinates method do not conform well to problems with irregular geometries, suffer from ray effects (i.e. unnatural oscillations in the flux distributions owing to the way the angular variable is being discretized) and can produce negative scalar fluxes especially when the mesh is not sufficiently fine (and hence impose greater computer storage requirements). The Monte Carlo method, although well suited for irregular geometries, is cost prohibitive because a large number of particles need to be tracked before any statistically significant results can be obtained.

So, bearing the disadvantages of the discrete-ordinates and Monte Carlo methods in mind, there is an impetus for introducing new methods in solving the Boltzmann transport equation. To this end the finite element method shows great promise. The FEM is an established method in the sense that its foundations are thoroughly laid and that it has met with considerable success in a multitude of applications. One great advantage of the FEM is its ability to cope with irregular geometries (that is why it has met with so much success in structural engineering).

Direct elimination methods, rather than iterative ones, are usually employed to solve the system of equations set up in the finite element analysis and this affords an advantage in execution speeds. Besides such solutions are unlikely to suffer from unnatural oscillations. Therefore there is potential for the FEM as an alternative method for solving the Boltzmann transport equation.

1.5 Current Status

There are, as we have seen, two approaches when employing the FEM, the method of weighted residuals and the method of variational principles. To date both methods have been employed in trying to solve the Boltzmann transport equation although when the variational method is used the even-parity second-order form of the Boltzmann equation is used in order to obtain a variational principle. This lack of an extremal variational principle for the first-order equation has now been remedied by Ackroyd [2]. This will be discussed in more detail in the next chapter, where it will also be seen that the Boltzmann equation is generally expressed in a multigroup form owing to the dependence of the materials cross-sections on incident particle speed. Besides, the diffusion equations usually refer to the lowest order of the Boltzmann transport equation. The following is a very concise review of the work done by other researchers.

In the initial stages Ohnishi [77] initiated work on the FEM. This was responded when Semenza et al [88], Kang

and Hansen [50], Kaper et al [51], Komoriya and Walters [56], Deppe and Hansen [25], Biswas et al [13] and Schmidt et al [85,86] reported work achieved on the diffusion aspects. In particular emphasis was on one or few groups problems with the exception of Schmidt et al where they developed a package called DIFGEN which has been thoroughly exercised on analysing practical problems concerned with the High Temperature Reactor at Jülich. Later on and in parallel with the development of the diffusion aspects, the FEM was also being applied to transport problems. Miller et al [71] and Kaper et al [53] reported results for x-y geometry using the Rayleigh-Ritz approach, and in the same vein Pitkaranta [78] reported results for spherical systems. This was followed on by Briggs et al [15] who discussed the elimination of ray effects with finite elements and further work by Blomquist and Lewis [14], Martin and Duderstadt [66], Mordant [73], Lillie and Robinson [65] and Galliara and Williams [33].

On the local front previous work has been achieved on a systematic study basis starting with the theoretical considerations of Ackroyd [1]. Ziver [104] has dealt with the study of linear elements in x-y geometry for up to two groups and two moments (the meaning of moments will be discussed in Chapter 3) while Issa [46] has also achieved some results for three-dimensional diffusion problems and in parallel with this work has also investigated higher order elements but for simple systems. Splawski [90] working in collaboration with Ziver had performed studies on the angular aspects of the work.

The present work is a continuation of the efforts mentioned above but extended to contain multigroup and multiregion capability, generalised angular treatment, a choice of Lagrangian elements, a treatment on the solution aspects and attention to ease of data handling. Moreover, for the first time, after separating the wheat from the chaff, a truly modular computer code has been developed the structure of which will remain intact when future work is continued, in which new features can be added or old features deleted with the minimum of interference to the structure.

For the remainder of this thesis, Chapter 2 will be concerned with the Boltzmann transport equation and the variational functional. This will be followed by a chapter on the treatment of the angular variable while finite elements are discussed in the fourth chapter. Results follow and this is concluded with the final chapter on summary and recommendations.

CHAPTER 2

THE BOLTZMANN EQUATION AND A VARIATIONAL FUNCTIONAL

"Here and elsewhere we shall not obtain the best insight into things until we actually see them growing from the beginning."

Aristotle

2.1 The Boltzmann Transport Equation

The Boltzmann transport equation is very often referred to when neutron particle transport is discussed. It was during the 19th Century that Boltzmann derived his equation to describe the kinetic behaviour of very dilute gases. The behaviour of neutrons in nuclear reactors or penetrating media is of a similar nature [24] and hence the reference to Boltzmann's equation when the transport of neutrons are discussed.

Under rarefied conditions the gaseous particles tend to cover longer distances between interactions and as a result the mean free paths are rather long when compared with those for normal diffusion processes where interactions are more frequent. In neutron transport the only significant type of interaction is between neutrons and the nuclei of the media in which they are streaming. However the frequency of such interactions is rather low owing to the fact that neutronic densities are very sparse in most media through which they are travelling. Hence the mean free paths of neutron-nuclei interactions are also rather long and therefore the fundamental ideas used in deriving the Boltzmann transport equation are similar to those used in deriving the neutron transport equation, the major difference being that in the latter only one species involved in the interactions is considered to be mobile.

In order to know the distribution of neutrons in a given medium, and hence the various reaction rates,

it would be necessary to solve the neutron transport equation. Analytical solutions are not possible for practical problems owing to the complexity of the equation. Numerical solutions are usually sought for whenever such situations arise. The complex nature of the equation is further enhanced by the fact that the neutronic cross-sections and their relation with the incident neutron energy is very complicated. Therefore averaging procedures and approximation techniques, especially the multigroup form of the transport equation, are used to remove this complexity. In practice, engineering constraints dictate the choice of materials used in nuclear reactor cores and shields. As a result such systems are highly heterogeneous and this further complicates the dictates on the equation. In the eventuality even before numerical techniques can be used to solve the Boltzman transport equation a number of simplifications and approximations have to be made.

By considering conservation principles one arrives at the integro-differential form of the Boltzmann transport equation [28]:

$$\frac{1}{v}\frac{\partial \phi}{\partial t} + \underline{\Omega}.\nabla\phi(\underline{r},E,\underline{\Omega},t) + \Sigma_t(\underline{r},E)\phi(\underline{r},E,\underline{\Omega},t)$$
$$= \int_{4\pi} d\Omega' \int_0^{\infty} \Sigma_s(\underline{r},E'\rightarrow E,\underline{\Omega}'\rightarrow\underline{\Omega})\phi(\underline{r},E',\underline{\Omega}',t)\,dE' \qquad (2.1)$$
$$+ S(\underline{r},E,\underline{\Omega},t)$$

where,

$\phi(\underline{r},E,\underline{\Omega},t)$ = angular flux

v = neutron speed

$\Sigma_t(\underline{r},E)$ = total macroscopic cross-section

$\Sigma_s(\underline{r},E'\to E,\underline{\Omega}'\to\underline{\Omega})$ = differential form of the macroscopic scattering cross-section

source

and the independent variables being

$\underline{r}$ = position vector

E = energy

$\underline{\Omega}$ = unit directional vector

t = time

The source term is expressed as the sum of the contributions due to a fixed source and fission:

$$S(\underline{r},E,\underline{\Omega},t) = Q(\underline{r},E,\underline{\Omega},t) + \frac{\chi(E)}{4\pi}\int_0^\infty \nu\Sigma_f(\underline{r},E')\int_{4\pi}\phi(\underline{r},E',\underline{\Omega}',t)\,dE'd\underline{\Omega}' \qquad (2.2)$$

where

$Q(\underline{r},E,\underline{\Omega},t)$ = fixed source contribution

$\nu\Sigma_f(\underline{r},E')$ = product of average number of neutrons per fission and the macroscopic fission cross-section

$\chi(E)$ = fission spectrum

Although complicated in appearance Eq.(2.1) is nothing more than an expression for the rate of change of neutron density as the difference between the rates of production

and loss at a point $\underline{r}$ in space and at a particular velocity, v. It can be seen that in addition to the temporal variable the equation involves 3 spatial variables, 2 angular variables and 1 energy variable. The first simplification to this equation involves the steady-state form only thereby removing the temporal variable. Therefore, Eq.(2.1) simplifies to:

$$\underline{\Omega}\cdot\nabla\phi(\underline{r},E,\underline{\Omega})+\Sigma_t(\underline{r},E)\phi(\underline{r},E,\underline{\Omega})$$

$$=\int_{4\pi}d\Omega'\int_0^{\infty}\Sigma_s(\underline{r},E'\to E,\underline{\Omega}'\to\underline{\Omega})\phi(\underline{r},E',\underline{\Omega}')\,dE' \qquad (2.3)$$

$$+S(\underline{r},E,\underline{\Omega})$$

2.1.1 Boundary conditions

In practice two types of exterior boundary conditions are considered:

(i) the bare surface (or vacuum) condition,

and (ii) the perfect reflector condition.

The surface sources that are sometimes used for shielding calculations are not treated because they are, in practice, the distributed or volume sources of the present method.

The first condition, when expressed for a non re-entrant body, means that no neutrons are entering the body from the outside, i.e.:

$$\phi(\underline{r}_s,E,\underline{\Omega})=0 \quad \text{for} \quad \underline{\Omega}\cdot\underline{n}<0 \qquad (2.4)$$

where,

$\underline{r}_s$ is on the bare surface

and $\underline{n}$ is the outward drawn normal to the surface at $\underline{r}_s$.

The perfect reflector condition represents a symmetry condition.

In diffusion problems the zero flux boundary condition is sometimes considered. This is the situation in which the flux on an extrapolated boundary in a vacuum is set to zero. Usually this condition is not applied when the choice of the rather more elegant vacuum condition is available. However in Section 5.2 where the ZION-1 reactor problem is discussed the zero flux boundary condition was introduced by the original investigators. Nevertheless a good approximation for the flux within a system can be made with this condition if the distance of the extrapolated boundaries from the true boundary is chosen appropriately.

2.2 The Multigroup Approximation

In the operation of a typical reactor, neutrons spanning the energy range from 10 MeV to less than 0.01 eV are present. The behaviour of the neutronic cross-sections in this enormous energy range is rather complicated. Any interaction could not be represented by a constant cross-section. Hence, in order to use nuclear data in a practical manner, the multigroup approximation is introduced in which the whole energy spectrum of interest is discretized into a finite number of energy groups. The number

of energy groups employed in a particular analysis depends to a large extent on the type of problem and the accuracy desired. Sometimes, only 2 or 3 groups suffice for thermal reactor calculations whereas for fast reactors the number of energy groups employed is of the order of ten.

Details of the multigroup approximation have been described elsewhere [16,18] but it can be written as:

$$\underline{\Omega}\cdot\nabla\phi_g(\underline{r},\underline{\Omega}) + \Sigma_{t_g}(\underline{r})\phi_g(\underline{r},\underline{\Omega})$$

$$= \int_{4\pi} \sum_{g'=1}^{G} \Sigma_{s_{g'g}}(\underline{r},\underline{\Omega}\cdot\underline{\Omega}')\phi_{g'}(\underline{r},\underline{\Omega}')\,d\Omega' \qquad (2.5)$$

$$+ S_g(\underline{r},\underline{\Omega}) \qquad g=1,2,\ldots G$$

where,

G = total number of energy groups considered.

The other variables in the equation are as defined in Eq.(2.1) except that they refer to a particular energy group g. The fastest group in this approximation assumes the value $g=1$ with the slowest being group G.

Before writing out the contributions in the group source term, $S_g(\underline{r},\underline{\Omega})$, it would be usual to separate the in-scattering contributions in the scattering term from within the group scattering component and lump it together with the source term. Therefore:

$$\underline{\Omega}\cdot\nabla\phi_g(\underline{r},\underline{\Omega}) + \Sigma_{t_g}(\underline{r})\phi_g(\underline{r},\underline{\Omega})$$

$$= \int_{4\pi} \Sigma_{s_{gg}}(\underline{r},\underline{\Omega}\cdot\underline{\Omega}')\phi_g(\underline{r},\underline{\Omega}')\,d\Omega'$$

$$+ S_g(\underline{r},\underline{\Omega}) \qquad (2.6)$$

in which

$$S_g(\underline{r},\underline{\Omega}) = \int_{4\pi} \sum_{\substack{g'=1 \\ g'\neq g}}^{G} \Sigma_{s_{g'g}}(\underline{r},\underline{\Omega}\cdot\underline{\Omega}')\phi_{g'}(\underline{r},\underline{\Omega}')\,d\Omega'$$

$$+ \frac{\chi_g}{4\pi} \sum_{g'=1}^{G} \nu\Sigma_{f_{g'}}(\underline{r}) \int_{4\pi} \phi_{g'}(\underline{r},\underline{\Omega}')\,d\Omega' \qquad (2.7)$$

$$+ Q_g(\underline{r},\underline{\Omega})$$

In order of appearance, the source contributions are the scattering, fission and fixed source terms. At each stage the contributions from other groups to the group under consideration is assumed to be known, while the within-group scattering term involves the unknown group flux. If a direct, as opposed to iterative, method is to be used for each group the within-group scattering term must be retained explicitly while the inter-group scattering terms are incorporated into the source.

If only downscattering is considered then the summation index for the scattering term in Eq.(2.7) can be written as $g' = g-1$ i.e.

$$S_g(\underline{r},\underline{\Omega}) = \int_{4\pi} \sum_{g'=1}^{g-1} \Sigma_{s_{g'g}}(\underline{r},\underline{\Omega}\cdot\underline{\Omega}')\phi_{g'}(\underline{r},\underline{\Omega}')\,d\Omega'$$

$$+ \sum_{g'=1}^{G} \nu\Sigma_{f_{g'}}(\underline{r}) \int_{4\pi} \phi_g(\underline{r},\underline{\Omega}')\,d\Omega' \qquad (2.8)$$

$$+ Q_g(\underline{r},\underline{\Omega})$$

2.3 The Second-Order Transport Equation

As was outlined in Section 1.3 there are two main approaches in a finite element formulation of the neutron transport equation. The first method is the application of the method of weighted residuals to the first-order equation whilst the second utilises a variational principle for the second-order equation. Since the latter approach is the method employed in this thesis, it is necessary then to mention the properties of the second-order equation. The inherent advantage of the second-order equation is that the leakage and removal operators are positive-definite and self-adjoint and this makes it fairly easy to establish variational principles of the extremal kind. The variational approach leads to a set of linear equations with a sparse, symmetric and positive-diagonal matrix. Besides, the variational principles are boundary free [1].

2.3.1 Even- and odd-parity definitions

The even- and odd-parity fluxes are defined as:

$$\Phi^{+}(\pm,\underline{\Omega}) = \frac{1}{2}\left\{\Phi(\pm,\underline{\Omega}) + \Phi(\pm,-\underline{\Omega})\right\}$$
$$\Phi^{-}(\pm,\underline{\Omega}) = \frac{1}{2}\left\{\Phi(\pm,\underline{\Omega}) - \Phi(\pm,-\underline{\Omega})\right\} \qquad (2.9)$$

The group subscript, g, has been omitted from the above definition but nevertheless the meaning is implied.

Similarly, the even- and odd-parity sources and scattering cross-sections are defined as:

$$S^{\pm}(\pm,\underline{\Omega}) = \frac{1}{2}\left\{S(\pm,\underline{\Omega}) \pm S(\pm,-\underline{\Omega})\right\} \qquad (2.10)$$

$$\Sigma_s^{\pm}(\pm,\underline{\Omega}\cdot\underline{\Omega}') = \frac{1}{2}\left\{\Sigma_s(\pm,\underline{\Omega}\cdot\underline{\Omega}') \pm \Sigma_s(\pm,-\underline{\Omega}\cdot\underline{\Omega})\right\} \qquad (2.11)$$

Starting with these definitions, the second-order transport equation is derived as will be seen in the next few sub-sections. The angular flux can then be expressed as a sum of the even- and odd-parity fluxes by

$$\Phi(\pm,\underline{\Omega}) = \Phi^{+}(\pm,\underline{\Omega}) + \Phi^{-}(\pm,\underline{\Omega}) \qquad (2.12)$$

2.3.2 Coupled first order even- and odd-parity equations

Since Eq. (2.6) holds for the whole range of the vector $\underline{\Omega}$, it can also be written as

$$-\underline{\Omega}\cdot\nabla\phi(\pm,-\underline{\Omega}) + \Sigma_t(\pm)\phi(\pm,-\underline{\Omega})$$

$$= \int_{4\pi} \Sigma_s(\pm,-\underline{\Omega}\cdot\underline{\Omega}')\phi(\pm,\underline{\Omega}')\,d\Omega' + S(\pm,-\underline{\Omega}) \qquad (2.13)$$

On adding and subtracting Eq.(2.6) and (2.13) the following equations result:

$$\underline{\Omega}\cdot\nabla\phi^-(\pm,\underline{\Omega}) + \Sigma_t(\pm)\phi^+(\pm,\underline{\Omega})$$

$$= \int_{4\pi} \Sigma_s^+(\pm,\underline{\Omega}\cdot\underline{\Omega}')\phi(\pm,\underline{\Omega}')\,d\Omega' + S^+(\pm,\underline{\Omega}) \qquad (2.14)$$

$$\underline{\Omega}\cdot\nabla\phi^+(\pm,\underline{\Omega}) + \Sigma_t(\pm)\phi^-(\pm,\underline{\Omega})$$

$$= \int_{4\pi} \Sigma_s^-(\pm,\underline{\Omega}\cdot\underline{\Omega}')\phi(\pm,\underline{\Omega}')\,d\Omega' + S^-(\pm,\underline{\Omega}) \qquad (2.15)$$

Substituting Eq.(2.12) into these two equations it is seen

$$\int_{4\pi} \Sigma_s^+(\pm,\underline{\Omega}\cdot\underline{\Omega}')\phi^-(\pm,\underline{\Omega}')\,d\Omega'$$

$$= \int_{4\pi} \Sigma_s^-(\pm,\underline{\Omega}\cdot\underline{\Omega}')\phi^+(\pm,\underline{\Omega}')\,d\Omega' = 0 \qquad (2.16)$$

because the integral over all directions of the product of an even and odd function of $\underline{\Omega}$ is zero.

We finally arrive at the following pair of coupled first-order differential-integro equations:

$$\underline{\Omega}.\nabla\phi^{-}(\pm,\underline{\Omega}) + \Sigma_t(\pm)\phi^{+}(\pm,\underline{\Omega}) = \int_{4\pi} \Sigma_s^{+}(\pm,\underline{\Omega}.\underline{\Omega}')\phi^{+}(\pm,\underline{\Omega}')\,d\Omega' + S^{+}(\pm,\underline{\Omega}) \tag{2.17}$$

$$\underline{\Omega}.\nabla\phi^{+}(\pm,\underline{\Omega}) + \Sigma_t(\pm)\phi^{-}(\pm,\underline{\Omega}) = \int_{4\pi} \Sigma_s^{-}(\pm,\underline{\Omega}.\underline{\Omega}')\phi^{-}(\pm,\underline{\Omega}')\,d\Omega' + S^{-}(\pm,\underline{\Omega}) \tag{2.18}$$

2.3.3 Expansion of the scattering cross-section

The scattering cross-section can be expanded in terms of Legendre Polynomials [16], i.e.:

$$\Sigma_s(\pm,\underline{\Omega}.\underline{\Omega}') = \sum_{l=0}^{\infty}\left(\frac{2l+1}{4\pi}\right)\Sigma_{s_l}(\pm)P_l(\underline{\Omega}.\underline{\Omega}') \tag{2.19}$$

in which $\Sigma_{s_l}(\pm)$, the scattering coefficients, are generated via the relation

$$\Sigma_{s_\ell}(\pm) = 2\pi \int_{-1}^{1} \Sigma_s(\pm, \underline{\Omega}.\underline{\Omega}') P_\ell(\underline{\Omega}.\underline{\Omega}') d(\underline{\Omega}.\underline{\Omega}') \qquad (2.20)$$

Recalling the odd-parity scattering cross-section from Eq.(2.11) using Eq.(2.16) and observing the relation

$$P_\ell(\underline{\Omega}.\underline{\Omega}') = P_\ell(-\underline{\Omega}.\underline{\Omega}') \qquad (2.21)$$

for ℓ even

the odd-parity scattering cross-section becomes

$$\Sigma_s^-(\pm, \underline{\Omega}.\underline{\Omega}') = \sum_{\ell\ \text{odd}} \left(\frac{2\ell+1}{4\pi}\right) \Sigma_{s_\ell}(\pm) P_\ell(\underline{\Omega}.\underline{\Omega}') \qquad (2.22)$$

2.3.4 Spherical harmonics representation

The following relation is derived from the Addition Theorem of Legendre Polynomials

$$P_\ell(\underline{\Omega}.\underline{\Omega}') = \left(\frac{4\pi}{2\ell+1}\right) \sum_{m=-\ell}^{\ell} Y_{\ell m}(\underline{\Omega}) Y_{\ell m}^*(\underline{\Omega}') \qquad (2.23)$$

where,

$Y^{*}_{\ell m}(\underline{\Omega})$ is the complex conjugate of $Y_{\ell m}(\underline{\Omega})$

From Eq.(2.22) and (2.23),

$$\Sigma_s^{-}(\pm, \underline{\Omega}.\underline{\Omega}') = \sum_{\ell\ \text{odd}} \Sigma_{s_\ell}(\pm) \sum_{m=-\ell}^{\ell} Y_{\ell m}(\underline{\Omega}) Y^{*}_{\ell m}(\underline{\Omega}) \tag{2.24}$$

which on substitution into Eq.(2.18) results in

$$\begin{aligned} &\underline{\Omega}.\nabla\phi^{+}(\pm,\underline{\Omega}) + \Sigma_t(\pm)\phi^{-}(\pm,\underline{\Omega}) \\ &= \sum_{\ell\ \text{odd}} \Sigma_{s_\ell}(\pm) \sum_{m=-\ell}^{\ell} Y_{\ell m}(\underline{\Omega}) \int Y^{*}_{\ell m}(\underline{\Omega}')\phi^{-}(\pm,\underline{\Omega}')\, d\Omega' \\ &+ S^{-}(\pm,\underline{\Omega}) \end{aligned} \tag{2.25}$$

2.3.5 Orthogonality relationship

Let

$$f(\pm,\underline{\Omega}) = -\underline{\Omega}.\nabla\phi^{+}(\pm,\underline{\Omega}) + S^{-}(\pm,\underline{\Omega}) \tag{2.26}$$

and Eq.(2.25) becomes

$$\begin{aligned} f(\pm,\underline{\Omega}) &= \Sigma_t(\pm)\phi^{-}(\pm,\underline{\Omega}) \\ &- \sum_{\ell\ \text{odd}} \Sigma_{s_\ell}(\pm) \sum_{m=-\ell}^{\ell} Y_{\ell m}(\underline{\Omega}) \int_{4\pi} Y^{*}_{\ell m}(\underline{\Omega}')\phi^{-}(\pm,\underline{\Omega}')\, d\Omega' \end{aligned} \tag{2.27}$$

Multiplying throughout by $Y^{*}_{\ell'm'}(\underline{\Omega})$ and integrating over Ω and using the Orthogonality Relationship

$$\int_{4\pi} Y^{*}_{\ell'm'}(\underline{\Omega}) Y_{\ell m}(\underline{\Omega})\, d\Omega = \delta_{\ell\ell'}\,\delta_{mm'} \tag{2.28}$$

we arrive at

$$\int_{4\pi} Y^{*}_{\ell m}(\underline{\Omega}')\,\phi^{-}(\pm,\underline{\Omega}')\, d\Omega'$$

$$= \left[\Sigma_t(\pm)-\Sigma_{s_\ell}(\pm)\right]^{-1}\int_{4\pi} Y^{*}_{\ell m}(\underline{\Omega}')\, f(\pm,\underline{\Omega}')\, d\Omega' \tag{2.29}$$

2.3.6 The odd-parity flux equation

Finally substituting Eq.(2.29) and (2.26) into (2.25) results in an expression for the odd-parity flux,

$$\phi^{-}(\pm,\underline{\Omega}) = \frac{1}{\Sigma_t(\pm)}\left\{S^{-}(\pm,\underline{\Omega}) - \underline{\Omega}.\nabla\phi^{+}(\pm,\underline{\Omega})\right.$$

$$+\sum_{\ell\ \mathrm{odd}}^{L}\frac{\Sigma_{s_\ell}(\pm)}{\Sigma_t(\pm)-\Sigma_{s_\ell}(\pm)}\sum_{m=-\ell}^{\ell} Y_{\ell m}(\underline{\Omega})\int_{4\pi} Y^{*}_{\ell m}(\underline{\Omega}') \tag{2.30}$$

$$\left.\times\left[S^{-}(\pm,\underline{\Omega}')-\underline{\Omega}'.\nabla\phi^{+}(\pm,\underline{\Omega}')\right] d\Omega'\right\}$$

A similar expression is obtained for the even-parity flux when the stages from Eq.(2.22) till (2.29) are observed except that the even-parity scattering cross-section is used as the starting point and Eq.(2.17) is used instead of Eq.(2.18).

2.3.7 The final expression

Substituting Eq.(2.30) into (2.17) yields the second-order even-parity form of the transport equation, i.e.

$$\begin{aligned}
&\underline{\Omega}\cdot\nabla\left\{\frac{1}{\Sigma_t(\underline{r})}\left[S^-(\underline{r},\underline{\Omega})-\underline{\Omega}\cdot\nabla\phi^+(\underline{r},\underline{\Omega})\right]\right.\\
&+\sum_{\ell\ \text{odd}}\frac{\Sigma_{s_\ell}(\underline{r})}{\Sigma_t(\underline{r})\left(\Sigma_t(\underline{r})-\Sigma_{s_\ell}(\underline{r})\right)}\sum_{m=-\ell}^{\ell}Y_{\ell m}(\underline{\Omega})\int_{4\pi}Y_{\ell m}^{*}(\underline{\Omega}')\\
&\left.\times\left[S^-(\underline{r},\underline{\Omega})-\underline{\Omega}'\cdot\nabla\phi^+(\underline{r},\underline{\Omega}')\right]d\Omega'\right\}+\Sigma_t(\underline{r})\phi^+(\underline{r},\underline{\Omega})\\
&=\sum_{\ell\ \text{even}}\Sigma_{s_\ell}(\underline{r})\sum_{m=-\ell}^{\ell}Y_{\ell m}(\underline{\Omega})\int_{4\pi}Y_{\ell m}^{*}(\underline{\Omega}')\phi^+(\underline{r},\underline{\Omega}')\,d\Omega'\\
&+S^+(\underline{r},\underline{\Omega})
\end{aligned}\tag{2.31}$$

2.4 The Leakage and Removal Operators

At this stage of the discussion it is necessary to introduce two operators. One reason is that they can be shown to be both self-adjoint and positive-definite [1] The properties allow one to establish extremal variational principles. We introduce operators G and C to describe the equations in a compact manner. These operators, serve as a shorthand for the lengthy expression in Eq.(2.31).

If $u(\underline{r},\underline{\Omega})$ be any arbitrary function of $\underline{r}$ and $\underline{\Omega}$, the leakage operator, G, can be defined as

$$Gu(\underline{r},\underline{\Omega}) = \frac{u(\underline{r},\underline{\Omega})}{\Sigma_t(\underline{r})} + \int_{4\pi} g(\underline{r},\underline{\Omega}.\underline{\Omega}')u(\underline{r},\underline{\Omega}')\,d\Omega' \qquad (2.32)$$

where,

$$g(\underline{r},\underline{\Omega}.\underline{\Omega}') = \sum_{l\ odd} \frac{\Sigma_{s_l}(\underline{r})}{\Sigma_t(\underline{r})\left(\Sigma_t(\underline{r})-\Sigma_{s_l}(\underline{r})\right)}\left(\frac{2l+1}{4\pi}\right)P_l(\underline{\Omega}.\underline{\Omega}') \qquad (2.33)$$

or using the expression for $P_l(\underline{\Omega}.\underline{\Omega}')$ from Eq.(2.23)

$$g(\underline{r},\underline{\Omega}.\underline{\Omega}') = \sum_{l\ odd} \frac{\Sigma_{s_l}(\underline{r})}{\Sigma_t(\underline{r})\left(\Sigma_t(\underline{r})-\Sigma_{s_l}(\underline{r})\right)} \sum_{m=-l}^{l} Y_{lm}(\underline{\Omega})Y_{lm}^{*}(\underline{\Omega}') \qquad (2.34)$$

The other operator is the removal operator, and is defined as

$$C u(\pm,\underline{\Omega}) = \Sigma_t(\pm,\underline{\Omega})\,u(\pm,\underline{\Omega}) - \int_{4\pi} \Sigma_s^{+}(\pm,\underline{\Omega}\cdot\underline{\Omega}')\,\phi^{+}(\pm,\underline{\Omega}\cdot\underline{\Omega}')\,d\Omega' \tag{2.35}$$

or, in terms of spherical harmonics

$$C u(\pm,\underline{\Omega}) = \Sigma_t(\pm,\underline{\Omega})\,u(\pm,\underline{\Omega}) - \sum_{\ell\ \text{even}} \Sigma_{s_\ell}(\pm) \sum_{m=-\ell}^{\ell} Y_{\ell m}(\underline{\Omega}) \int_{4\pi} Y_{\ell m}^{*}(\underline{\Omega})\,\phi^{+}(\pm,\underline{\Omega}')\,d\Omega' \tag{2.36}$$

Hence it can readily be seen that Eq.(2.31) becomes

$$\underline{\Omega}\cdot\nabla\left\{G\left[S^{-}(\pm,\underline{\Omega}) - \underline{\Omega}\cdot\nabla\phi^{+}(\pm,\underline{\Omega})\right]\right\} + C\phi^{+}(\pm,\underline{\Omega}) = S^{+}(\pm,\underline{\Omega}) \tag{2.37}$$

or in the more usual form

$$-\underline{\Omega}\cdot\nabla\left\{G\left[\underline{\Omega}\cdot\nabla\phi^{+}(\pm,\underline{\Omega})\right]\right\} + C\phi^{+}(\pm,\underline{\Omega}) = S^{+}(\pm,\underline{\Omega}) - \underline{\Omega}\cdot\nabla G\left[S^{-}(\pm,\underline{\Omega})\right] \tag{2.38}$$

2.5 Self-Adjoint and Positive Definite Conditions

In order to apply variational methods to obtain maximum principles, the two conditions of self-adjointness and positive-definiteness must be met by both the leakage and removal operators.

Taking the removal operator C as an example, the definitions of these two conditions are [1];

(i) The operator C is self-adjoint if

$$\int_{4\pi} u(\pm,\underline{\Omega})\, C\, v(\pm,\underline{\Omega})\, d\Omega = \int_{4\pi} v(\pm,\underline{\Omega})\, C\, u(\pm,\underline{\Omega})\, d\Omega \qquad (2.39)$$

or using the notation for the inner product,

$$\left\langle u(\pm,\underline{\Omega}), C\, v(\pm,\underline{\Omega}) \right\rangle = \left\langle v(\pm,\underline{\Omega}), C\, u(\pm,\underline{\Omega}) \right\rangle \qquad (2.40)$$

in which,

$$\left\langle u,v \right\rangle = \int_{4\pi} u(\pm,\underline{\Omega})\, v(\pm,\underline{\Omega})\, d\Omega \qquad (2.41)$$

(ii) The operator C is positive-definite if

$$\left\langle u(\underset{\sim}{r},\underset{\sim}{\Omega}), Cu(\underset{\sim}{r},\underset{\sim}{\Omega}) \right\rangle \geq 0 \tag{2.42}$$

with equality if $u(\underset{\sim}{r},\underset{\sim}{\Omega})$ is zero.

Kaplan and Davis [55] have shown that both the leakage and removal operators are self-adjoint and positive definite when the scattering cross-section was expanded in terms of Legendre Polynomials as in Eq.(2.19) and (2.22). Ackroyd [1] has extended this proof for a general scattering law.

2.6 The $K(\hat{\phi})$ -Functional from Maximum Principles

If $\hat{\phi}(\underset{\sim}{r},\underset{\sim}{\Omega})$ be an admissible function, chosen as an approximation for $\phi^{+}(\underset{\sim}{r},\underset{\sim}{\Omega})$, it can then be shown [1] that, by applying maximum principles to Eq.(2.38), the following functional results:

$$\begin{aligned} K(\hat{\phi}) = \int_V \Big\{ & -\left\langle \underset{\sim}{\Omega}\cdot\nabla\hat{\phi}(\underset{\sim}{r},\underset{\sim}{\Omega}), G\left[\underset{\sim}{\Omega}\cdot\nabla\hat{\phi}(\underset{\sim}{r},\underset{\sim}{\Omega})\right]\right\rangle \\ & -\left\langle \hat{\phi}(\underset{\sim}{r},\underset{\sim}{\Omega}), C\hat{\phi}(\underset{\sim}{r},\underset{\sim}{\Omega})\right\rangle + 2\left\langle \hat{\phi}(\underset{\sim}{r},\underset{\sim}{\Omega}), S^{+}(\underset{\sim}{r},\underset{\sim}{\Omega})\right\rangle \\ & + 2\left\langle \underset{\sim}{\Omega}\cdot\nabla\hat{\phi}(\underset{\sim}{r},\underset{\sim}{\Omega}), GS^{-}(\underset{\sim}{r},\underset{\sim}{\Omega})\right\rangle \Big\}\, dV \\ & - \int_S \left\langle |\underset{\sim}{\Omega}\cdot\underset{\sim}{n}|, \hat{\phi}^{2}(\underset{\sim}{r},\underset{\sim}{\Omega})\right\rangle dS \end{aligned} \tag{2.43}$$

where,

dV, dS are the volume and surface differentials

$\underline{n}$ is the outward normal to the surfaces.

Consideration of the boundary conditions for bare surfaces and perfect reflectors has resulted in the surface integral term. When perfect reflectors are considered that term vanishes as it only applies here to bare surfaces. The present treatment can be generalised so that surface sources can be accounted for [3].

2.7 Explicit Expression for $K(\hat{\phi})$

$$
\begin{aligned}
K(\hat{\phi}) = \int_V \Bigg\{ & - \int_{4\pi} \underline{\Omega}.\nabla\hat{\phi}(\underline{r},\underline{\Omega}) \Bigg[\frac{1}{\Sigma_t(\underline{r})}\underline{\Omega}.\nabla\hat{\phi}(\underline{r},\underline{\Omega}) \\
& + \sum_{\ell\ \mathrm{odd}} \frac{\Sigma_{s_\ell}(\underline{r})}{\Sigma_t(\underline{r})(\Sigma_t(\underline{r})-\Sigma_{s_\ell}(\underline{r}))} \sum_{m=-\ell}^{\ell} Y_{\ell m}(\underline{\Omega}) \int_{4\pi} Y^*_{\ell m}(\underline{\Omega}')\underline{\Omega}'.\nabla\hat{\phi}(\underline{r},\underline{\Omega}')\,d\Omega' \Bigg] d\Omega \\
& - \int_{4\pi} \hat{\phi}(\underline{r},\underline{\Omega}) \Bigg[\Sigma_t(\underline{r})\hat{\phi}(\underline{r},\underline{\Omega}) - \sum_{\ell\ \mathrm{even}} \Sigma_{s_\ell}(\underline{r}) \sum_{m=-\ell}^{\ell} Y_{\ell m}(\underline{\Omega}) \int_{4\pi} Y^*_{\ell m}(\underline{\Omega}')\hat{\phi}(\underline{r},\underline{\Omega}')d\Omega' \Bigg] d\Omega \\
& + 2\int_{4\pi} \hat{\phi}(\underline{r},\underline{\Omega}) S^+(\underline{r},\underline{\Omega})\,d\Omega + 2\int_{4\pi} \underline{\Omega}.\nabla\hat{\phi}(\underline{r},\underline{\Omega}) \Bigg[\frac{1}{\Sigma_t(\underline{r})} S^-(\underline{r},\underline{\Omega}) \\
& + \sum_{\ell\ \mathrm{odd}} \frac{\Sigma_{s_\ell}(\underline{r})}{\Sigma_t(\underline{r})(\Sigma_t(\underline{r})-\Sigma_{s_\ell}(\underline{r}))} \sum_{m=-\ell}^{\ell} Y_{\ell m}(\underline{\Omega}) \int_{4\pi} Y^*_{\ell m}(\underline{\Omega}') S^-(\underline{r},\underline{\Omega}')\,d\Omega' \Bigg] d\Omega \Bigg\} dV \\
& - \int_S \int_{4\pi} |\underline{\Omega}.\underline{n}|\,\hat{\phi}^2(\underline{r},\underline{\Omega})\,d\Omega\,dS
\end{aligned}
\tag{2.44}
$$

Equ.(2.44) is the general expression of the functional. Again, simplifications are required. Two non-geometrical assumptions are made in this thesis:

(i) The source contribution is isotropic, i.e. the downscattering, fission and extraneous source contributions are equal in all directions. This leads to

$$S^{-}(\pm,\underline{\Omega}) = 0$$

and

$$S^{+}(\pm,\underline{\Omega}) = \frac{1}{4\pi} S(\pm)$$

The assumption is quite valid for the fission and extraneous source terms but the downscattering can be anisotropic to some degree. If anisotropic downscattering is significant, the above relation is not true.

(ii) The within-group scattering term is isotropic, i.e.

$$\Sigma_{s_\ell}(\pm) = 0 \qquad \text{for} \qquad \ell > 0$$

Applying condition (i) gives:

$$K(\hat{\phi}) = \int_V \Bigg\{ -\int_{4\pi} \underline{\Omega}\cdot\nabla\hat{\phi}(\underline{r},\underline{\Omega}) \Bigg[\frac{1}{\Sigma_t(\underline{r})}\,\underline{\Omega}\cdot\nabla\hat{\phi}(\underline{r},\underline{\Omega})$$

$$+ \sum_{\ell\ \text{odd}} \frac{\Sigma_{s_\ell}(\underline{r})}{\Sigma_t(\underline{r})\left(\Sigma_t(\underline{r})-\Sigma_{s_\ell}(\underline{r})\right)} \sum_{m=-\ell}^{\ell} Y_{\ell m}(\underline{\Omega}) \int_{4\pi} Y^*_{\ell m}(\underline{\Omega}')\,\underline{\Omega}\cdot\nabla\hat{\phi}(\underline{r},\underline{\Omega}')\,d\Omega' \Bigg] d\Omega$$

$$- \int_{4\pi} \hat{\phi}(\underline{r},\underline{\Omega}) \Bigg[\Sigma_t(\underline{r})\,\hat{\phi}(\underline{r},\underline{\Omega})$$

$$- \sum_{\ell\ \text{even}} \Sigma_{s_\ell}(\underline{r}) \sum_{m=-\ell}^{\ell} Y_{\ell m}(\underline{\Omega}) \int_{4\pi} Y^*_{\ell m}(\underline{\Omega}')\,\hat{\phi}(\underline{r},\underline{\Omega}')\,d\Omega' \Bigg] d\Omega$$

$$+ 2\int_{4\pi} \hat{\phi}(\underline{r},\underline{\Omega})\,S^+(\underline{r},\underline{\Omega})\,d\Omega \Bigg\}\, dV$$

$$- \int_S \int_{4\pi} \left|\underline{\Omega}\cdot\underline{n}\right| \hat{\phi}^2(\underline{r},\underline{\Omega})\, d\Omega\, dS \qquad (2.45)$$

Applying condition (ii) in addition gives

$$K(\hat{\phi}) = \int_V \left\{ \int_{4\pi} \frac{1}{\Sigma_t(\pm)} \left[\underline{\Omega} \cdot \nabla \hat{\phi}(\pm, \underline{\Omega}) \right]^2 d\Omega \right.$$

$$- \int_{4\pi} \hat{\phi}(\pm, \underline{\Omega}) \left[\Sigma_t(\pm) \hat{\phi}(\pm, \underline{\Omega}) \right.$$

$$\left. - \frac{1}{4\pi} \Sigma_{s_0}(\pm) Y_{00}(\underline{\Omega}) \int_{4\pi} Y_{00}^*(\underline{\Omega}') \hat{\phi}(\pm, \underline{\Omega}') d\Omega' \right] d\Omega$$

$$\left. + 2 \int_{4\pi} \hat{\phi}(\pm, \underline{\Omega}) S^+(\pm, \underline{\Omega}) d\Omega \right\} dV \qquad (2.46)$$

$$- \iint_S \int_{4\pi} \left| \underline{\Omega} \cdot \underline{n} \right| \hat{\phi}^2(\pm, \underline{\Omega}) d\Omega \, dS$$

As

$$Y_{00}(\underline{\Omega}) = Y_{00}^*(\underline{\Omega}) = \frac{1}{2\sqrt{\pi}}$$

(Refer Appendix A in which $\underline{\Omega}$ has been explicitly expressed as (μ,ω) defined in Fig.2.1) Eq.(2.46) is simplified to

$$K(\hat{\phi}) = \int_V \left\{ -\frac{1}{\Sigma_t(\underline{r})} \int_{4\pi} \left[\underline{\Omega}.\nabla \hat{\phi}(\underline{r},\underline{\Omega}) \right]^2 d\Omega \right.$$

$$- \int_{4\pi} \hat{\phi}(\underline{r},\underline{\Omega}) \left[\Sigma_t(\underline{r}) \hat{\phi}(\underline{r},\underline{\Omega}) - \frac{1}{4\pi} \Sigma_{s_0}(\underline{r}) \int_{4\pi} \hat{\phi}(\underline{r},\underline{\Omega}') d\Omega' \right] d\Omega$$

$$\left. + 2 \int_{4\pi} \hat{\phi}(\underline{r},\underline{\Omega}) S^+(\underline{r},\underline{\Omega}) \, d\Omega \right\} dV \qquad (2.47)$$

$$- \int_S \int_{4\pi} \left| \underline{\Omega}.\underline{n} \right| \hat{\phi}^2(\underline{r},\underline{\Omega}) \, d\Omega \, dS$$

Eq.(2.47) represents the K-Functional for a general geometry with isotropic source contributions and within-group scatter.

2.8 The $K(\hat{\phi})$ -Functional for Rectangular Geometry

The present work lays emphasis on obtaining solutions to problems in rectangular geometry. In particular only two-dimensional (or x-y) problems are solved. Therefore it is necessary to express Eq.(2.47) for such a system. Any differences in the $K(\hat{\phi})$ -Functional for different

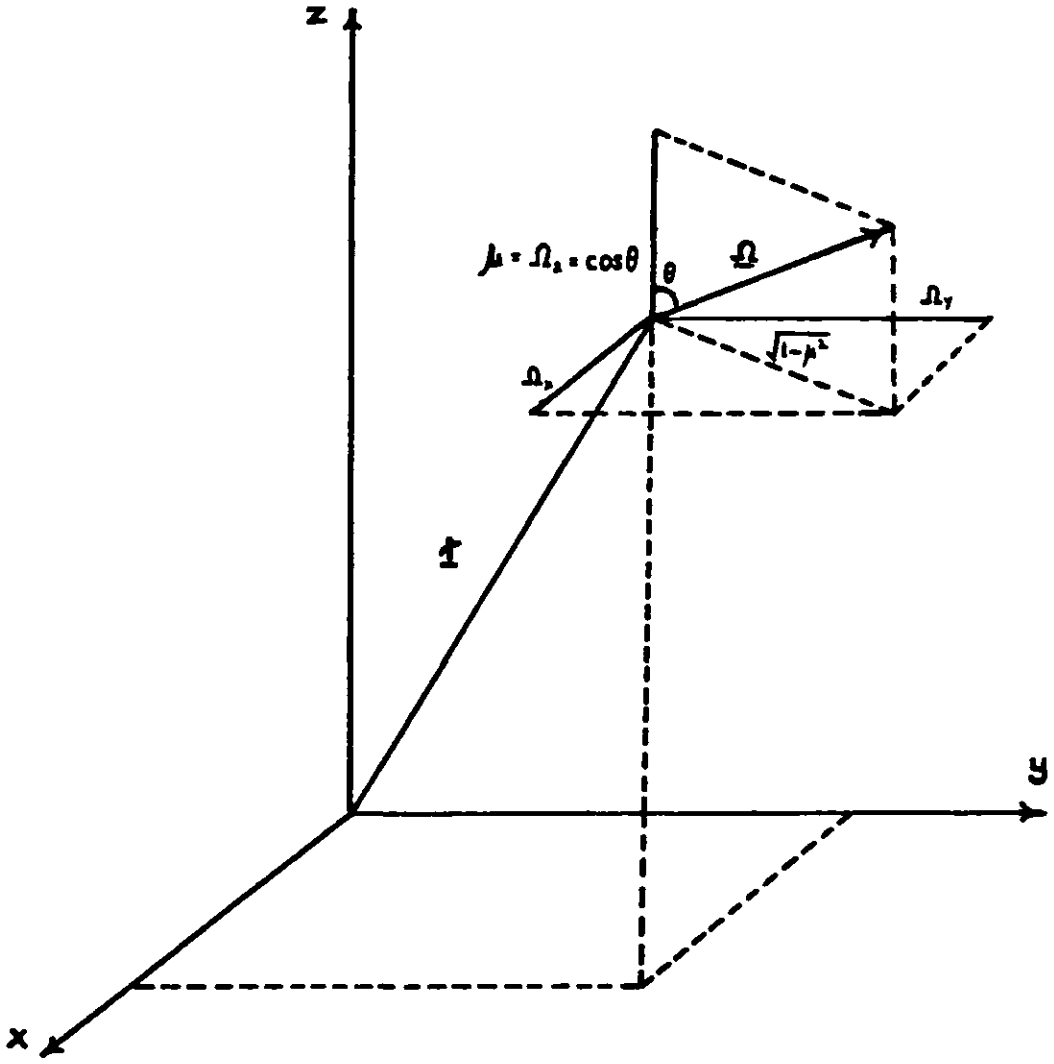

Fig.2.1 The Rectangular Coordinate System

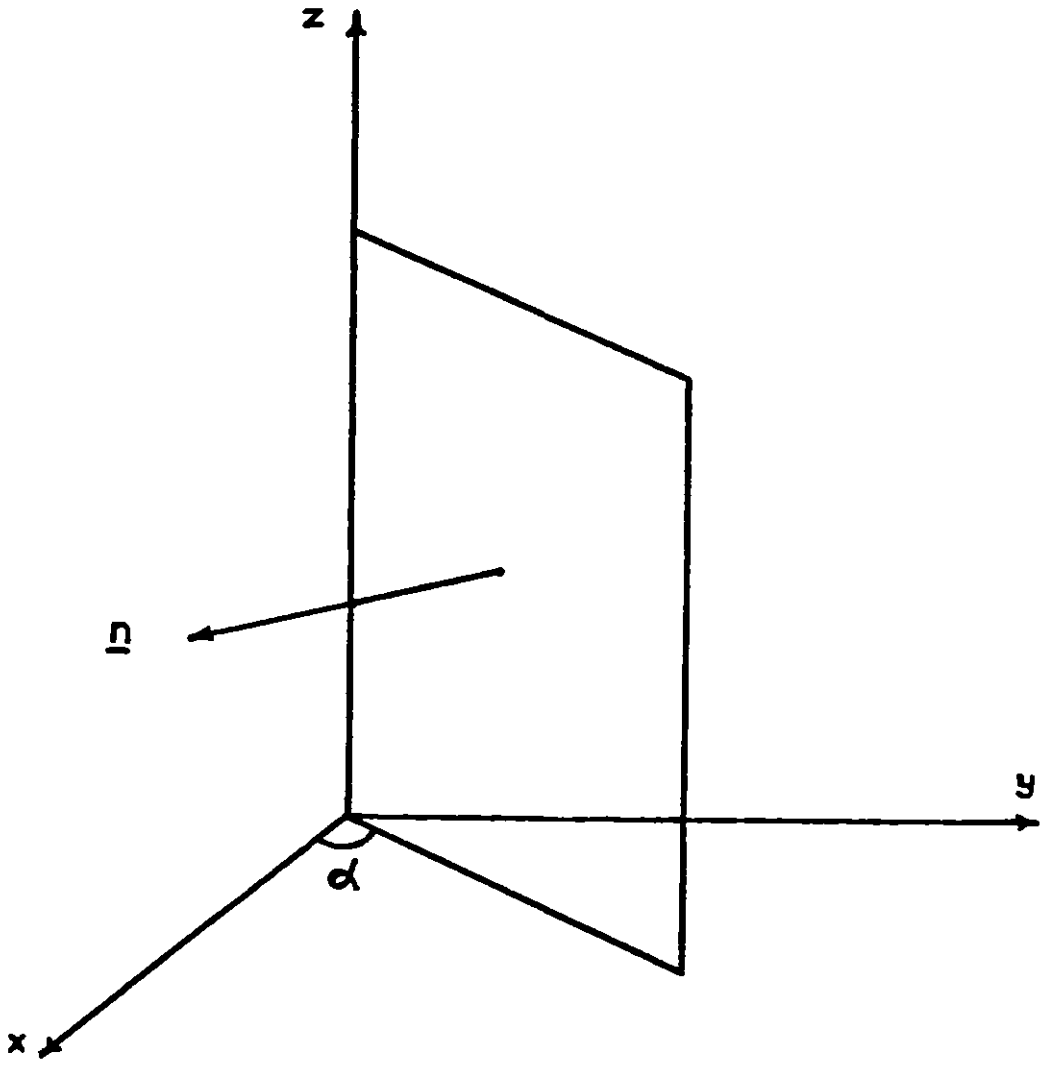

Fig.2.2 Inclination of a Bare Surface to the X-Axis

geometries will originate from the expressions for $\underline{\Omega}.\nabla$ and $|\underline{\Omega}.\underline{n}|$.

For x-y geometry, with reference to Fig.2.1 and 2.2, it is known that

$$\underline{\Omega}.\nabla = \sqrt{1-\mu^2}\left(\cos\omega\frac{\partial}{\partial x} + \sin\omega\frac{\partial}{\partial y}\right) \tag{2.48}$$

and

$$|\underline{\Omega}.\underline{n}| = \left|\sqrt{1-\mu^2}\,\sin(\alpha-\omega)\right| \tag{2.49}$$

in which α is the angle between the x-axis and the bare surface. To be more precise, α must be measured from the x-axis to the side of the bare surface where $\underline{n}$ is directed outwards.

In such a geometrical system

$$\int_{4\pi} d\Omega \equiv \int_{-1}^{1} d\mu \int_{0}^{2\pi} d\omega \tag{2.50}$$

as can be readily seen from Fig.2.1.

Using Eq.(2.48) to (2.50), it is seen that

$$K(\hat{\phi}) = \int_V \left\{ -\frac{1}{\Sigma_t(\pm)} \int_{-1}^{1} (1-\mu^2)\, d\mu \right.$$

$$\times \int_0^{2\pi} \left[\cos^2\omega \left(\frac{\partial\hat{\phi}}{\partial x}\right)^2 + \sin 2\omega \left(\frac{\partial\hat{\phi}}{\partial x}\right)\left(\frac{\partial\hat{\phi}}{\partial y}\right) + \sin^2\omega \left(\frac{\partial\hat{\phi}}{\partial y}\right)^2 \right] d\omega$$

$$- \int_{-1}^{1}\int_0^{2\pi} \hat{\phi}(\pm,\mu,\omega) \left[\Sigma_t(\pm)\, \hat{\phi}(\pm,\mu,\omega) \right.$$

$$\left. - \frac{1}{4\pi} \Sigma_{s_0}(\pm) \int_{-1}^{1}\int_0^{2\pi} \hat{\phi}(\pm,\mu',\omega')\, d\mu' d\omega' \right] d\mu\, d\omega$$

$$\left. + 2\int_{-1}^{1}\int_0^{2\pi} \hat{\phi}(\pm,\mu,\omega)\, S^+(\pm,\mu,\omega)\, d\mu\, d\omega \right\} dV$$

$$- \int_S \int_{-1}^{1}\int_0^{2\pi} \left| \sqrt{1-\mu^2}\, \sin(\alpha-\omega) \right| \hat{\phi}^2(\pm,\mu,\omega)\, d\mu\, d\omega\, dS \qquad (2.51)$$

Eq.(2.51) then represents the $K(\hat{\phi})$-Functional in x-y geometry for the specific case of isotropic scattering and isotropic source components. Before we conclude it is necessary to express the even parity source, in terms of the downscattering, fission and extraneous source components in a relevant form.

2.8.1 The even-parity source term

In the present discussion the group g subscript will be introduced for the quantities expressed in Eq.(2.9) and (2.10). Recalling the group g source expression from Eq.(2.8) and using the definition of the even-parity source term in Eq.(2.10) it can easily be shown that

$$S_g^+(\pm,\underline{\Omega}) = \sum_{g'=1}^{g-1} \int_{4\pi} \Sigma^+_{s_{g'g}}(\pm,\underline{\Omega}.\underline{\Omega}')\,\phi^+_{g'}(\pm,\underline{\Omega}')\,d\Omega'$$

$$+ \frac{\chi_g}{4\pi} \sum_{g'=1}^{G} \nu\Sigma_{f_{g'}}(\pm) \int_{4\pi} \phi^+_{g'}(\pm,\underline{\Omega}')\,d\Omega' \qquad (2.52)$$

$$+ Q^+_g(\pm,\underline{\Omega}) \qquad g=1,2\ldots G$$

in which the even-parity inter-group scattering cross-section and the even-parity extraneous source term are defined in a similar manner as in Eq.(2.9) to (2.11), i.e.

$$\Sigma^{+}_{s_{g'g}}(\pm,\underline{\Omega}.\underline{\Omega}') = \frac{1}{2}\left\{\Sigma_{s_{g'g}}(\pm,\underline{\Omega}.\underline{\Omega}') + \Sigma_{s_{g'g}}(\pm,-\underline{\Omega}.\underline{\Omega}')\right\} \tag{2.53}$$

$$Q^{+}_{g}(\pm,\underline{\Omega}) = \frac{1}{2}\left\{Q_{g}(\pm,\underline{\Omega}) + Q_{g}(\pm,-\underline{\Omega})\right\} \tag{2.54}$$

In a similar manner to the stages from Eq.(2.22) to (2.24),

$$\Sigma^{+}_{s_{g'g}}(\pm,\underline{\Omega}.\underline{\Omega}') = \sum_{\ell\ \text{even}} \Sigma_{s_{\ell g'g}}(\pm) \sum_{m=-\ell}^{\ell} Y_{\ell m}(\underline{\Omega}) Y^{*}_{\ell m}(\underline{\Omega}') \tag{2.55}$$

Therefore,

$$S^{+}_{g}(\pm,\underline{\Omega}) = \sum_{g'=1}^{g-1} \sum_{\ell\ \text{even}} \Sigma_{s_{\ell g'g}}(\pm) \sum_{m=-\ell}^{\ell} Y_{\ell m}(\underline{\Omega}) \int_{4\pi} Y^{*}_{\ell m}(\underline{\Omega}') \Phi^{+}_{g'}(\pm,\underline{\Omega}')\, d\Omega'$$

$$+ \frac{\chi_g}{4\pi} \sum_{g'=1}^{G} \omega \Sigma_{f_{g'}}(\pm) \int_{4\pi} \Phi^{+}_{g'}(\pm,\underline{\Omega}')\, d\Omega' \tag{2.56}$$

$$+ Q^{+}_{g}(\pm,\underline{\Omega}) \qquad g = 1,2 \ldots G$$

Since only isotropic scattering is considered then

$$\sum_{s_{\ell g'g}}(\pm) = 0$$

for ℓ greater than 0.

Besides extraneous sources, when they are considered, are always isotropic. Thus $Q_g^{+}(\pm,\underline{\Omega})$ can be replaced by $\frac{1}{4\pi} Q_g(\pm)$. Hence

$$S_g^{+}(\pm,\underline{\Omega}) = \frac{1}{4\pi}\sum_{g'=1}^{g-1} \Sigma_{s_{0g'g}}(\pm)\int_{4\pi} \phi_{g'}^{+}(\pm,\underline{\Omega}')\,d\Omega'$$

$$+\frac{\chi_g}{4\pi}\sum_{g'=1}^{G} \omega\Sigma_{f_{g'}}(\pm)\int_{4\pi} \phi_{g'}^{+}(\pm,\underline{\Omega}')\,d\Omega' \qquad (2.57)$$

$$+\frac{1}{4\pi} Q_g(\pm) \qquad g=1,2\ldots G$$

Although the angular integrals are not explicitly expressed in terms of μ and ω in Eq.(2.57), nevertheless Eq.(2.51) and (2.57) represent the $K(\hat{\phi})$-Functional and source term for x-y geometry but only for isotropic scattering.

2.8.2 The odd-parity source term

To conclude this chapter we indicate how anistropic sources can be accounted for through the odd-parity source

term. This term is also essential if one were to treat anisotropic scattering between groups as can be seen from Eq.(2.44). Hence

$$S_g^-(\underline{r},\underline{\Omega}) = \sum_{g'=1}^{g-1} \sum_{\ell\ \text{odd}} \Sigma_{s_{\ell g'g}}(\underline{r}) \sum_{m=-\ell}^{\ell} Y_{\ell m}(\underline{\Omega}) \int_{4\pi} Y_{\ell m}^*(\underline{\Omega}')\, \phi_{g'}^-(\underline{r},\underline{\Omega}')\, d\Omega'$$

$$+ Q_g^-(\underline{r},\underline{\Omega}) \qquad g=1,2\ldots G \qquad (2.58)$$

The order of anisotropic scattering to be treated will thus govern the limit to which summation over ℓ is to be taken in the above equation.

CHAPTER 3

CORFU

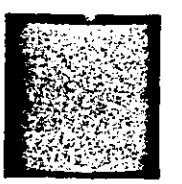

"One should never forget that the functions like all mathematical constructions, are only our own creations, and that when the definition with which one begins ceases to make sense, one should not ask: what is it, but what is it convenient to assume in order that it remain significant?"

Karl Friedrich Gauss

3.1 Introduction

CORFU, as the title of this chapter, is an acronym for Constants Of the Reduced-FUnctional. As was seen in the previous chapter, the $K(\hat{\phi})$ -Functional involves both a spatial and an angular integration of each of the terms. Naturally the order of the integration is arbitrary but in the present work angular integrations are performed first with the result that the $K(\hat{\phi})$ -Functional is reduced to one in which the integrand depends directly on space only. This functional is referred to as the Reduced-Functional and the results of the angular integrations being constants, hence the acronym CORFU. The constants are dependent on the geometry under consideration which happens to be rectangular in this case. The number of constants depend on the accuracy of the angular representation desired which is connected through the order of the trial function. This will be discussed in the next section but, suffice to say, a higher order trial function is used whenever a more accurate transport order solution is required. However, the number of constants will also be greater. The number of terms representing a trial function is equal to the square of its order and since the $K(\hat{\phi})$ -Functional is quadratic in $\hat{\phi}(\pm,\underline{\Omega})$, the number of constants associated with a trial function is equal to its order exponentiated to four. For example, a 1-moment trial function (the simplest) gives only one constant while a 2-moment trial function gives sixteen constants when angular integrations are performed. The term 'moment' describes the order of the trial function.

Spatial integrations are performed after the Reduced-Functional is obtained but this is the subject of the next chapter.

3.2 The Trial Function

The admissible function $\hat{\phi}(\pm,\Omega)$ chosen as an approximation for $\phi^{+}(\pm,\Omega)$ as shown in Section 2.6 can be represented as:

$$\hat{\phi}(\pm,\Omega)=\sum_{\ell=0}^{\infty}\sum_{m=-\ell}^{\ell}\Phi_{\ell m}(\pm)Y_{\ell m}(\Omega) \qquad (3.1)$$

in which the angular dependency has been represented by the set of Spherical Harmonics $Y_{\ell m}(\Omega)$ and whereby $\Phi_{\ell m}(\pm)$ are the moments of the spatial fluxes. The expression in Eq.(3.1) constitutes a trial function for the $K(\hat{\phi})$ Functional.

As seen from Appendix A, the Spherical Harmonics for x-y geometry are expressed in terms of μ and ω . Hence Eq.(3.1) needs to be manipulated into a form containing the shape functions and the angular components μ and ω.

From Appendix B, the trial function can therefore be written as

$$\hat{\phi}(\pm,\mu,\omega)=\sum_{\ell=0}^{M-1}\left\{\sqrt{\frac{4\ell+1}{4\pi}}\,P_{2\ell}^{o}(\mu)\phi_{(\ell^2+1)}(\pm)\right.$$

$$\left.+\sum_{m=1}^{L}\sqrt{\frac{4\ell+1}{4\pi}\cdot\frac{(2\ell+1)!}{(2\ell+2m)!}}\left[\phi_{(\ell^2+2m)}(\pm)\cos 2m\omega+\phi_{(\ell^2+2m+1)}(\pm)\sin 2m\omega\right]\right\} \qquad (3.2)$$

where

M = no. of moments in the trial function.

The manner in which the spatial fluxes have been subscripted ensures that they will be numbered in an ascending order commencing with unity.

In a similar manner the extraneous source is thereby expanded as in Eq.(3.2) but since only the isotropic case is considered,

$$Q_g(\pm,\mu,\omega) = \frac{1}{\sqrt{4\pi}} \tilde{Q}_g(\pm)$$

3.3 An Alternative Formulation

From Eq.(3.2) it can be seen that every term in the expression can be expressed in the following manner:

T_i = constant x Associated Legendre Polynomial
x Function of ω
x $\phi_{g_i}(\pm)$ (3.3)

where,

T_i = i^{th} term of the trial function

and the subscript g is now re-introduced for the spatial fluxes.

If we denote,

C_i = constant

$H_i(\mu)$ = Associated Legendre Polynomial

$G_i(\omega)$ = Function of ω

for the i^{th} term,

$$T_i = C_i H_i(\mu) G_i(\omega) \phi_{g_i}(\pm) \quad (3.4)$$

and

$$\hat{\phi}_g(\pm,\mu,\omega) = \sum_{i=1}^{M^2} T_i = \sum_{i=1}^{M^2} c_i H_i(\mu) G_i(\omega) \phi_{g_i}(\pm) \qquad (3.5)$$

Eq.(3.5) is a more compact expression for the trial function than Eq.(3.2) and therefore easier to handle when the trial function is substituted into the $K(\hat{\phi})$-Functional.

The discussion in the next few sections will deal wth the substitution of the trial function in the $K(\hat{\phi})$-Functional. The leakage term is the first to be considered. This will be followed by the removal, source and bare surface terms.

3.4 The Reduced Form of the Leakage Term

If L denotes the leakage term, then from Eq.(2.51) it is readily seen that

$$L = \int_V -\frac{1}{\Sigma_{t_g}(\pm)} \int_{-1}^{1} (1-\mu^2)\, d\mu \qquad (3.6)$$

$$\times \int_0^{2\pi} \left[\cos^2\omega \left(\frac{\partial \phi_g}{\partial x}\right)^2 + \sin 2\omega \left(\frac{\partial \phi_g}{\partial x}\right)\left(\frac{\partial \phi_g}{\partial y}\right) + \sin^2\omega \left(\frac{\partial \phi_g}{\partial y}\right)^2\right] d\omega\, dV$$

From Eq.(3.5) we have

$$\left(\frac{\partial \hat{\phi}_g}{\partial x}\right)^2 = \sum_{i=1}^{M^2} \sum_{j=1}^{M^2} c_i c_j H_i H_j G_i G_j \left(\frac{\partial \phi_{g_i}}{\partial x}\right)\left(\frac{\partial \phi_{g_i}}{\partial x}\right) \qquad (3.7)$$

$$\left(\frac{\partial \hat{\phi}_g}{\partial x}\right)\left(\frac{\partial \hat{\phi}_g}{\partial y}\right) = \sum_{i=1}^{M^2}\sum_{j=1}^{M^2} c_i c_j H_i H_j G_i G_j \left(\frac{\partial \phi_{gi}}{\partial x}\right)\left(\frac{\partial \phi_{gj}}{\partial y}\right) \qquad (3.8)$$

$$\left(\frac{\partial \hat{\phi}_g}{\partial y}\right)^2 = \sum_{i=1}^{M^2}\sum_{j=1}^{M^2} c_i c_j H_i H_j G_i G_j \left(\frac{\partial \phi_{gi}}{\partial y}\right)\left(\frac{\partial \phi_{gj}}{\partial y}\right) \qquad (3.9)$$

where,

the dependence on μ, ω and $\pm$ have been dropped from the notation for brevity.

Substituting (3.7) to (3.9) in (3.6),

$$L = \int_V -\frac{1}{\Sigma_{tg}(\pm)} \sum_{i=1}^{M^2}\sum_{j=1}^{M^2} c_i c_j \int_{-1}^{1} (1-\mu^2) H_i H_j \, d\mu$$

$$\times \left[\int_0^{2\pi} \cos^2\omega \, G_i G_j \, d\omega \left(\frac{\partial \phi_{gi}}{\partial x}\right)\left(\frac{\partial \phi_{gj}}{\partial y}\right) \right. \qquad (3.10)$$

$$+ \int_0^{2\pi} \sin 2\omega \, G_i G_j \, d\omega \left(\frac{\partial \phi_{gi}}{\partial x}\right)\left(\frac{\partial \phi_{gj}}{\partial y}\right)$$

$$\left. + \int_0^{2\pi} \sin^2\omega \, G_i G_j \, d\omega \left(\frac{\partial \phi_{gi}}{\partial y}\right)\left(\frac{\partial \phi_{gj}}{\partial y}\right) \right] dV$$

If,

$$I_{1ij} = \int_{-1}^{1} (1-\mu^2)\, H_i H_j \, d\mu \tag{3.11}$$

$$J_{1ij} = \int_{0}^{2\pi} \cos^2\omega \, G_i G_j \, d\omega \tag{3.12}$$

$$J_{2ij} = \int_{0}^{2\pi} \sin 2\omega \, G_i G_j \, d\omega \tag{3.13}$$

$$J_{3ij} = \int_{0}^{2\pi} \sin^2\omega \, G_i G_j \, d\omega \tag{3.14}$$

Therefore,

$$L = \int_V -\frac{1}{\Sigma_{t_g}(\pm)} \sum_{i=1}^{M^2} \sum_{j=1}^{M^2} c_i c_j I_{1ij}$$

$$X\left[J_{1ij}\left(\frac{\partial \phi_{gi}}{\partial x}\right)\left(\frac{\partial \phi_{gj}}{\partial x}\right) + J_{2ij}\left(\frac{\partial \phi_{gi}}{\partial x}\right)\left(\frac{\partial \phi_{gj}}{\partial y}\right) + J_{3ij}\left(\frac{\partial \phi_{gi}}{\partial y}\right)\left(\frac{\partial \phi_{gj}}{\partial y}\right)\right] dV \tag{3.15}$$

Finally, let

$$\left.\begin{aligned} E_{1ij} &= c_i c_j I_{1ij} J_{1ij} \\ E_{2ij} &= c_i c_j I_{1ij} J_{2ij} \\ E_{3ij} &= c_i c_j I_{1ij} J_{3ij} \end{aligned}\right\} \qquad (3.16)$$

whereby

$$L = \int_V -\frac{1}{\Sigma_{t_g}(\pm)} \sum_{i=1}^{M^2} \sum_{j=1}^{M^2} \left[E_{1ij} \left(\frac{\partial \phi_{gi}}{\partial x}\right)\left(\frac{\partial \phi_{gj}}{\partial x}\right) \right.$$

$$\left. + E_{2ij} \left(\frac{\partial \phi_{gi}}{\partial x}\right)\left(\frac{\partial \phi_{gj}}{\partial y}\right) + E_{3ij} \left(\frac{\partial \phi_{gi}}{\partial y}\right)\left(\frac{\partial \phi_{gj}}{\partial y}\right) \right] dV \qquad (3.17)$$

Hence, the quantities E_{1ij} , E_{2ij} , E_{3ij} are the constants of the Reduced Functional for the leakage term.

3.5 The Reduced Form of the Removal Term

Let R represent the removal term which from Eq.(2.51) is shown to be

$$R = -\int_V \int_{-1}^{1} \int_0^{2\pi} \hat{\phi}_g(\pm,\mu,\omega) \left[\Sigma_{t_g}(\pm)\, \hat{\phi}_g(\pm,\mu,\omega) \right.$$

$$\left. - \frac{\Sigma_{s_{ogg}}(\pm)}{4\pi} \int_{-1}^{1} \int_0^{2\pi} \hat{\phi}_g(\pm,\mu',\omega')\, d\mu'\, d\omega' \right] d\mu\, d\omega\, dV \qquad (3.18)$$

Therefore,

$$R = -\int_V \int_{-1}^{1} \int_0^{2\pi} \Big[\Sigma_{t_g}(\pm) \sum_{i=1}^{M^2} \sum_{j=1}^{M^2} c_i c_j H_i H_j G_i G_j \phi_{g_i} \phi_{g_j}$$

$$- \frac{\Sigma_{s_{0gg}}}{4\pi} \sum_{i=1}^{M^2} c_i H_i G_i \phi_{g_i} \sum_{j=1}^{M^2} c_j \phi_{g_j} \int_{-1}^{1} H_j \, d\mu' \int_0^{2\pi} G_j \, d\omega' \Big] d\mu \, d\omega \, dV \qquad (3.19)$$

Finally,

$$R = -\int_V \Big[\Sigma_{t_g}(\pm) \sum_{i=1}^{M^2} \sum_{j=1}^{M^2} c_i c_j \phi_{g_i} \phi_{g_j} \int_{-1}^{1} H_i H_j \, d\mu \int_0^{2\pi} G_i G_j \, d\omega$$

$$- \frac{\Sigma_{s_{0gg}}}{4\pi} \sum_{i=1}^{M^2} c_i \phi_{g_i} \int_{-1}^{1} H_i \, d\mu \int_0^{2\pi} G_i \, d\omega \sum_{j=1}^{M^2} c_j \phi_{g_j} \int_{-1}^{1} H_j \, d\mu' \int_0^{2\pi} G_j \, d\omega' \Big] dV \qquad (3.20)$$

As before,

$$I_{2ij} = \int_{-1}^{1} H_i H_j \, d\mu \qquad (3.21)$$

$$I_{3i} = \int_{-1}^{1} H_i \, d\mu \qquad (3.22)$$

$$I_{4ij} = \int_0^{2\pi} G_i G_j \, d\omega \qquad (3.23)$$

$$I_{5i} = \int_0^{2\pi} G_i \, d\omega \qquad (3.24)$$

Therefore,

$$R = -\int_V \Big[\Sigma_{t_g}(\pm) \sum_{i=1}^{M^2} \sum_{j=1}^{M^2} c_i c_j I_{2ij} J_{4ij} \phi_{gi} \phi_{gj} - \frac{\Sigma_{s_{ogg}}(\pm)}{4\pi} \sum_{i=1}^{M^2} c_i I_{3i} J_{5i} \phi_{gi} \sum_{j=1}^{M^2} c_j I_{3j} J_{5j} \phi_{gj} \Big] dV \quad (3.25)$$

Finally, let

$$F_{ij} = c_i c_j I_{2ij} J_{4ij} \quad (3.26)$$

$$D_i = c_i I_{3i} J_{5i} \quad (3.27)$$

and so

$$R = -\int \Big[\Sigma_{t_g}(\pm) \sum_{i=1}^{M^2} \sum_{j=1}^{M^2} F_{ij} \phi_{gi} \phi_{gj} - \frac{\Sigma_{s_{ogg}}}{4\pi} \sum_{i=1}^{M^2} D_i \phi_{gi} \sum_{j=1}^{M^2} D_j \phi_{gj} \Big] dV \quad (3.28)$$

The quantities F_{ij} , D_i are therefore the constants of the removal term in the reduced functional.

3.6 The Reduced Form of the Source Term

This is represented as

$$S = 2 \int_V \int_{-1}^{1} \int_0^{2\pi} \hat{\phi}_g(\pm,\mu,\omega) S_g^+(\pm,\mu,\omega) d\mu d\omega dV \quad (3.29)$$

Substituting for $S_g^+(\pm,\mu,\omega)$ from Eq.(2.64)

$$S = 2\int_V\int_{-1}^{1}\int_0^{2\pi} \hat{\phi}_g(\pm,\mu,\omega)$$

$$\times\left[\frac{1}{4\pi}\sum_{g'=1}^{g-1}\Sigma_{s_{0g'g}}(\pm)\int_{-1}^{1}\int_0^{2\pi}\hat{\phi}_{g'}(\pm,\mu',\omega')\,d\mu'd\omega'\right.$$

$$\left.+\frac{\chi_g}{4\pi}\sum_{g'=1}^{G}\nu\Sigma_{f_{g'}}(\pm)\int_{-1}^{1}\int_0^{2\pi}\hat{\phi}_{g'}(\pm,\mu',\omega')\,d\mu'd\omega'\right. \qquad (3.30)$$

$$\left.+\frac{1}{\sqrt{4\pi}}\tilde{Q}_g(\pm)\right.$$

As in the previous sections, upon substituting for the flux,

$$S = 2\int_V\left[\frac{1}{4\pi}\sum_{g'=1}^{g-1}\Sigma_{s_{0g'g}}(\pm)\sum_{i=1}^{M^2}c_i\phi_{g_i}\int_{-1}^{1}H_i\,d\mu\int_0^{2\pi}G_i\,d\omega\right.$$

$$\times\sum_{j=1}^{M^2}c_j\phi_{g_j}\int_{-1}^{1}H_j\,d\mu'\int_0^{2\pi}G_j\,d\omega$$

$$+\frac{\chi_g}{4\pi}\sum_{g'=1}^{G}\nu\Sigma_{f_{g'}}(\pm)\sum_{i=1}^{M^2}c_i\phi_{g_i}\int_{-1}^{1}H_i\,d\mu\int_0^{2\pi}G_i\,d\omega\sum_{j=1}^{M^2}c_j\phi_{g_j}\int_{-1}^{1}H_j\,d\mu'\int_0^{2\pi}G_j\,d\omega'$$

$$\left.+\frac{1}{\sqrt{4\pi}}\tilde{Q}_g(\pm)\sum_{i=1}^{M^2}c_i\phi_{g_i}\int_{-1}^{1}H_i\,d\mu\int_0^{2\pi}G_i\,d\omega\right]dV \qquad (3.31)$$

Finally via Eq.(3.22), (3.24) and (3.27),

$$S = 2\int_V \Bigg[\frac{1}{4\pi}\sum_{g'=1}^{g-1}\Sigma_{s_{0g'g}}(\pm)\sum_{i=1}^{M^2} D_i\phi_{gi}\sum_{j=1}^{M^2} D_j\phi_{gj} + \frac{\chi_g}{4\pi}\sum_{g'=1}^{G}\nu\Sigma_{f_{g'}}(\pm)\sum_{i=1}^{M^2} D_i\phi_{gi}\sum_{j=1}^{M^2} D_j\phi_{gj} + \frac{1}{\sqrt{4\pi}}\tilde{Q}_g(\pm)\sum_{i=1}^{M^2} D_i\phi_{gi}\Bigg] dV \qquad (3.32)$$

3.7 The Reduced Form of the Bare Surface Term

Let this be represented as

$$P = -\int_S\int_{-1}^{1}\int_0^{2\pi}\left|\sqrt{1-\mu^2}\sin(\alpha-\omega)\right|\hat{\phi}_g^2(\pm,\mu,\omega)\,d\mu\,d\omega\,dS \qquad (3.33)$$

Substituting for $\hat{\phi}_g$,

$$P = -\int_S\sum_{i=1}^{M^2}\sum_{j=1}^{M^2} C_iC_j\phi_{gi}\phi_{gj}\int_{-1}^{1}\left|\sqrt{1-\mu^2}\right|H_iH_j\,d\mu \qquad (3.34)$$

$$\times\int_0^{2\pi}\left|\sin(\alpha-\omega)\right|G_iG_j\,d\omega$$

Let,

$$I_{4ij} = \int_{-1}^{1} \left|\sqrt{1-\mu^2}\right| H_i H_j \, d\mu \tag{3.35}$$

$$J_{6ij} = \int_{0}^{2\pi} \left|\sin(\alpha-\omega)\right| G_i G_j \, d\omega \tag{3.36}$$

$$\therefore P = -\int_S \sum_{i=1}^{M^2} \sum_{j=1}^{M^2} c_i c_j I_{4ij} J_{6ij} \phi_{gi} \phi_{gj} \, dS \tag{3.37}$$

And, if

$$B_{ij} = c_i c_j I_{4ij} J_{6ij} \tag{3.38}$$

$$P = -\int_S \sum_{i=1}^{M^2} \sum_{j=1}^{M^2} B_{ij} \phi_{gi} \phi_{gj} \, dS \tag{3.39}$$

3.8 <u>The Reduced Functonal</u>

Finally, since

$$K(\hat{\phi}_g) = L + R + S + P$$

therefore,

$$\tilde{K}(\hat{\phi}_g) = \int_V \Bigg\{ -\frac{1}{\Sigma_{t_g}(\pm)} \sum_{i=1}^{M^2} \sum_{j=1}^{M^2} \Bigg[E_{1ij} \left(\frac{\partial \phi_{gi}}{\partial x}\right)\left(\frac{\partial \phi_{gj}}{\partial y}\right) + E_{2ij} \left(\frac{\partial \phi_{gi}}{\partial x}\right)\left(\frac{\partial \phi_{gj}}{\partial y}\right) + E_{3ij} \left(\frac{\partial \phi_{gi}}{\partial y}\right)\left(\frac{\partial \phi_{gj}}{\partial y}\right) \Bigg]$$

$$- \Bigg[\Sigma_{t_g}(\pm) \sum_{i=1}^{M^2} \sum_{j=1}^{M^2} F_{ij} \phi_{gi} \phi_{gj} - \frac{\Sigma_{s_{0gg}}}{4\pi} \sum_{i=1}^{M^2} D_i \phi_{gi} \sum_{j=1}^{M^2} D_j \phi_{gj} \Bigg]$$

$$+ 2 \Bigg[\frac{1}{4\pi} \sum_{g'=1}^{g-1} \Sigma_{s_{0g'g}}(\pm) \sum_{i=1}^{M^2} D_i \phi_{gi} \sum_{j=1}^{M^2} D_j \phi_{gj}$$

$$+ \frac{\chi_g}{4\pi} \sum_{g'=1}^{G} \omega \Sigma_{f_{g'}}(\pm) \sum_{i=1}^{M^2} D_i \phi_{gi} \sum_{j=1}^{M^2} D_j \phi_{gj} \qquad (3.40)$$

$$+ \frac{1}{\sqrt{4\pi}} \tilde{Q}_g(\pm) \sum_{i=1}^{M^2} D_i \phi_{gi} \Bigg] \Bigg\} \, dV$$

$$- \int_S \sum_{i=1}^{M^2} \sum_{j=1}^{M^2} B_{ij} \phi_{gi} \phi_{gj} \, dS$$

by substituting from (3.17), (3.28), (3.32) and (3.39)

Eq.(3.40) is the general form of the Reduced Functional for x-y geometry for a trial function of moment M. As can be seen by the double summation and the limit of in each term, the number of constants increases as M^4

for those with double subscripts and as M^2 for those with single subscripts. Clearly then there will always be a practical limit to the number of moments chosen for the trial function.

Tables 3.1 to 3.3 summarises the expressions for the constants as obtained in the last few sections.

TABLE 3.1

EXPRESSIONS FOR THE CONSTANTS OF THE REDUCED-FUNCTIONAL

Term	Expression
E_{1ij}	$c_i c_j I_{1ij} J_{1ij}$
E_{2ij}	$c_i c_j I_{1ij} J_{2ij}$
E_{3ij}	$c_i c_j I_{1ij} J_{3ij}$
F_{ij}	$c_i c_j I_{2ij} J_{4ij}$
B_{ij}	$c_i c_j I_{4ij} J_{6ij}$
D_i	$c_i I_{3i} J_{5i}$

TABLE 3.2

THE INTEGRALS OVER μ

Term	Expression
I_{1ij}	$\int_{-1}^{1}(1-\mu^2)H_iH_j\,d\mu$
I_{2ij}	$\int_{-1}^{1}H_iH_j\,d\mu$
I_{3i}	$\int_{-1}^{1}H_i\,d\mu$
I_{4ij}	$\int_{-1}^{1}\lvert\sqrt{1-\mu^2}\rvert H_iH_j\,d\mu$

TABLE 3.3

THE INTEGRALS OVER ω

Term	Expression
J_{1ij}	$\int_{0}^{2\pi}\cos^2\omega\,G_iG_j\,d\omega$
J_{2ij}	$\int_{0}^{2\pi}\sin 2\omega\,G_iG_j\,d\omega$
J_{3ij}	$\int_{0}^{2\pi}\sin^2\omega\,G_iG_j\,d\omega$
J_{4ij}	$\int_{0}^{2\pi}G_iG_j\,d\omega$
J_{5i}	$\int_{0}^{2\pi}G_i\,d\omega$
J_{6ij}	$\int_{0}^{2\pi}\lvert\sin(\alpha-\omega)\rvert G_iG_j\,d\omega$

3.9 Implementation

A computer package has been written to evaluate the angular constants for a trial function of any order. In practice there will always be a limit to the order of the trial function employed because of problems related to core storage, processing time and because of the necessary compromise between accuracy and cost. (This argument assumes that enough groups are chosen for the problem and that neutronic data are accurate.)

The CORFU package can be extended to include evaluation of angular integrals for other types of geometries and also to evaluate those constants that will arise when anisotropic scattering is considered (and in this case an option for the level of scattering desired).

3.9.1 Solution of the Integrals over μ

This constitutes the solutions of I_1 to I_4 as tabulated in Table 3.2. In CORFU the associated Legendre Polynomials are systematically generated. The number of terms constructed is, of course, dependent on the order of the trial function.

The integrals are solved by using Gauss-Legendre Quadrature Sets [19]. In particular the NAG subroutines at Imperial College (and also widely available elsewhere) were relied upon. The specific algorithm employed allows one to use up to 64 quadrature points. Naturally, fewer points were required when evaluating the integrals which contain the lower order Legendre Polynomials.

Analytical integration was not used here because numerical integrations for polynomials using the Gauss-Legendre Quadrature Sets are accurate [19] and can be easily performed on a computer. Of course the other reason for using numerical integration is because the Legendre Polynomials associated with any moment trial function are systematically generated and therefore numerically integrated.

3.9.2 Solution of the integrals over ω

The integrals over ω are as shown in Table 3.3. However these integrals involve trigonometric functions and it was trivial to solve them analytically, thereby avoiding the use of Gauss-Legendre Quadrature Sets, as was performed for the integrals over μ . The results of these integrations are summarised in Appendix C. These results are also systematically produced by the CORFU module for trial functions of any order.

3.10 Discussion

With reference to Table 3.1, all those terms with double indices can be regarded as elements of $(M^2 \times M^2)$ matrices where M is the order of the chosen trial function. However, these constants are symmetric. For example E_{ij} is equal to E_{ji} . Therefore when high order trial functions are used, this fact can be utilised to minimise the calculations and subsequent storage of the constants.

The constants E_{1ij} and E_{3ij} are equal in magnitude when the subscripts correspond but some of them differ only in the signs.

Although the constants F_{ij} are considered symmetric, due to orthogonality of spherical harmonics in actuality

$$F_{ij} = 0 \qquad \text{if} \quad i \neq j$$

This fact is utilised in storage and computation considerations when the global matrix is assembled.

The values of B_{ij} are dependent upon α, i.e. the angle between a bare surface and the x-axis as shown in Fig.2.2 In x-y problems the values of α are naturally 0, $\pi/2, \pi, 3\pi/2$ if only horizontal and vertical sides are considered. When these values of α are considered it was found that the values of B_{ij} are similar for $\alpha=0$ and $\alpha=\pi$ on the one hand and for $\alpha=\pi/2$ and $\alpha=3\pi/2$ on the other because

$$|\sin(\alpha \pm \pi - \omega)| = |-\sin(\alpha-\omega)| = |\sin(\alpha-\omega)|$$

Even then the only difference in the two sets lie in differences in signs while the magnitudes remain the same.

As for D_i, the only set of constants with a singular subscript, it was found that

$$D_i = \sqrt{4\pi} \qquad \text{for} \quad i = 1$$

$$= 0 \qquad \text{for} \quad i > 1$$

Again this result will be utilised in reducing the complexity of Eq.(3.40).

Hence with the observed results from CORFU Eq.(3.40) is now simplified as

$$\tilde{K}(\hat{\phi}_g) = \int_V \Bigg\{ -\frac{1}{\Sigma_{t_g}(\pm)} \sum_{i=1}^{M^2} \sum_{j=1}^{M^2} \Bigg[E_{1ij} \left(\frac{\partial \phi_{g_i}}{\partial x}\right)\left(\frac{\partial \phi_{g_j}}{\partial x}\right) + E_{2ij} \left(\frac{\partial \phi_{g_i}}{\partial x}\right)\left(\frac{\partial \phi_{g_j}}{\partial y}\right) + E_{3ij} \left(\frac{\partial \phi_{g_i}}{\partial}\right)\left(\frac{\partial \phi_{g_j}}{\partial y}\right) - \Big[\Sigma_{t_g}(\pm) \sum_{i=1}^{M^2} F_{ii} \phi_{g_i}^2 - \Sigma_{s_{0gg}}(\pm) \phi_{g_i}^2 \Big] + 2 \Big[\sum_{g'=1}^{g-1} \Sigma_{s_{0g'g}}(\pm) \phi_{g_1}^2 + \chi_g \sum_{g'=1}^{G} \nu \Sigma_{f_{g'}}(\pm) \phi_{g_1}^2 + \tilde{Q}_g(\pm) \phi_{g_1} \Big] \Bigg\} dV - \int_S \sum_{i=1}^{M^2} \sum_{j=1}^{M^2} B_{ij} \phi_{g_i} \phi_{g_j} \, dS \qquad (3.41)$$

To conclude this chapter, the constants for a 3-moment trial function are displayed in Tables 3.4 to 3.6 to emphasise the points discussed above. Table 3.4 contains the constants for the three components of the leakage term. The results for F_{ij} and D_i have been grouped together in Table 3.5. Finally Table 3.6 display the two sets of results for the bare surfaces determined by the value of α.

TABLE 3.4

THE CONSTANTS OF THE LEAKAGE TERM

VALUES OF E1

1	3.33333E-01	-1.49071E-01	1.82574E-01	0	0
2	-1.49071E-01	2.38095E-01	-1.16642E-01	0	-1.27775E-01
3	1.82574E-01	-1.16642E-01	2.14286E-01	0	2.60820E-02
4	-4.12393E-02	0	1.09109E-01	2.14286E-01	0
5	0	-4.12393E-02	0	1.09109E-01	2.46753E-01
6	-1.23206E-01	-1.27775E-01	2.60820E-02	0	-1.23206E-01
7	0	1.01015E-01	-4.12393E-02	0	0
8	1.49351E-01	0	-3.43604E-02	-4.12393E-02	0
9	0	1.49351E-01	0	-3.43604E-02	0
	0	0	1.09109E-01	0	0
	-3.43604E-02	0	2.27273E-01	1.09109E-01	0
	0	-3.43604E-02	0	2.27273E-01	

VALUES OF E2

1	0	0	0	3.65148E-01	0
2	0	0	0	0	0
3	0	2.02031E-01	0	-2.33285E-01	0
4	0	0	0	0	0
5	3.65148E-01	-2.33285E-01	0	2.18218E-01	5.21641E-02
6	0	0	-2.18218E-01	0	0
7	0	-2.46411E-01	0	5.21641E-02	0
8	0	0	0	0	0
9	0	2.02031E-01	0	-6.87208E-02	-2.46411E-01
	0	0	6.87208E-02	0	0
	0	6.87208E-02	0	-2.18218E-01	0
	-6.87208E-02	0	2.18218E-01	0	0

VALUES OF E3

1	3.33333E-01	-1.49071E-01	-1.82574E-01	0	0
2	-1.49071E-01	2.38095E-01	1.16642E-01	0	-1.27775E-01
3	-1.82574E-01	1.16642E-01	2.14286E-01	0	-2.60820E-02
4	-4.12393E-02	0	-1.09109E-01	2.14286E-01	0
5	0	-4.12393E-02	0	-1.09109E-01	2.46753E-01
6	1.23206E-01	-1.27775E-01	-2.60820E-02	0	1.23206E-01
7	0	-1.01015E-01	-4.12393E-02	0	0
8	1.49351E-01	0	3.43604E-02	-4.12393E-02	0
9	0	1.49351E-01	0	3.43604E-02	0
	0	0	-1.09109E-01	0	0
	3.43604E-02	0	2.27273E-01	-1.09109E-01	0
	0	3.43604E-02	0	2.27273E-01	

TABLE 3.5

THE CONSTANTS OF THE REMOVAL AND SOURCE TERMS

VALUES OF F

1	1.000000E+00	0	0	0	0
2	0	1.000000E+00	0	0	0
3	0	0	5.000000E-01	0	0
4	0	0	0	5.000000E-01	0
5	0	0	0	0	1.000000E+00
6	0	0	0	0	0
7	5.000000E-01	0	0	0	0
8	0	5.000000E-01	0	0	0
9	0	0	5.000000E-01	0	0
	0	0	0	5.000000E-01	

VALUES OF D

3.544491E+00

TABLE 3.6

THE CONSTANTS OF THE BARE SURFACE TERM FOR HORIZONTAL AND VERTICAL INCLINATIONS OF THE BARE SURFACE WITH THE X-AXIS

VALUES OF B (ALPHA=0 OR π)

1	5.00021E-01	-1.39708E-01	-1.71163E-01	0	-2.33736E-02
	-2.47050E-02	0	-3.26820E-02	0	
2	-1.39708E-01	3.90730E-01	9.56833E-02	0	-1.40702E-01
	-1.07032E-01	0	2.28373E-02	0	
3	-1.71163E-01	9.56833E-02	2.73438E-01	0	-1.20347E-02
	-2.96005E-02	0	-1.06285E-01	0	
4	0	0	0	3.12500E-01	0
	0	-3.38291E-02	0	-8.95034E-02	
5	-2.33736E-02	-1.40702E-01	-1.20347E-02	0	3.99551E-01
	1.19860E-01	0	-6.89387E-03	0	
6	-2.47050E-02	-1.07032E-01	-2.96005E-02	0	1.19860E-01
	2.23023E-01	0	2.76137E-02	0	
7	0	0	0	-3.38291E-02	0
	0	2.54883E-01	0	2.32537E-02	
8	-3.26820E-02	2.28373E-02	-1.06285E-01	0	-6.89387E-03
	2.76137E-02	0	2.98004E-01	0	
9	0	0	0	-8.95034E-02	0
	0	2.32537E-02	0	3.07617E-01	

VALUES OF B (ALPHA= $\pi/2$ OR $3\pi/2$)

1	5.00021E-01	-1.39708E-01	1.71163E-01	0	-2.33736E-02
	2.47050E-02	0	-3.26820E-02	0	
2	-1.39708E-01	3.90730E-01	-9.56833E-02	0	-1.40702E-01
	1.07032E-01	0	2.28373E-02	0	
3	1.71163E-01	-9.56833E-02	2.73438E-01	0	1.20347E-02
	-2.96005E-02	0	1.06285E-01	0	
4	0	0	0	3.12500E-01	0
	0	-3.38291E-02	0	8.95034E-02	
5	-2.33736E-02	-1.40702E-01	1.20347E-02	0	3.99551E-01
	-1.19860E-01	0	-6.89387E-03	0	
6	2.47050E-02	1.07032E-01	-2.96005E-02	0	-1.19860E-01
	2.23023E-01	0	-2.76137E-02	0	
7	0	0	0	-3.38291E-02	0
	0	2.54883E-01	0	-2.32537E-02	
8	-3.26820E-02	2.28373E-02	1.06285E-01	0	-6.89387E-03
	-2.76137E-02	0	2.98004E-01	0	
9	0	0	0	8.95034E-02	0
	0	-2.32537E-02	0	3.07617E-01	

CHAPTER 4

ELEMENTS, BANDS AND SOLVERS

"Finite elements ceased to burgeon long ago, and the first harvest is in. Most consumers are satisfied. Those suppliers who planted their programs early are jubilant. It is a growth industry....."

Irons and Ahmad [45]

4.1 Introduction

In the previous chapter the Reduced-Functional, $\tilde{K}(\hat{\phi}_3)$, was obtained together with the constants resulting from the angular integrations. The stage is now set for incorporating the finite element techniques into the analysis. Performing spatial integrations is one of the features at this stage. This is performed by approximating the spatial fluxes using the shape functions of the chosen type of element in terms of its nodal values, i.e. values at prescribed points of the element. However before this is embarked upon the essential features of elements and shape functions are reviewed in the next two sections.

To begin with, the shape functions and associated nodal values are substituted into the Reduced-Functional. Since the Functional is derived from maximum principles, its first derivatives with respect to the nodal values will be zero. Once this is obtained the spatial integrations in terms of the shape functions are then performed. This results in a set of equations (equal to the number of nodal variables) to represent the conditions governing the element. In matrix notation these equations can be represented by the element stiffness matrix, the unknown nodal values and source vectors. Detailed discussion of these aspects are found in Section 4.4.

The next section then discusses the union of the individual elements into the complete system that describes the problem. In the final sections discussion will dwell upon the types of problems encountered, nature of the global stiffness matrix and its relation to storage requirements, solution algorithms

and the implementation of the computer code that has been set up.

4.2 The Element

The selection of particular elements and the definition of the shape functions associated with the chosen element is a most important subject in finite element analysis. This is obvious because of the many types of elements available and certainly some types of elements would be better suited to the geometrical configurations of certain problems. Also it is mathematically more demanding to represent a complex or higher-ordered element and in general these elements yield more accurate results when compared with simpler elements. However, a trade-off sets in when one takes into account the level of accuracy required and additional computation effort and storage required in utilising a higher-ordered element.

In order to fully describe the type of element employed one needs four pieces of information [42]:

(i) shape of the element;

(ii) number and type of nodes;

(iii) number of nodal variables;

(iv) type of shape functions.

The shape of the element and the number of nodes are easily discernible. When one refers to the type of nodes it means that nodes are either exterior or interior nodes. Exterior nodes are those lying on the corners or along the edges of elements. They represent the point of connection between bordering elements. On the other hand, interior

nodes lie inside the element and do not connect with neighbouring elements.

The number of nodal variables is related to the number of degrees of freedom per node and the number of nodes per element. In the previous chapter it was shown that the number of terms in the expansion of the angular flux was equal to the square of the order of the trial function. Hence, if a two-moment trial function was used over a domain discretised by quadilaterals with four nodes per element then the number of nodal variables per element would be sixteen.

The last category, i.e. item (iv) refers to the many types of functions that could serve as shape functions. Polynomials are by far the most popularly used functions. This is because they are easy to manipulate mathematically, i.e. they can be differentiated and integrated without difficulty, a point that will be emphasised in the later sections of this chapter when the element stiffness matrix is derived. Needless to say then only polynomials are considered in the derivation of the shape functions used here.

Since the fundamental premise of the finite element method is that a continuous domain can be accurately modelled by an assemblage of simple shapes it is not surprising that most finite elements are geometrically simple. The 3-node straightsided triangular element is the simplest two-dimensional element and is the most popularly used, since an assemblage of triangles can represent fairly well a two-dimensional domain of any shape.

Next in vogue is the four-node rectangular element. It enjoys the advantage that an assemblage of such elements can be easily constructed because of its regular shape.

In addition to the various types of straight-edged elements that have been discussed it is also possible to construct elements with curved boundaries. The so-called isoparametric family of elements belong to this category. Experience has shown that these elements have been especially helpful in the solution of three-dimensional problems where it is often necessary to reduce the cost of computations by choosing fewer elements [42]. However isoparametric elements are not employed here since the problems solved are confined to regular geometry.

In the present work because of the restriction to regular geometry only right-angled trianges and rectangles are used in the choice of elements.

4.3 The Shape Functions

To illustrate how shape functions arises the simple example of a 3-node triangle is exemplified. For such an element,

$$\phi = \alpha_0 + \alpha_1 x + \alpha_2 y \qquad (4.1)$$

is the form of the polynomial used to approximate the flux within the element.

Let (x_k, y_k) for k = 1,2,3 be the coordinates of the nodes of the triangle and ϕ_k the corresponding values of

the flux. Therefore one can write three equations using relation (4.1) and from the solution of these three equations α_0, α_1 and α_2 can be obtained in terms of (x_k, y_k, ϕ_k) for k = 1,2,3. Substitutiing back in (4.1) and re-arranging one arrives at

$$\phi = N_1\phi_1 + N_2\phi_2 + N_3\phi_3 \qquad (4.2)$$

Here, the N_k are functions of x,y and the coordinates of the nodes and they represent the shape functions of the triangular element.

In general the spatial flux can be represented over the ith element as

$$\phi_g^i(x,y) = \sum_{k=1}^{L} N_k u_k^{ig} \qquad (4.3)$$

where,

L = number of nodes in the element
N_k = the shape functions of the element
u_k^{ig} = nodal values of the spatial flux ϕ_g^i

Note that the group representation g is posed as a superscript for the nodal fluxes purely for the convenience of notation.

An important property of the shape functions is that a shape function, N_k , will be unity if the coordinates of its associated node is substituted into it and it will be zero if the substitution is achieved with the coordinates of the other nodes, i.e.

$$N_k(x_\ell, y_\ell) = \begin{cases} 1 & k = \ell \\ 0 & k \neq \ell \end{cases} \qquad (4.4)$$

$$k = 1, 2, \ldots L$$

The Lagrangian family of rectangular elements provide an easy and systematic method of generating shape functions of any order [102]. This is achieved by the multiplication of appropriate polynomials in the x- and y-axes. The derivation of the shape functions for the Lagrangian elements is shown in Appendix D. Fig.4.1 shows the first three members of the Lagrangian family with equal number of nodes in both the x- and y-directions. The number of nodes are 4, 9 and 16 respectively and because of the form of the shape functions produced (see Appendix D) they are naturally referred to as the bi-linear, bi-quadratic and bi-cubic elements. For brevity they will be referred to as linear, quadratic and cubic elements. In the present work all the elements used are Lagrangian elements.

In passing, the Serendipity family of elements must be mentioned as they relate to rectangular elements. These elements, whose name was coined by Zienkiewicz [102], resemble the Lagrangian family of elements except that they do not possess any internal nodes. Although they are not employed at all in the present work they will be recommended for further investigation by future workers. This investigation is worthwhile because of the presence of the large number of internal nodes and better curve-fitting properties of the higher order Serendipity elements [102].

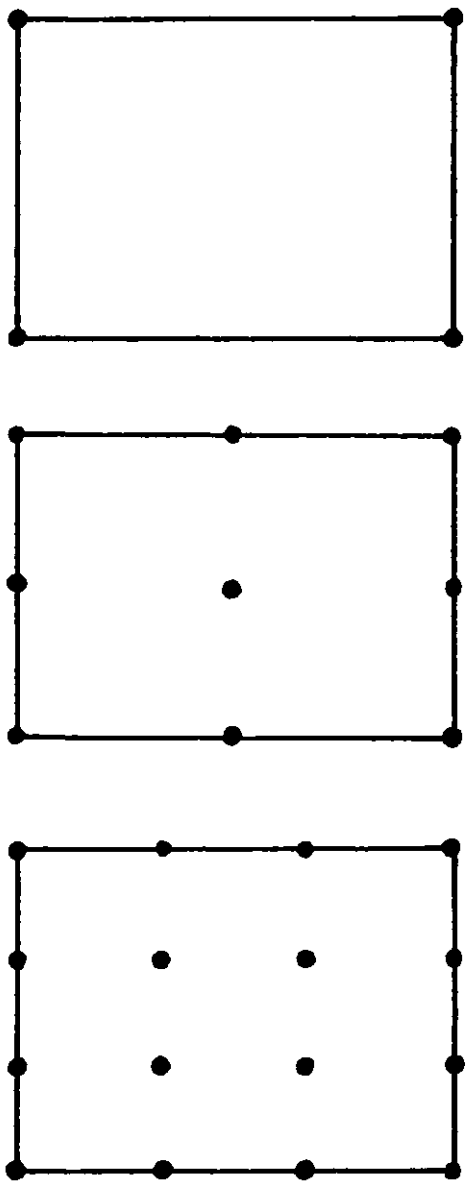

Fig.4.1 The first three members of the Langrangian family of elements

Is there any economic or other types of advantages to be gained by increasing the order (and hence the complexity) of an element? The answer is not an easy one although generally as the order of an element increases the total number of unknowns in the whole domain can be reduced for a given level of accuracy. However economic advantage requires a reduction in the total amount of computations and the effort in setting up the input data; and this does not necessarily follow from a reduction in the total number of unknowns (in which case the equation solving times may be reduced) as the time required for formulating the element increases. Nevertheless it will be seen that linear elements do not perform as well as the higher-ordered elements. In general quadratic elements appear to produce optimum results.

4.4 The Element Stiffness Matrix

As was outlined in Section 4.1, the element stiffness matrix together with the unknown and source vectors constitute the set of linear equations governing the conditions within the element under consideration. To arrive at this stage we need to carry on from where we left off in the last chapter with the equation of the Reduced-Functional, i.e. Eq.(3.41). First, each moment of the spatial flux is replaced by its finite element form in general terms, i.e. Eq.(4.3) and hence,

$$\tilde{K}(\hat{\phi}_g) = \int_V \left\{ -\frac{1}{\Sigma_{t_g}(\pm)} \sum_{i=1}^{M^2} \sum_{j=1}^{M^2} \left[E_{1ij} \sum_{k=1}^{L} \sum_{\ell=1}^{L} \frac{\partial N_k}{\partial x} \frac{\partial N_\ell}{\partial x} u_{ik}^g u_{j\ell}^g \right.\right.$$

$$+ E_{2ij} \sum_{k=1}^{L} \sum_{\ell=1}^{L} \frac{\partial N_k}{\partial x} \frac{\partial N_\ell}{\partial y} u_{ik}^g u_{j\ell}^g + E_{3ij} \sum_{k=1}^{L} \sum_{\ell=1}^{L} \frac{\partial N_k}{\partial y} \frac{\partial N_\ell}{\partial y} u_{ik}^g u_{j\ell}^g \Big]$$

$$- \left[\Sigma_{t_g}(\pm) \sum_{i=1}^{M^2} F_{ij} \sum_{k=1}^{L} \sum_{\ell=1}^{L} N_k N_\ell u_{ik}^g u_{i\ell}^g - \Sigma_{s_{0gg}}(\pm) \sum_{k=1}^{L} \sum_{\ell=1}^{L} N_k N_\ell u_{ik}^g u_{i\ell}^g \right]$$

$$+ 2 \Bigg[\sum_{g'=1}^{g-1} \Sigma_{s_{0g'g}}(\pm) \sum_{k=1}^{L} \sum_{\ell=1}^{L} N_k N_\ell u_{ik}^{g'} u_{i\ell}^{g'}$$

$$+ \chi_g \sum_{g'=1}^{G} \omega \Sigma_{f_{g'}}(\pm) \sum_{k=1}^{L} \sum_{\ell=1}^{L} N_k N_\ell u_{ik}^{g'} u_{i\ell}^{g'} \qquad (4.5)$$

$$+ \tilde{Q}_g(\pm) \sum_{k=1}^{L} N_k u_{ik}^g \Bigg] \Bigg\} dV$$

$$- \int_S \sum_{i=1}^{M^2} \sum_{j=1}^{M^2} B_{ij} \sum_{k=1}^{L} \sum_{\ell=1}^{L} N_k N_\ell u_{ik}^g u_{j\ell}^g \; dS$$

From the maximum principles, the first derivatives of $\tilde{K}(\hat{\phi}_g)$ with respect to the nodal fluxes are zero,

$$\frac{\partial \tilde{K}(\hat{\phi}_g)}{\partial u_{h,m}} = 0 \qquad (4.6)$$

$h = 1, 2, \ldots M^2$

$m = 1, 2, \ldots L$

and so,

$$\begin{aligned}
\frac{\partial \tilde{K}(\hat{\phi}_g)}{\partial u_{h,m}} = \int_V \Bigg\{ & -\frac{1}{\Sigma_{t_g}(\pm)} \Bigg[\frac{\partial N_m}{\partial x} \sum_{j=1}^{M^2} \left(E_{1hj} \sum_{\ell=1}^{L} u_{j\ell}^g \frac{\partial N_\ell}{\partial x} + E_{1jh} \sum_{\ell=1}^{L} u_{j\ell}^g \frac{\partial N_\ell}{\partial x} \right) \\
& + \frac{\partial N_m}{\partial x} \sum_{j=1}^{M^2} E_{2hj} \sum_{\ell=1}^{L} u_{j\ell}^g \frac{\partial N_\ell}{\partial y} + \frac{\partial N_m}{\partial y} \sum_{j=1}^{M^2} E_{2jh} \sum_{\ell=1}^{L} u_{j\ell}^g \frac{\partial N_\ell}{\partial y} \\
& + \frac{\partial N_m}{\partial y} \sum_{j=1}^{M^2} \left(E_{3hj} \sum_{\ell=1}^{L} u_{j\ell}^g \frac{\partial N_\ell}{\partial y} + E_{3jh} \sum_{\ell=1}^{L} u_{j\ell}^g \frac{\partial N_\ell}{\partial y} \right) \Bigg] \\
& - 2 \left[\Sigma_{t_g}(\pm) F_{hh} N_m \sum_{\ell=1}^{L} N_\ell u_{h\ell}^g - \Sigma_{s_{0gg}}(\pm) \delta_{1,h} N_m \sum_{\ell=1}^{L} N_\ell u_{h\ell}^g \right] \\
& + 2 \Bigg[2 \sum_{g'=1}^{g-1} \Sigma_{s_{0g'g}}(\pm) \delta_{1,h} N_m \sum_{\ell=1}^{L} N_\ell u_{h\ell}^{g'} \\
& + 2\chi_g \sum_{g'=1}^{G} \nu \Sigma_{f_{g'}}(\pm) \delta_{1,h} N_m \sum_{\ell=1}^{L} N_\ell u_{h\ell}^{g'} \\
& + \tilde{Q}_g(\pm) \delta_{1,h} N_m \Bigg] \Bigg\} dV \\
& - \int_S N_m \sum_{j=1}^{M^2} \left\{ B_{hj} \sum_{\ell=1}^{L} N_\ell u_{j\ell}^g + B_{jh} \sum_{\ell=1}^{L} N_\ell u_{j\ell}^g \right\} dS = 0
\end{aligned} \qquad (4.7)$$

$h = 1, 2, \ldots M^2$

$m = 1, 2, \ldots L$

Recalling the results of Section 3.10 it is known that owing to symmetry the paired values (E_{1hj}, E_{1jh}), (E_{2hj}, E_{2jh}), (E_{3hj}, E_{3jh}) and (B_{hj}, B_{jh}) are equal. Since in x-y geometry the volume integrals are double integrals over x and y and the surface integral is a single integral over either x or y, Eq.(4.7) can be written as:

$$\frac{\partial \tilde{K}(\hat{\Phi}_g)}{\partial u_{h,m}} = -\frac{1}{\Sigma_{t_g}(\pm)} \sum_{j=1}^{M^2} \Bigg[2E_{1jh} \iint \frac{\partial N_m}{\partial x} \sum_{\ell=1}^{L} u_{j\ell}^{g} \frac{\partial N_\ell}{\partial x} \, dx\,dy$$

$$+ E_{2jh} \iint \frac{\partial N_m}{\partial x} \sum_{\ell=1}^{L} u_{j\ell}^{g} \frac{\partial N_\ell}{\partial y} \, dx\,dy + E_{2jh} \iint \frac{\partial N_m}{\partial y} \sum_{\ell=1}^{L} u_{j\ell}^{g} \frac{\partial N_\ell}{\partial x} \, dx\,dy$$

$$+ 2E_{3jh} \iint \frac{\partial N_m}{\partial y} \sum_{\ell=1}^{L} u_{j\ell}^{g} \frac{\partial N_\ell}{\partial y} \, dx\,dy \Bigg]$$

$$-2 \Big[\Sigma_{t_g}(\pm) F_{hh} \iint N_m \sum_{\ell=1}^{L} N_\ell u_{h\ell}^{g} \, dx\,dy - \delta_{1,h} \Sigma_{s_{ogg}}(\pm) \iint N_m \sum_{\ell=1}^{L} N_\ell u_{h\ell}^{g} \, dx\,dy \Big]$$

$$+ 2\delta_{1,h} \Bigg[2 \sum_{g'=1}^{g-1} \Sigma_{s_{ogg}}(\pm) \iint N_m \sum_{\ell=1}^{L} N_\ell u_{h\ell}^{g'} \, dx\,dy$$

$$+ 2\chi_g \sum_{g'=1}^{G} \nu \Sigma_{f_{g'}}(\pm) \iint N_m \sum_{\ell=1}^{L} N_\ell u_{h\ell}^{g'} \, dx\,dy + \tilde{Q}_g(\pm) \iint N_m \, dx\,dy$$

$$-2 \sum_{j=1}^{M^2} B_{jh} \int N_m \sum_{\ell=1}^{L} N_\ell u_{j\ell}^{g} \, dp = 0$$

$h = 1, 2, \ldots M^2$

$m = 1, 2, \ldots L$

in which dp takes up dx or dy according to the surface.

At this stage it would be proper to compact Eq.(4.8) by using a notation for the spatial integrals. This is helpful when the evaluation of the spatial integrals are discussed later on.

Let,

$$
\left.
\begin{aligned}
W_{m\ell}^{xx} &= \iint \frac{\partial N_m}{\partial x}\,\frac{\partial N_\ell}{\partial x}\,dx\,dy \\
W_{m\ell}^{xy} &= \iint \frac{\partial N_m}{\partial x}\,\frac{\partial N_\ell}{\partial y}\,dx\,dy \\
W_{m\ell}^{yx} &= \iint \frac{\partial N_m}{\partial y}\,\frac{\partial N_\ell}{\partial x}\,dx\,dy \\
W_{m\ell}^{yy} &= \iint \frac{\partial N_m}{\partial y}\,\frac{\partial N_\ell}{\partial y}\,dx\,dy \\
V_{m\ell} &= \iint N_m N_\ell\,dx\,dy \\
U_m &= \iint N_m\,dx\,dy \\
T_{m\ell} &= \int N_m N_\ell\,dp
\end{aligned}
\right\} \qquad (4.9)
$$

Substituting the expressions from Eq.(4.9) into (4.8) and grouping the source components to one side of the equation,

$$\frac{1}{\Sigma_{t_g}(\pm)} \sum_{j=1}^{M^2} \sum_{\ell=1}^{L} \left[2E_{1jh} W_{m\ell}^{xx} + E_{2jh}(W_{m\ell}^{xy} + W_{m\ell}^{yx}) + 2E_{3jh} W_{m\ell}^{yy} \right] u_{j\ell}^{g}$$

$$+ 2 \sum_{\ell=1}^{L} \left[\Sigma_{t_g}(\pm) F_{hh} - \delta_{1,h} \Sigma_{s_{0gg}}(\pm) \right] V_{m\ell} u_{h\ell}^{g}$$

$$+ 2 \sum_{j=1}^{M^2} B_{jh} \sum_{\ell=1}^{L} T_{m\ell} u_{j\ell}^{g}$$

$$= 2\delta_{1,h} \left[2 \sum_{g'=1}^{g-1} \Sigma_{s_{0g'g}}(\pm) \sum_{\ell=1}^{L} V_{m\ell} u_{h\ell}^{g'} \right. \qquad (4.10)$$

$$+ 2\chi_g \sum_{g'=1}^{G} \nu \Sigma_{f_{g'}}(\pm) \sum_{\ell=1}^{L} V_{m\ell} u_{h\ell}^{g'}$$

$$\left. + \tilde{Q}_g(\pm) U_m \right]$$

$h = 1, 2, \ldots M^2$

$m = 1, 2, \ldots L$

Gathering the terms on the L.H.S. under the common summations,

$$\sum_{j=1}^{M^2}\sum_{\ell=1}^{L}\left\{\frac{1}{\Sigma_{t_g}(\pm)}\left[2E_{1jh}W_{m\ell}^{xx}+E_{2jh}(W_{m\ell}^{xy}+W_{m\ell}^{yx})+2E_{3jh}W_{m\ell}^{yy}\right]\right.$$

$$+2\left[\delta_{j,h}\Sigma_{t_g}(\pm)F_{hh}-\delta_{1,h}\Sigma_{s_{0gg}}(\pm)\right]V_{m\ell}$$

$$\left.+2B_{jh}T_{m\ell}\right\}U_{j\ell}^{g}$$

$$=2\delta_{1,h}\left[2\sum_{g'=1}^{g-1}\Sigma_{s_{0g'g}}(\pm)\sum_{\ell=1}^{L}V_{m\ell}U_{h\ell}^{g'}\right.$$

$$+2\chi_g\sum_{g'=1}^{G}\omega\Sigma_{f_{g'}}(\pm)\sum_{\ell=1}^{L}V_{m\ell}U_{h\ell}^{g'} \qquad (4.11)$$

$$\left.+\tilde{Q}_g(\pm)U_m\right]$$

$h=1,2,\ldots M^2$

$m=1,2,\ldots L$

If we now introduce

$$a_{j\ell}^{hm} = \frac{1}{\Sigma_{t_g}(\pm)}\left[2E_{1jh}W_{m\ell}^{xx} + E_{2jh}(W_{m\ell}^{xy} + W_{m\ell}^{yx}) + 2E_{3jh}W_{m\ell}^{yy}\right]$$

$$+2\left[\delta_{j,h}\Sigma_{t_g}(\pm)F_{hh} - \delta_{i,h}\Sigma_{s_{0_{gg}}}(\pm)\right]V_{m\ell} + 2B_{jh}T_{m\ell} \qquad (4.12)$$

and

$$d^{hm} = 2\delta_{i,h}\left[2\sum_{g'=1}^{g-1}\Sigma_{s_{0_{g'g}}}(\pm)\sum_{\ell=1}^{L}V_{m\ell}\,u_{h\ell}^{g'}\right.$$

$$+ 2\chi_g\sum_{g'=1}^{G}\nu\Sigma_{f_{g'}}(\pm)\sum_{\ell=1}^{L}V_{m\ell}\,u_{h\ell}^{g'} \qquad (4.13)$$

$$\left.+ \tilde{Q}_g(\pm)U_m\right]$$

Eq.(4.11) is now re-written as

$$\sum_{j=1}^{M^2}\sum_{\ell=1}^{L} a_{j\ell}^{hm}\,u_{j\ell}^{g} = d^{hm} \qquad (4.14)$$

$$h = 1, 2, \ldots M^2$$

$$m = 1, 2, \ldots L$$

The double subscripted from of Eq.(4,14) is rather unwieldy. To simplify matters the indexing over j and ℓ can be combined and another similar one for h and m. If the new subscripts are now p and q, we have

$$\sum_{p=1}^{T} a_{qp} u_p^g = d_q \qquad q = 1, 2, \ldots . T \tag{4.15}$$

where,

$$T = LM^2$$

and p and q can be related to the original indices in the following manner:

$$\left.\begin{aligned} p &= (\ell - 1)L + j \\ q &= (m-1)L + h \end{aligned}\right\} \tag{4.16}$$

The indexing achieved in this manner ensures that all the components of the angular flux at a node can be physically located at the same nodal point.

In matrix notation, the system of equations in (4.15) can be expressed as

$$\underline{\underline{A}}_g^e \, \underline{u}_g^e = \underline{d}_g^e \tag{4.17}$$

in which matrix $\underline{\underline{A}}_g$ is of dimension (LM^2 x LM^2) and the vectors $\underline{u}_g^e$ and $\underline{d}_g^e$ are of length LM^2. The superscript e is introduced to signify that Eq.(4.17) represents the

element equation and subscript g of course denotes the neutronic group. The matrix $\underline{\underline{A}}^e_g$ is very often referred to as the element stiffness matrix, the parody on the word stiffness being due its coinage by structural engineers during the early days of the finite element method. In essence Eq.(4.17) is the simplest building block in the problem analysis.

4.5 Numerical Integration

Should the spatial integrals represented by Eq.(4.9) be evaluated numerically or analytically? According to Irons and Ahmad [45] numerical integration, in their own experience, always pays. This is attributed to the fact that analytical solutions take longer times and mistakes frequently occur. Also, with numerical methods the procedure is uniform and provides a modular feature to the code. In large codes modularity is important. When irregular meshes are used analytical integrations become impractical and this is also true when curved elements are employed. Hence it is not surprising that numerical integration has become an increasingly important part of the finite element technique.

During the initial stages of this work the integrals were evaluated numerically by the use of Gauss-Legendre quadrature sets. Since only regular elements were used a switch to analytical integration was made later on to provide a check. There was no difference when results

were compared, but the switch to analytical methods was based purely on grounds of regular elements and portability. However the module where integrations are performed numerically has been left intact as it is anticipated that numerical integrations would be performed when irregular elements become a feature during the later developments of the finite element techniques in neutronic applications.

4.6 Assembly

In Section 4.4 the single element equations for the nodal values were derived. Since the element is the basic unit of the whole continuum therefore the complete set of equations would come about from combining the elemental equations. This can be represented by

$$\underline{\underline{A}}_g \underline{u}_g = \underline{d}_g \tag{4.18}$$

in which

$$\left.\begin{aligned} A_{g_{ij}} &= \sum_{e=1}^{N} A^e_{g_{ij}} \\ u_{g_i} &= \sum_{e=1}^{N} u^e_{g_i} \\ d_{g_i} &= \sum_{e=1}^{N} d^e_{g_i} \end{aligned}\right\} \tag{4.19}$$

Here N denotes the number of elements in the system. The subscripts i,j here refer to the numbering system for

the global system. Note that the numbering system in the single element Eq.(4.15), (4.17) will take the values from 1 to LM^2 but when referred to the complete system there has to be a transformation into the appropriate global values.

Fig.4.2 demonstrates how the global stiffness matrix is constructed for a (2 x 2) grid of 4-node rectangular elements using a 1 moment trial function. The figure has been adapted from a more detailed illustration by Zienkiewicz [102]. As can be seen the global numbering of each element is different from its local numbering. Also nodes lying between elements receive contributions from each of the elements. For example node 5 receives contributions from all the elements while corner nodes 1, 3, 7 and 9 receive contributions from only 1 element each.

In all, Eq.(4.15) represents LM^2 equations. Therefore, if a 2-moment trial function were used to approximate the angular flux in a 4-node rectangular element then there would be 16 unknowns embodied in 16 equations. This can be contrasted against only 4 unknowns in 4 equations for a 1-moment trial function. Of course the large number of unknowns and equations for higher moments of the trial function means that there has to be a limit in the order of the trial function for practical purposes. When compared against other applications using the finite element method it can be seen that conditions are more demanding when trial functions of two or more moments are used.

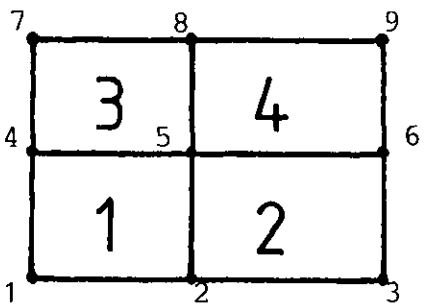

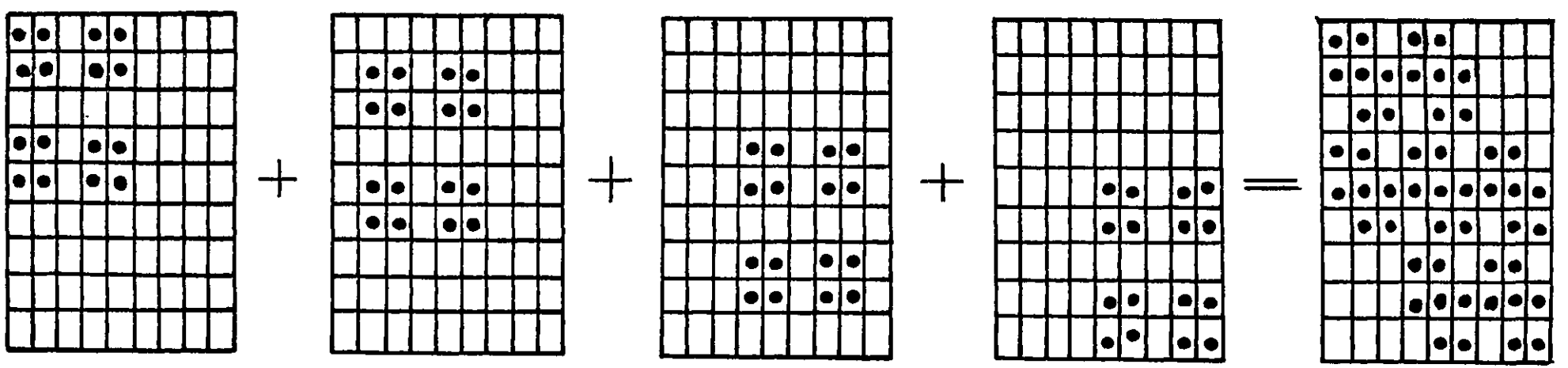

Fig.4.2 Construction of the global stiffness matrix

4.7 The Global Stiffness Matrix

The global stiffness matrix for group g, $\underline{\underline{A}}_g$, is symmetric and positive-definite. This is the result of using the variational formulation of the stiffness equations. On the other hand, had one approached the finite element formulation from a weighted residual point of view the resulting global matrix may not necessarily be symmetric and positive-definite except in the least squares case.

Another feature of the matrix is that it is banded, that is to say the non-zero components are to be found in a banded region centred round the principal diagonal. Fig.4.3 exemplifies this point. The term half-bandwidth refers to the width of one-half of this band including the principal diagonal and is designated as N_b in Fig.4.3.

The banded and symmetric nature of $\underline{\underline{A}}_g$ ensures that the whole matrix of dimension ($N_{eq} \times N_{eq}$) need not be constructed and stored. Only the elements of shaded region of the matrix in Fig.4.3 need to be stored. This enables considerable savings in computer memory allocations. As an example, if we analyse a problem on a rectangular array of (15 x 15) linear elements using a 2-moment trial function then we would have to account for $16 \times 16 \times 2^2 = 1024$ equations due to the 1024 unknowns. Storing all the elements of $\underline{\underline{A}}_g$ means that (1024 x 1024) storage locations have to be allowed for. However in such a problem by using an appropriate global ordering system the half-bandwidth is only 72 and so only (1024 x 72) storage locations are

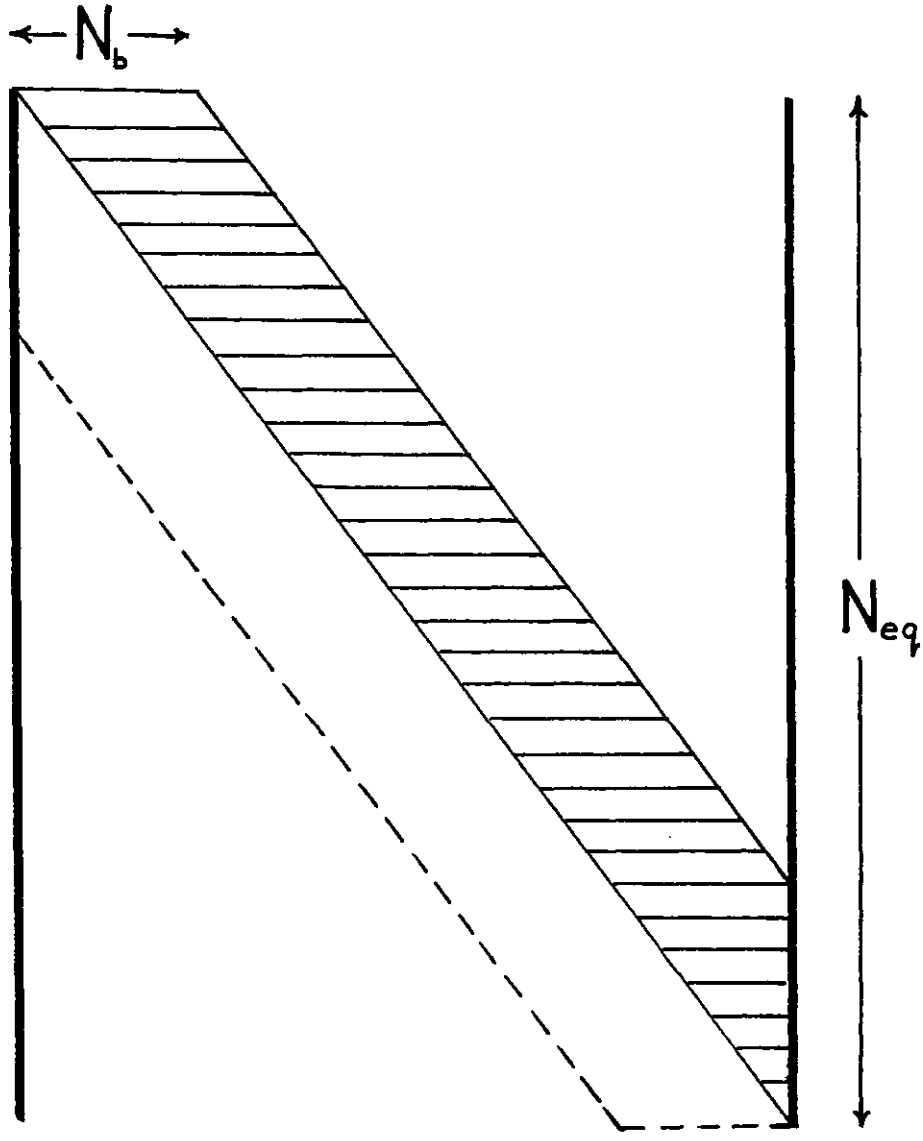

Fig.4.3 The banded and symmetrical nature of $\underline{\underline{A}}_g$

required, which is a saving of approximately 92% in storage terms. Of course in this instance one does not talk about the additional computing time in filling up a full matrix with unnecessary zeroes and the unnecessary operations that would have been done with them. It is clearly desirable to chose an ordering system which leads to a small bandwidth.

How does one achieve an optimal bandwidth? This comes about from the labelling of the nodes in the global numbering system. It depends on the largest difference between node numbers in a single element with all elements under consideration. In regular meshes the determination is simple and straightforward as shown in Fig.4.4. Segerlind [87] has shown the effects of variation in bandwidth due to different labelling patterns for an iregular grid.

4.8 Fixed Source and Eigenvalue Problems

Generally two types of problems are encountered depending on the nature of the sources arising from the problem. There is the fixed source problem in which the source contribution is known and on the other hand the eigenvalue problem poses the situation that the source contribution cannot be known until the unknowns in the problem are solved for. So, as to be expected an iteration cycle, known popularly as the outer iteration cycle, has to be imposed when solving eigenvalue problems. The outer iteration cycle is so called because there may or may not be an inner iteration cycle in solving for the unknowns

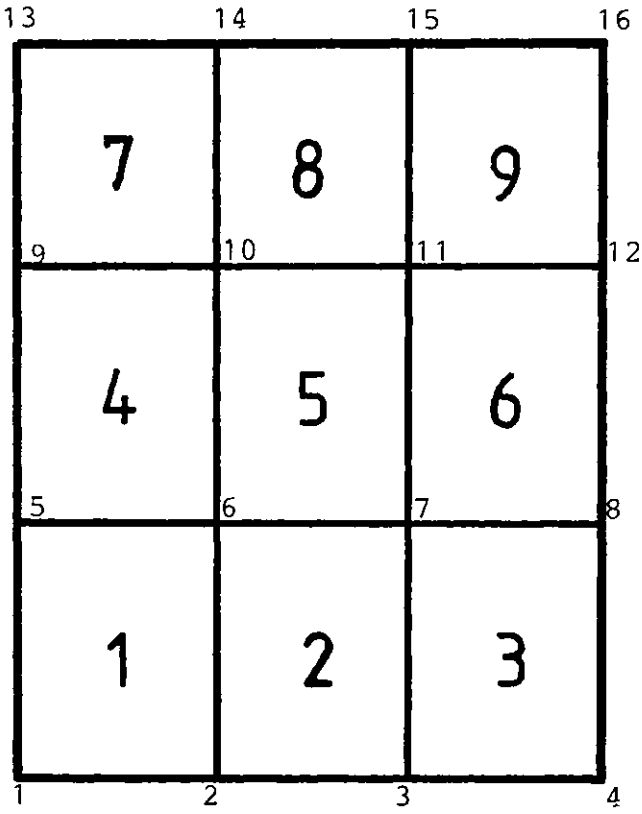

N_b = (Top right node - Bottom left node) of any element + 1

Fig.4.4 Half-bandwidth in a regular array of elements

depending on whether iteration techniques are used to solve the global set of equations.

To improve categorisation of these two classes of problems we recall that there are three types of contributions in the source term, i.e. scattering from one group to another, extraneous source and fission. Fixed source problems are those for which the sources for a group are due to extraneous sources and downscattering contributions. For eigenvalue problems the group sources have intergroup scattering and fission contributions. A fission source for a group has contributions from fission within the group and fissions from other groups.

Therefore, from Eq.(4.13) it can be seen that the source vector for an element would be

$$\underline{d}_g^e = 2\underline{\underline{U}}\,\tilde{Q}_g + 4\sum_{g'=1}^{g-1} \underline{\underline{D}}_{g'}\,\underline{U}_{g'} \qquad (4.20)$$

where

$$\left.\begin{aligned} \underline{\underline{U}} &= \{U_\ell\}^T && \ell = 1,2,\ldots L \\ \underline{\underline{D}}_{g'} &= \Sigma_{s_{0g'g}}\{V_{k\ell}\} && k,\ell = 1,2,\ldots L \\ \underline{U}_{g'} &= \{U_{g'(\ell-1)M^2+1}\} && \ell = 1,2,\ldots L \\ \underline{d}_g &= \{d_{g(\ell-1)M^2+1}\} && \ell = 1,2,\ldots L \end{aligned}\right\} \qquad (4.21)$$

For eigenvalue problems

$$\underline{d}_g^e = 4\sum_{g'=1}^{g-1} \underline{\underline{D}}_{g'}\underline{U}_{g'} + 4\chi_g \sum_{g'=1}^{G} \underline{\underline{F}}_{g'}\underline{U}_{g'}^* \qquad (4.22)$$

where,

$$\underline{\underline{F}}_{g'} = \nu\Sigma_{f_{g'}}\{V_{k\ell}\} \qquad k,\ell = 1,2,\ldots L \qquad (4.23)$$

and the other vectors and matrix are as defined in Eq.(4.21).

In the fission term the asterisk in the unknowns show that they are values from a previous iteration cycle. In both classes of problems upscattering is not considered. However if upscattering were to be considered the following additional term would have to be considered, i.e.

$$4\sum_{g'=g+1}^{G} \underline{\underline{D}}_{g'}\underline{U}_{g'}^*$$

and an iteration cycle for this would be required.

4.9 Solution Schemes

The solution of a set of linear equations can be obtained either by direct elimination or by iteration. In finite element analysis direct elimination, typified by Gaussian elimination, is by far the more popular method. It has also been reported that, in the application of the finite element method to radiation transport, direct

elimination methods are faster than iteration techniques [63]. Hence it is not surprising that Irons and Ahmad [45] have attributed the fact that finite element technology owes more to Gauss than to any other person in history since Gaussian quadrature is also widely used in numerical integration (see Section 4.5).

However in finite element analysis the effectiveness of direct solution methods depends on the specific properties of the finite element stiffness matrix, i.e. symmetry, positive definiteness and bandedness [10]. This is exactly the structure of the global matrix $\underline{\underline{A}}_g$ as described in the preceding section. So it is natural enough that direct solution schemes serve to bring about the results to which we sought for. However this is not to say that iterative methods should not be regarded at all. It has been found that even storing only the half-bandwidth of the global matrix there can be problems with computer memory capacity especially when fine mesh, high-order elements or high-order trial functions are used. This is where iterative methods can score over the direct elimination methods because in some iteration schemes there is effectively zero storage of a global matrix. The finite difference techniques have enjoyed this particular aspect of an iterative solution because the coefficients at a nodal point are assembled "on the spot" during the iteration. It is not so easy in a finite element scheme to assemble coefficients in this manner. Consequently only direct elimination schemes have been

considered in the present study especially since the global matrix $\underline{\underline{A}}_g$ is symmetric positive-definite and banded. The positive-definite nature of the matrix ensures that no pivotting is required and is highly desirable because pivotting could destroy the banded nature of the matrix.

One other reason for using direct solvers is that the available computing facilities nowadays have tremendous storage capacity and for two-dimensional analyses the storage aspect is not the most important factor. In the eventuality direct methods are faster than iterative methods and as such will always be preferred. Besides one does not face the problems of convergence and stability associated with iterative techniques.

Two types of direct solvers were used in this present work. One is called BANSOL [26] and is an in-core solver, i.e. the whole of the global matrix resides in the fast primary storage. The other is called SESOL [99] and is an out-of-core solver. Using this solver only part of the global matrix need to be in fast storage at any one time while the rest is held on the slower secondary storage and therefore it is understandable that SESOL would be used in those circumstances where storage is a limiting factor. The amount of savings achieved is dependable on the number of blocks as will be seen in Sections 4.10, 5.7 and 5.8. However SESOL has only been adapted to the stage where it can only handle source problems. Therefore BANSOL still handles all the eigenvalue problems besides the smaller sized source problems.

The out-of-core solver will be discussed in the next section while details about the mechanics of direct elimination methods have been discussed elsewhere [31,67]. A review of all available in-core direct elimination algorithms have been discussed by Mondaker and Powell [72].

This section would not be complete if no mention was made of the frontal solution technique first reported by Irons [44]. This is a direct elimination technique and is a storage saving algorithm. The basic essence is that in using this algorithm the global matrix is not assembled at one time. Instead solution is performed on the completely assembled part of the matrix as one proceeds through the whole structure of elements. The effect is rather like a wave front propagation and hence the name. Wilson [100] has examined the advantages and disadvantages of the frontal method against the other direct elimination methods. Although the frontal method was not used here it is hoped that this, as a proposal for future research and development, would be carried out.

4.10 The Out-of-Core Solver

As was mentioned in the previous section the out-of-core solver is one in which secondary storage is used to ease the problems associated with available primary storage. This technique greatly enhances the number of equations that can be solved as secondary storage can be very large depending on the computer and the computing environment (these aspects will not be discussed here).

To begin with it is necessary to introduce a most important concept, i.e. blocking techniques. This is because in using the out-of-core solver one needs to know into how many "blocks" the global matrix has been divided into. In using SESOL the blocks have to be of equal length which is an advantage for regular grids. Imagine a mesh of (4 x 6) linear elements as shown in Fig.4.5. The system has been divided into 7 blocks, each block consisting of equations relating to each row of the grid. If the same mesh were to contain quadratic elements then Fig.4.6 shows the blocking pattern, i.e. each block would consist of 2 consecutive rows of the grid except the last where it would be filled with the remaining row followed by a row of zeros. The technique is extended to three rows in the case of cubic elements.

The above technique is by no means the only method available for "blocking" a mesh of elements. Instead of considering one row of elements, multiple number of rows or fractions of a row could be considered. However, the advantage in the above technique is that since we are only dealing with regular grids it ensures that the elemental contributions are not calculated more than once. Besides when adding the bare surface effects there is no other simpler method.

When implementing SESOL into the finite element program several changes were made. The global matrix, which was originally assembled in one go for each energy group, is assembled block by block. When the assembly

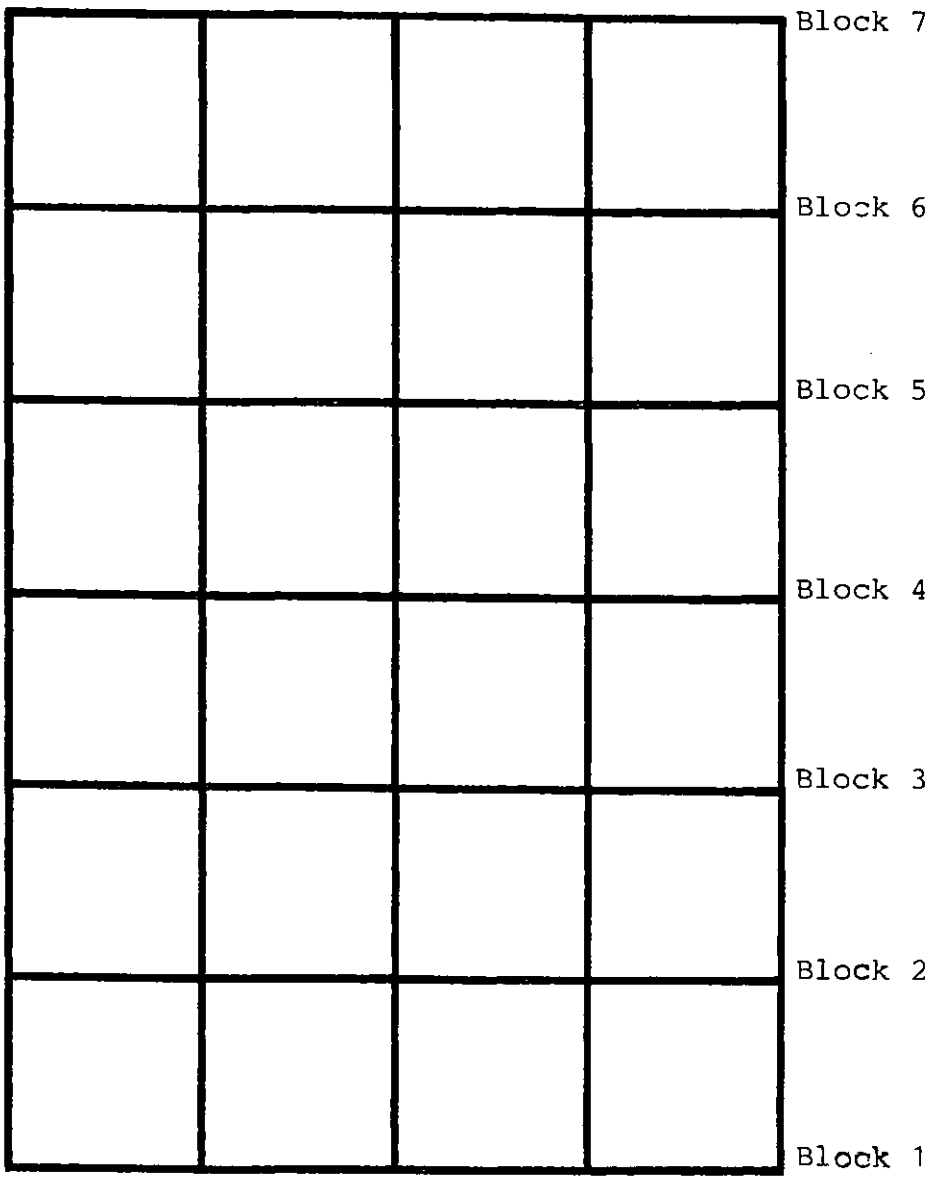

Fig.4.5 Blocking pattern for linear elements

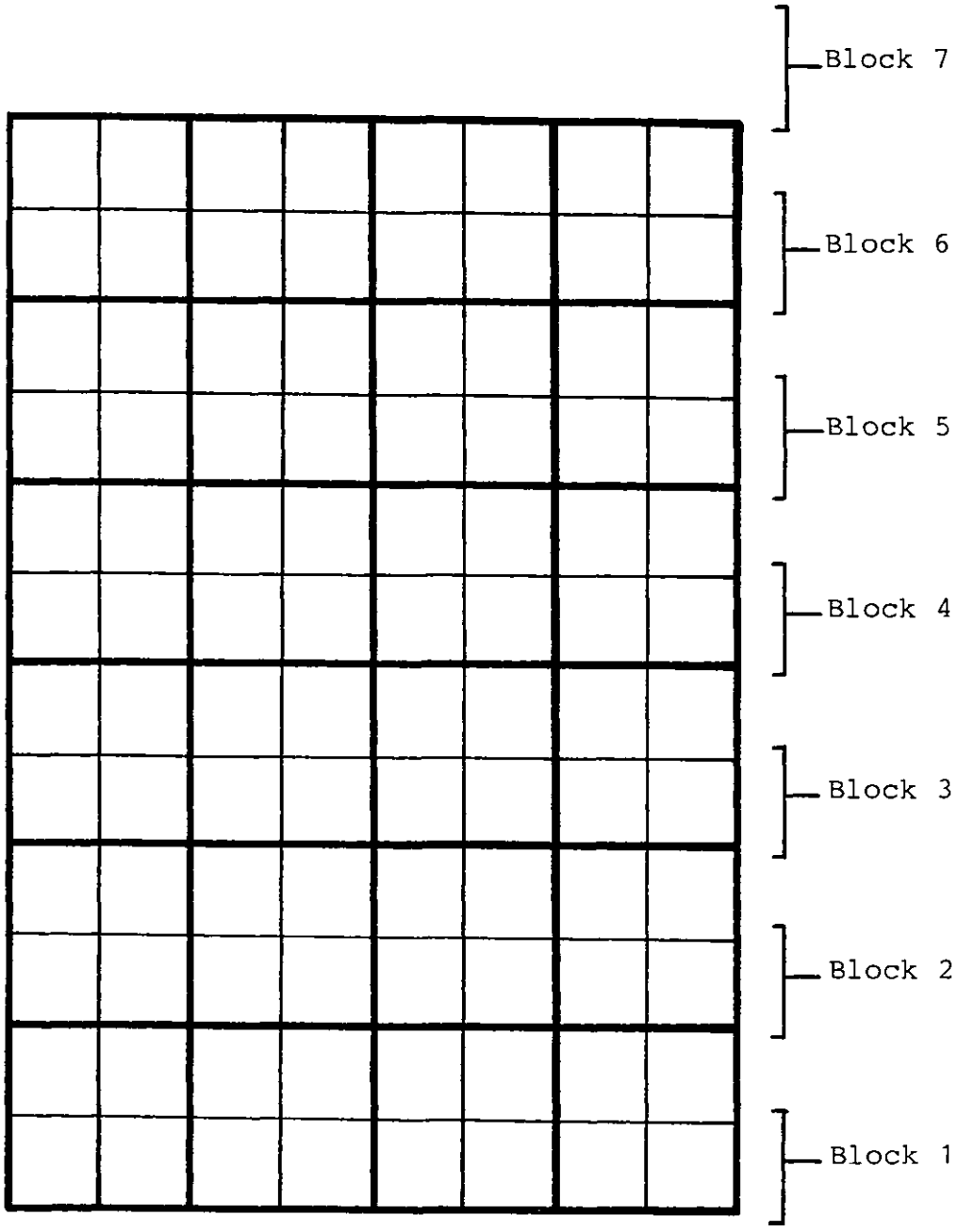

Fig.4.6 Blocking pattern for quadratic elements

for each block is complete (together with the boundary conditions) it is shifted to secondary storage. This requires the use of storage equivalent to 2 blocks in primary storage at any one time because blocks not on the boundary require contributions from different layers of elements. Nevertheless the minimum in-core storage is always 2 blocks because in the solution stage 2 blocks of data are required for manipulation by SESOL at any one time. Assembly is completed once all the blocks are shifted to secondary storage.

In the solution stage the process is reversed and each block is brought in turn into primary storage. The algorithm requires that 2 blocks of data should be manipulated at the same time in primary storage. The coefficients of the leading block are reduced and any coefficients of the second block affected by this process are suitably modified. The coefficients of the reduced leading block are returned to secondary storage, the trailing block then becomes the leading block and the next block from secondary storage is shifted in to occupy the position of trailing block. The process is repeated until all the blocks are reduced. Back substitution to determine the solutions require the calling of one block of the reduced matrix into primary storage at a time.

There is one important feature in SESOL that is not available in BANSOL and that is the ability to skip non-productive zero arithmetical operations. Consider the global matrix assembled from using cubic elements as shown in Fig.4.7. There are 4 bands of zero elements

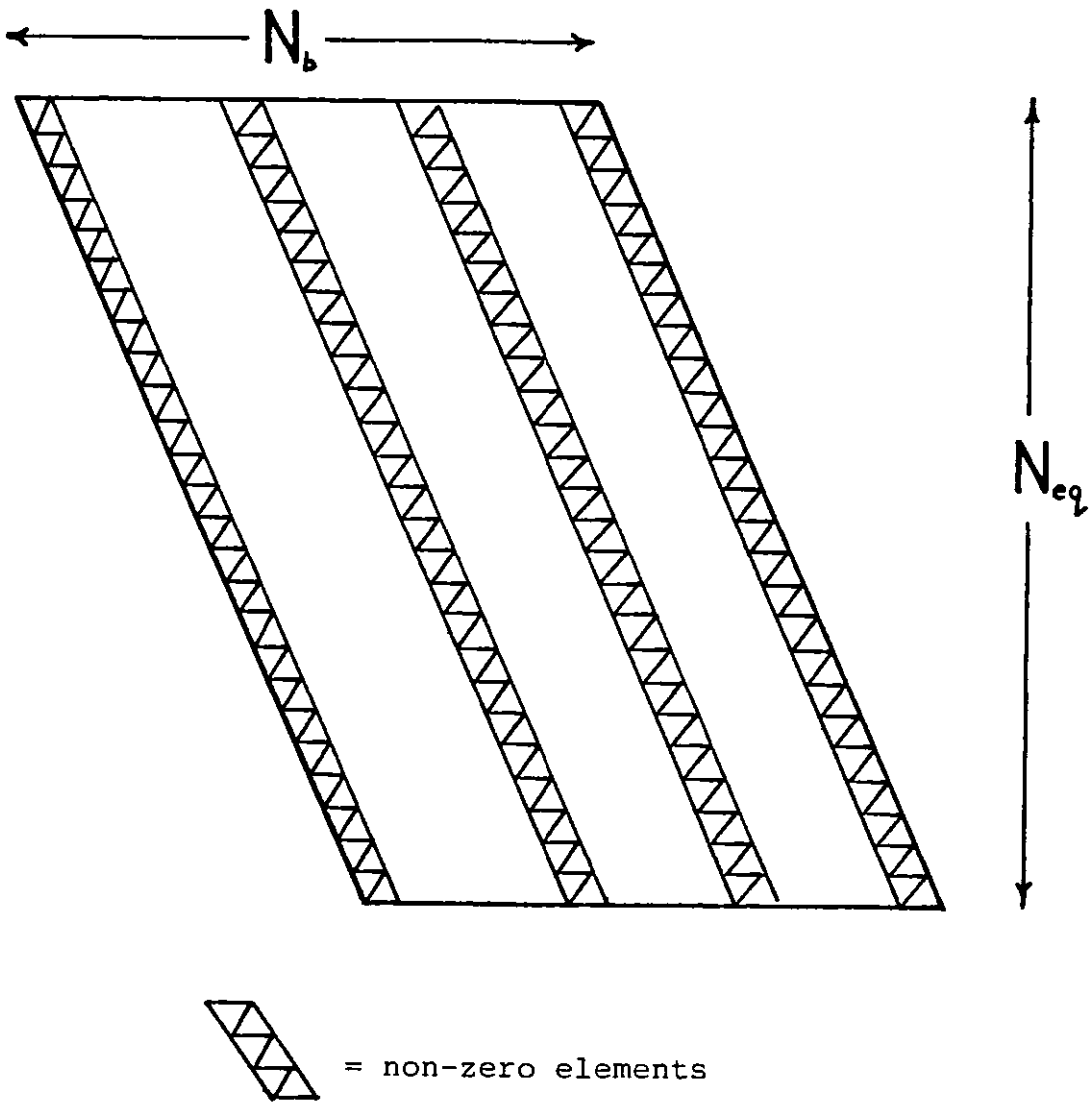

Fig.4.7 The banded nature of the symmetric half of the global matrix derived from using cubic elements

within the half-bandwidth. For quadratic elements there will be three and for linear elements, two. The number of zero elements will depend on the bandwidth for the system, being more for a larger bandwidth. Unproductive operations on these zero elements (i.e. the products of which are still zero) can be time consuming. If the above effect of band zeros were insignificant one would expect BANSOL to perform rather faster than SESOL when the same problem is considered by both algorithms, because SESOL is hindered by the relatively slower read and write processes between primary and secondary storage. Contrary to all expectations SESOL performs better than BANSOL when cubic elements are analysed but not with linear elements as will be seen from the results in Sections 5.7 and 5.8. This shows that the unproductive effect of zero operations is time consuming.

To end this section on the out-of-core solver we will consider the percentage savings achieved. Consider the (4 x 6) mesh of quadratic elements from Fig.4.6. Assume a 1-moment trial function (actually the percentage savings do not depend on the order of the trial function). Using SESOL there are 7 blocks, but the 2 blocks of storage employed is only 28.5% of the actual size of the global matrix. Therefore if more blocks were used then the percentage savings would be greater but then the dis-compensating factor would be computing time. On the other hand the actual size of a block, using this manner of partitioning, is dependent on the half-bandwidth of the system. Actually, as witnessed from Fig.4.7, there

are plenty of zero elements even within the half-bandwidth of the global matrix. Therefore one may ask whether it would be better to store only all the non-zero elements and re-order them by an alternative numbering scheme. However it has been shown by George and Liu [36] that the zero elements in the band of a banded matrix are filled in during the reduction process and therefore it is necessary to preserve the zero elements within the band. It should be noted that the zero arithmetic operations referred to above refers to the alteration of the zero coefficient by multiplication or division, the result of which is still zero, and that when these zero coefficients are filled in they result from the subtraction between the rows of the matrix.

4.11 Implementation

In order to implement the ideas discussed in the previous sections effectively it is necessary to construct an efficient computer code because it would be impossible to do any constructive analysis of difficult problems otherwise. In designing an efficient code there are several important objectives to be fulfilled otherwise the process of obtaining solutions to a problem can be particularly tedious. Efficiency must be associated with a flexible modular construction so that the addition or deletion of pertinent features in the code can be undertaken rapidly. Naturally enough the code should be constructed with the convenience of the user in mind so that only the minimum amount of data need to be read in.

Modifications to modules of the code, the addition of permanent features, and options must be clearly identified to the user. The pertinent features of the code are therefore encapsulated in separate modules; these modules can be pulled out and new ones plugged in without interfering with other parts of the code, except those where they interact (usually subroutine calls). It is with the fulfilment of these important characteristics that FELTRAN has been constructed. FELTRAN is the acronym for Finite ELement Techniques for solving TRANsport Problems.

In the construction of any code there has to be several characteristic stages, and Fig.4.8 serves to outline these pertinent features in the finite element analysis. The mesh generation stage can be very simple or complicated depending upon the geometry of the problem, the type of elements to be used and the mesh refinement required. In the present thesis since we are restricted to simple geometries and elements this aspect is not too complicated. The post-processing stage is usually not part of the computer code because, depending on the nature of the problem, the manner in which the solutions are edited can be quite varied. Therefore if post-processing edits are required these numerical values are usually written to an external device and stored. They are then retrieved and manipulated. For example they can be set up so that they can be automatically plotted or they can be used to calculate power ratios in different regions of a reactor core.

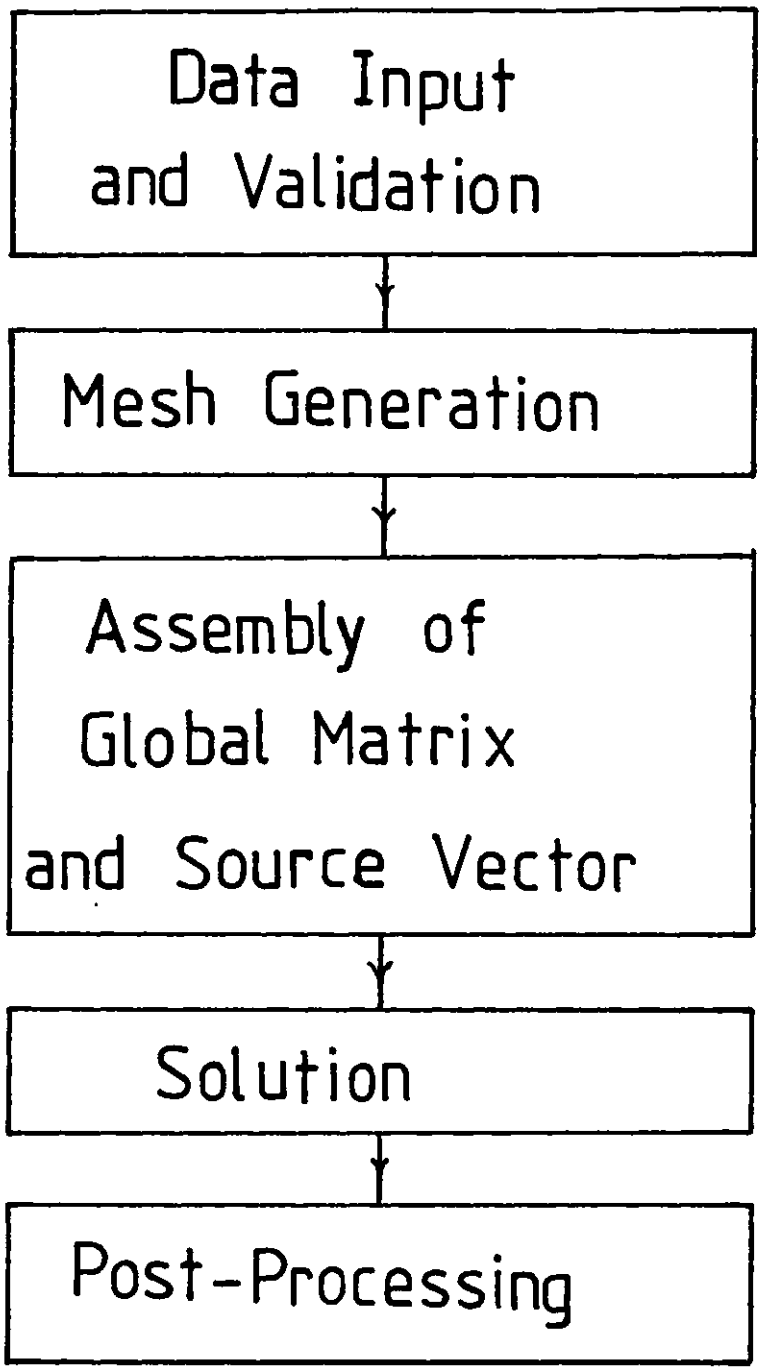

Fig.4.8 Main features in a finite element analysis

Fig.4.9 outlines the major modules that exist in FELTRAN. The DATA Module is concerned with data input and validation. INIT handles all the initialisation of variables that will be used later on in the program. The mesh is generated in MESH while SHAPE calculates the integrals for the shape functions. The assembly of the global stiffness matrix and source vector is handled by ASSEM.

After the ASSEM module there is a branch out into FIXSOR, which handles fixed source problems, and EIGENV where eigenvalue problems are solved. The details of both these modules are shown in Figs.4.10 and 4.11 and as can be seen some of the modules are common to both FIXSOR and EIGEN .

In FIXSOR the solution cycle is simple and straightforward. For each neutronic group starting from the fastest, the global matrix and source vector are assembled and solved. In EIGENV the global matrices for each group are first assembled, triangularised and then shifted to any external tape. This process necessarily saves computing time because the global matrices for each group are not assembled at each and every iteration. Also triangularisation is not repeated. Naturally the source vector is not stored as they are updated at every iteration.

Since SESOL is only used for fixed source problems Fig.4.12 shows how FIXSOR has been transformed to include SESOL. There is an inner loop over the number of blocks for the assembly stage which is available within the SESOL module.

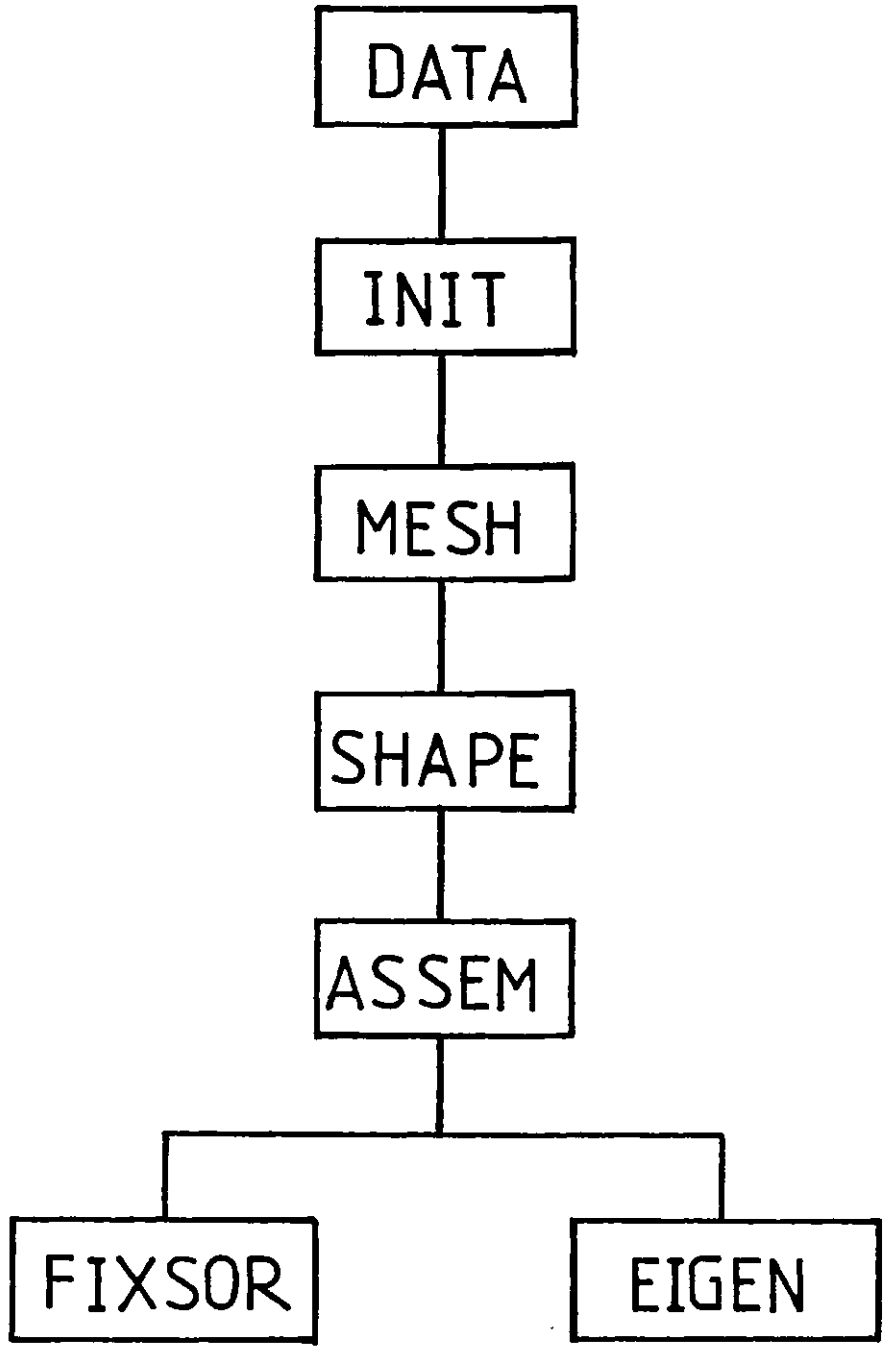

Fig.4.9 Major modules of FELTRAN

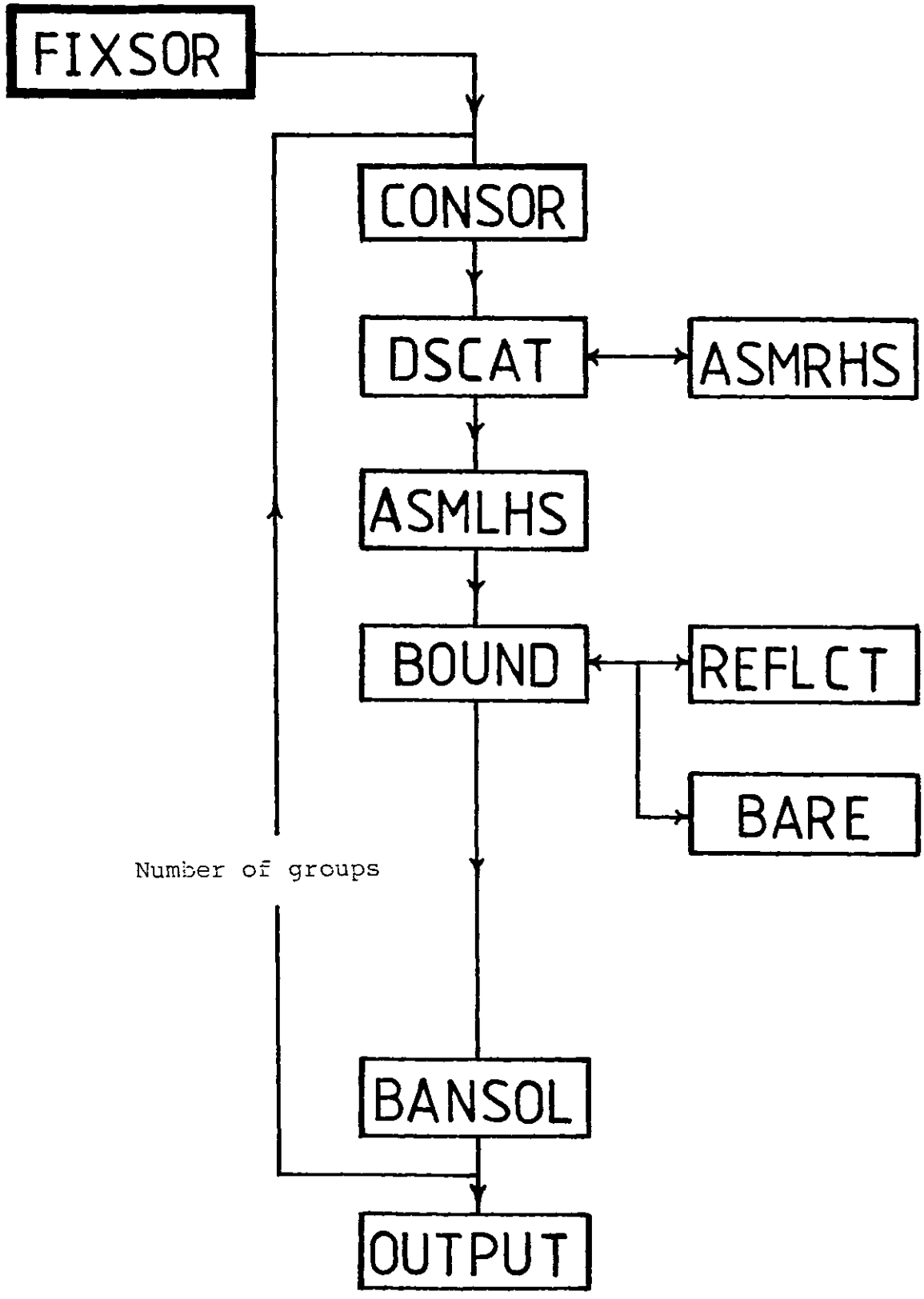

Fig.4.10 Outline of FIXSOR

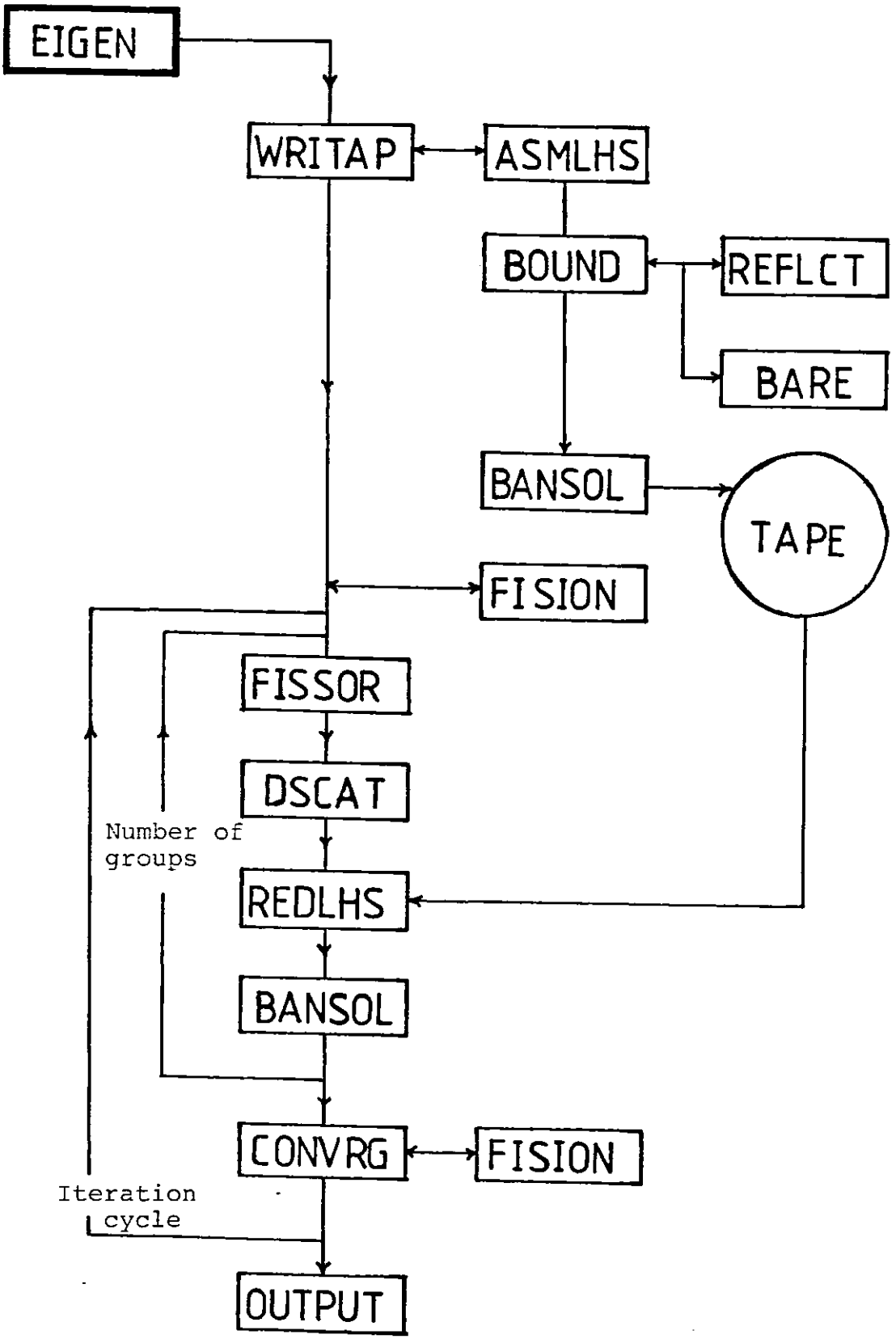

Fig.4.11 Outline of EIGEN

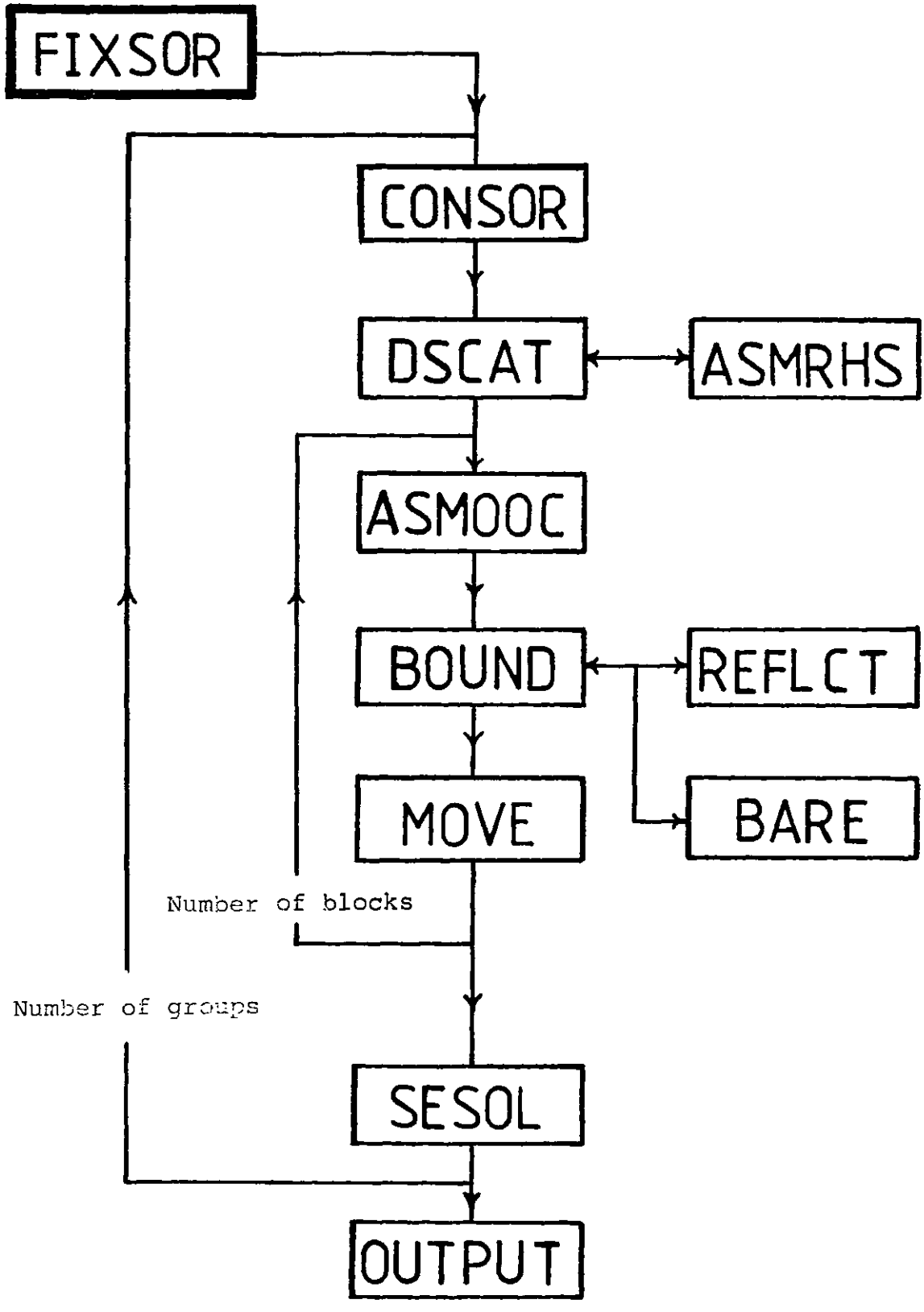

Fig.4.12 Adaptation of FIXSOR to accommodate SESOL

Finally it must be mentioned that in implementing and validating FELTRAN the CDC 6600 and AMDAHL 470/V8 computers at the University of London Computer Centre were used. Of particular importance was the AMDAHL computer in the sense that it provided an available primary storage of 8 Megabytes. In single precision arithmetic this is equivalent to 2 million storage locations, while it is 1 million for double precision arithmetic. When using the AMDAHL the source problems were performed by using single precision arithmetic whereas with the eigenvalue problems double precision arithmetic was used. The precision on the AMDAHL are 6 and 15 decimal places for single and double precision arithmetic respectively. Evidence that single precision arithmetic is accurate enough for source problems is shown in Section 5.7. For the CDC computer only single precision arithmetic is used since this is accurate to 14 decimal places. Besides these two computers at the University of London Computer Centre the CDC 6500 and CDC Cyber 174 at Imperial College were used especially for the smaller sized jobs.

CHAPTER 5

RESULTS

"Trying to find the solution, we may repeatedly change our point of view, our way of looking at the problem. We have to shift our position again and again. Our conception of the problem is likely to be incomplete when we start the work; our outlook is different when we have made some progress; it is again different when we have almost obtained the solution."

George Polya [79]

5.1 Introduction

In the last chapter the major modules of FELTRAN were outlined and the manner in which they were implemented shown. The success or failure of the implementation can be judged from the results produced by FELTRANwhen compared against results produced by established methods or those that are deemed accurate. Therefore accuracy is the most important factor otherwise FELTRAN cannot be said to be successfully implemented. There are also problems which cannot be solved successfully or which demand constraints on available resources. If FELTRAN can overcome these problems then it would not only be judged as accurate but it could be regarded as a potential for replacing the established methods when it comes to solving these difficult problems.

Seven problems are considered in this chapter. The first five are eigenvalue problems while the last two are fixed source problems. Eigenvalue problems are particularly interesting in the fact that values of k_{eff} are very sensitive and provides a gauge to the accuracy of the method. All the problems are multiregional and, with the exception of one, multigroup.

5.2 The ZION-1 Reactor

The quarter-core layout of the ZION-1 reactor is shown in Fig.5.1. ZION-1 is a modern PWR with a nominal capacity of 3250 MW (th). This is essentially a multi-region, two-group diffusion problem. There are three

Material legend:

1,2,3 - Fissile material of different enrichment
4 - Baffle
5 - Water

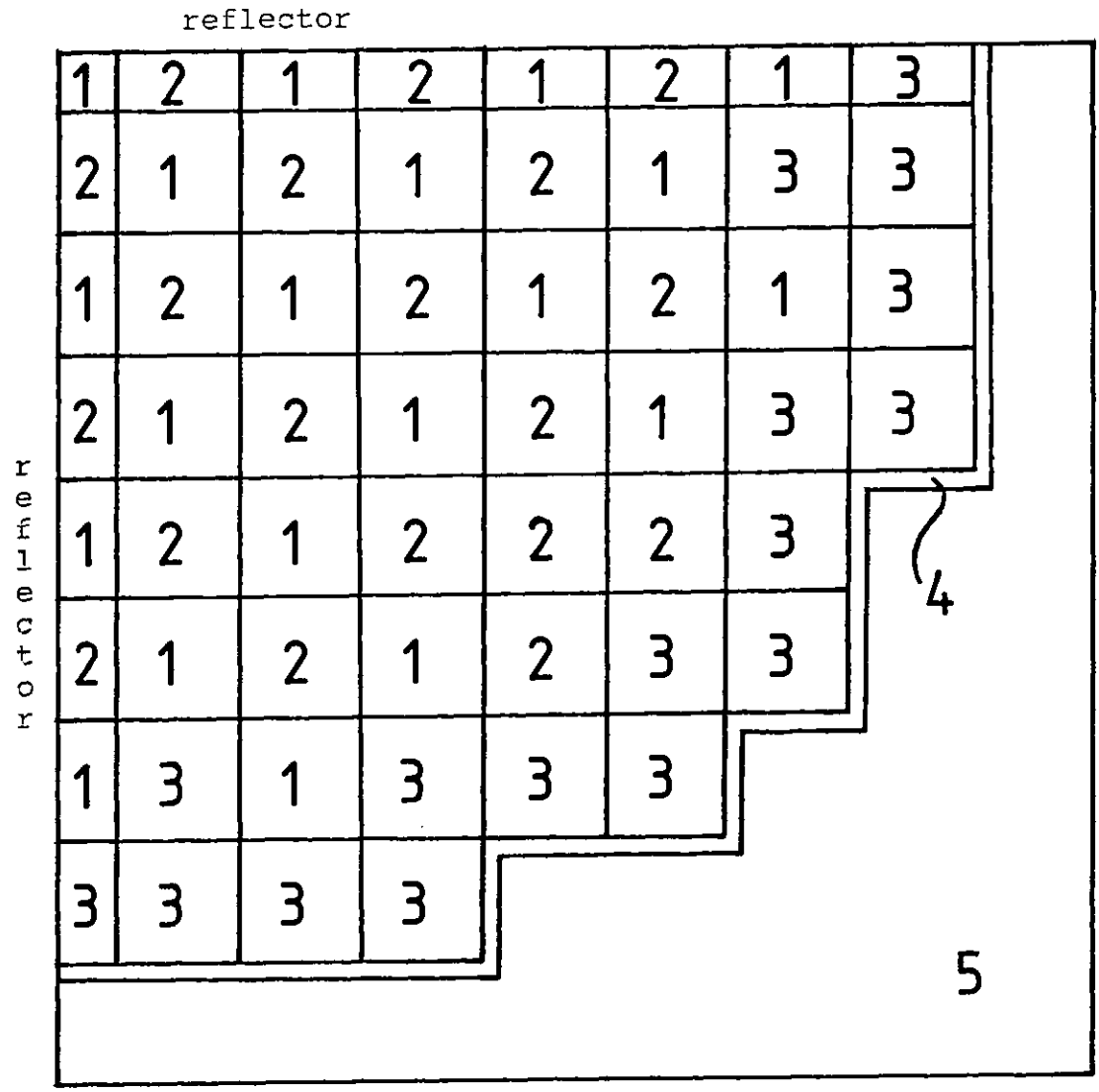

Fig.5.1 Quarter-core layout of the ZION-1 Reactor

types of materials in the fissile core whose differences lie in the degree of enrichment. A thin stainless steel baffle serves to separate this region from the water moderator. A composition number serves to identify each of the material present.

The dimensions of each composition region are illustrated in Fig.5.2. Only a sketch of the horizontal dimensions along the centre core line are shown. However owing to symmetry the vertical dimensions are the same.

Reflector conditions exist on the interior surfaces of the quarter-core layout. The exterior surfaces are subjected to zero flux boundary conditions. Bare surface conditions could have been imposed but results reported for this problem were those for the zero flux condition. The cross-sectional data are shown in Table 5.1. At this juncture a brief note must be made on the representation of the numbers under the heading POS. Let k represent any number under POS. When k = 1, the inference is that fission cross-sections $(\omega\Sigma_{f_g})$ are represented. Total cross-sections (Σ_{t_g}) are represented when k = 2 whilst for k = 3 we have the within-group scattering cross-section $(\Sigma_{s_{gg}})$. When $k \geqslant 4$ the representations are for the inter-group cross-sections. The representation refers to $\Sigma_{s_{ij}}$ where j assumes the value of the column number and $i = k - 3$, and $j > i$. Therefore, referring to Table 5.1, the non-zero entry when k = 4 refers to $\Sigma_{s_{12}}$. The cross-sections referred to in this chapter are the macroscopic cross-sections with dimensions of cm^{-1}.

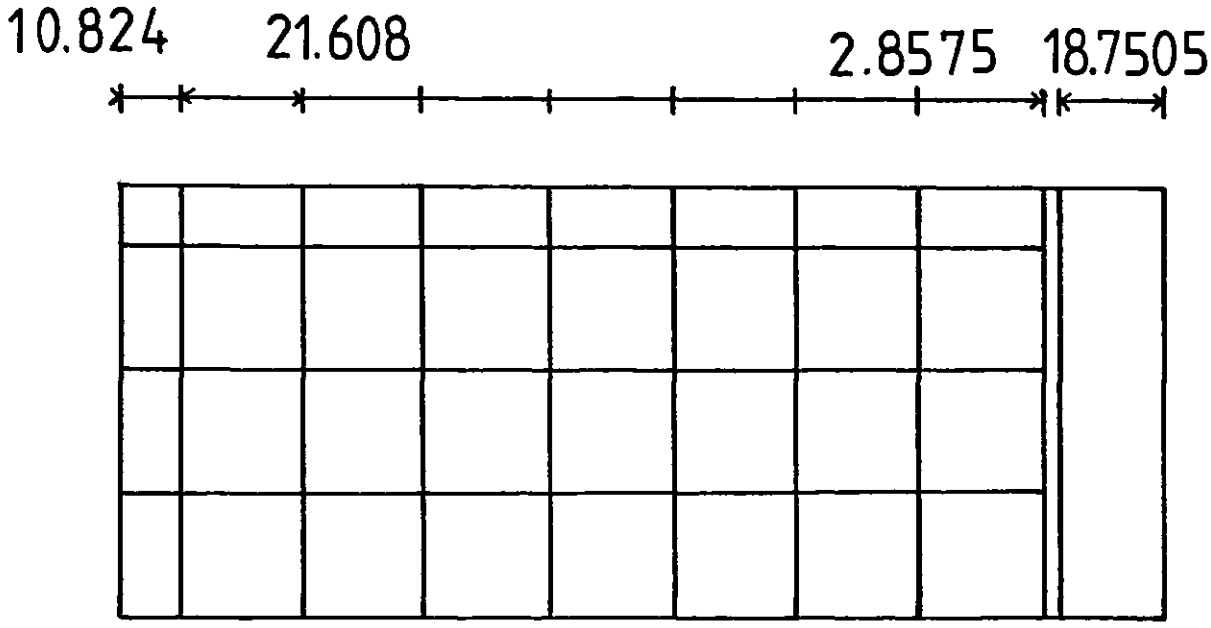

Fig.5.2 Dimensions (cm) of the composition regions in the ZION-1 reactor

TABLE 5.1

CROSS-SECTIONAL DATA FOR THE ZION-1 REACTOR

CROSS-SECTIONS

REGION NO 1

POS	GROUP 1	GROUP 2
1	5.3600E-03	1.0433E-01
2	2.3514E-01	8.9282E-01
3	2.0917E-01	8.2613E-01
4	0	1.7420E-02

REGION NO 2

POS	GROUP 1	GROUP 2
1	6.0100E-03	1.2472E-01
2	2.3479E-01	8.9198E-01
3	2.0903E-01	8.1592E-01
4	0	1.6940E-02

REGION NO 3

POS	GROUP 1	GROUP 2
1	6.5300E-03	1.4120E-01
2	2.3367E-01	8.9069E-01
3	2.0807E-01	8.0710E-01
4	0	1.6580E-02

REGION NO 4

POS	GROUP 1	GROUP 2
1	0	0
2	3.2638E-01	9.9360E-01
3	3.2316E-01	8.4764E-01
4	0	0

REGION NO 5

POS	GROUP 1	GROUP 2
1	0	0
2	2.2903E-01	1.1497E+00
3	1.9953E-01	1.1402E+00
4	0	2.9030E-02

FISSION SPECTRUM

GROUP 1	GROUP 2
1.0000E+00	0

This problem was first reported by Deppe and Hansen [25] when they compare finite element against finite difference results. Later on Komoriya and Walters[56] solved this problem with their own version of the finite element method and, as of late, Greenstadt [38] has analysed the problem using the cell discretization method, a technique not unlike the finite element method. Before comparing the results from FELTRAN against these reported results a brief description of these methods will first be presented.

The finite difference results were achieved using the codes PDQ-5 [40] and CITATION [30]. The results quoted from these codes were obtained from using finer mesh intervals, and therefore more mesh points, than the finite element results.

Deppe and Hansen used Hermite-type piecewise bi-cubic elements. Hermitian elements allow the preservation of the flux derivatives across the element interfaces but necessitates additional computations when compared with Lagrangian elements. The presence of the core baffle (as seen in Fig.5.1) disturbed the regular structure of the fuel elements which would otherwise have provided an excellent partition for the problem. Deppe and Hansen "defined a region with varying parameters on the outside of the core to include both baffle and water" in order to prevent what would otherwise have been a finer mesh. The alternative method is to homogenise the baffle and water. This latter alternative is attempted in the

FELTRAN results. In all Deppe and Hansen tried 3 different meshes of (10 x 10), (7 x 7) and (6 x 6). In the coarser meshes each element would contain contributions from different materials. Deppe and Hansen produced their results using their code called CHD.

Komoriya and Walters used Lagrangian bi-quadratic elements. However they also investigated energy-dependent spatial mesh schemes in which a finer mesh was used for the thermal group. This scaling was merited on the basis that the neutron diffusion length is generally smallest in the lower energy group and largest in the fast groups. Conventionally the finite element method has adhered to similar mesh sizes for all energy groups. The results were obtained by using a code called EDFEM (Energy Dependent Finite Element Method). In all they reported mesh refinements of L/8 (1 - 1), L/4 (1 - 2) and L/4 (1 - 1). For example in L/8 (1 - 1) the mesh refinement is (8 x 8) and the mesh is similar for both groups while in L/4 (1 - 2) the mesh is (4 x 4) for the fast group and (8 x 8) for the thermal group. No mention was made on how to account for the different compositions in an element or the baffle/water arrangement.

Finally, in the Cell Discretization (CD) method the similarity with finite elements lie in the subdivision of the problem domain into smaller regions called cells. The difference lies in the fact that approximations need not be polynomials and no attempt was made to establish *a priori* elemental continuity. However Greenstadt [39]

has established mathematically the distinction between CD and finite elements. The important concept in CD lies in the number of interfaces between the adjacent cells and also the number of interface conditions at each interface. The product gives the total number of unknowns for the problem. Greenstadt analysed the problem using 169 cells because of the presence of the baffle. However a "synthetic method" was introduced by constructing mixed interface conditions in order to homogenise the baffle with the water. This arrangement results in 81 cells.

In all eight sets of results were reported using FELTRAN using two different meshes. In the first instance no attempt was made to homogenise the baffle with the water. Such an arrangement results in a grid of (13 x 13) elements as shown in Fig.5.3 in which there is a presence of small and thin rectangular elements. An attempt was made at homogenising the baffle/water system which reduces the grid to (9 x 9) elements. The resulting system is shown in Fig.5.4. However homogenisation results in three new materials numbered from 6 to 8 whose percentile compositions are shown in Table 5.2. For each mesh specification results were reported using linear, quadratic and triangular elements.

The values of k_{eff} obtained from all the different codes are shown in Table 5.3. The following points should be noted: (i) the meshes referred to for PDQ-5 and CITATION are with respect to nodal points; (ii) the

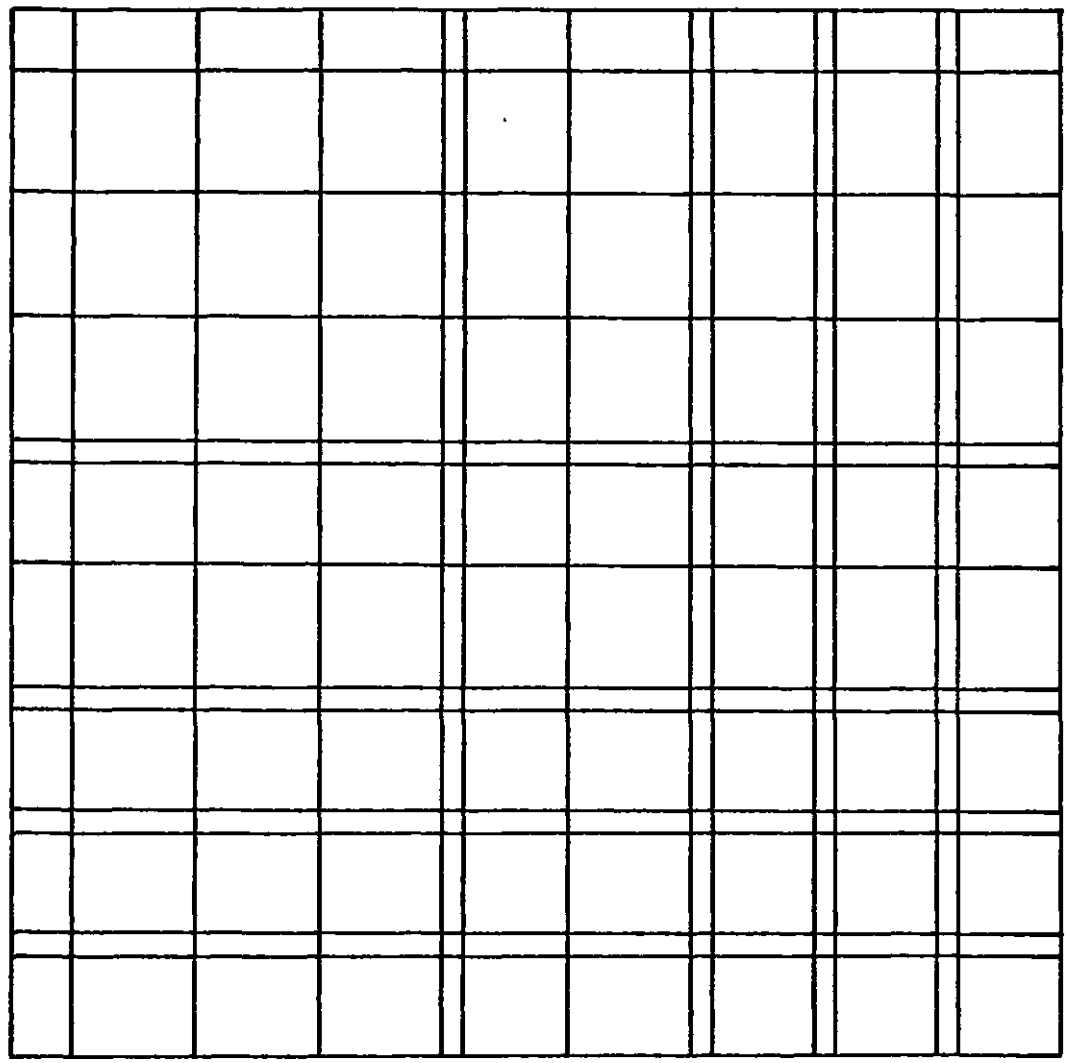

Fig.5.3 Mesh layout for unhomogenised arrangement of (13 x 13) elements

1	2	1	2	1	2	1	3	6
2	1	2	1	2	1	3	3	6
1	2	1	2	1	2	1	3	6
2	1	2	1	2	1	3	3	6
1	2	1	2	2	2	3	7	8
2	1	2	1	2	3	3	6	5
1	3	1	3	3	3	7	8	5
3	3	3	3	7	6	8	5	5
6	6	6	6	8	5	5	5	5

Fig.5.4 Mesh layout for homogenised arrangement of (9 x 9) elements

TABLE 5.2

COMPOSITION OF HOMOGENISED REGIONS

Material No.	% Baffle	% Water
6	15.24	84.76
7	24.70	75.30
8	1.75	98.25

TABLE 5.3

COMPARISON OF k_{eff} FROM VARIOUS CODES

Code	Run No.	Mesh	No. of Unknowns per Group	Element Type	k_{eff}
PDQ-5	1	44 x 44	1936	-	1.2749
CITATION	1	44 x 44	1936	-	1.27313
	2	75 x 75	5625	-	1.27508
CHD	1	10 x 10	348	Hermite Cubic	1.27469
	2	7 x 7	190	Hermite Cubic	1.27474
	3	6 x 6	128	Hermite Cubic	1.27554
EDFEM	1	L/8 (1-1)	289-289	Quadratic	1.27502
	2	L/4 (1-2)	81-289	Quadratic	1.27453
	3	L/4 (1-1)	81-81	Quadratic	1.27529
CD	1	13 x 13	312	-	1.275068
	2	13 x 13	624	-	1.274896
	3	13 x 13	936	-	1.274893
	4	13 x 13	1248	-	1.274890
	5	13 x 13	1560	-	1.274874
	6	9 x 9	576	-	1.274494
FELTRAN	1	13 x 13	196	Linear	1.27509
	2	13 x 13	729	Quadratic	1.27478
	3	13 x 13	1600	Cubic	1.27472
	4	26 x 13	196	Triangular	1.27462
	5	9 x 9	100	Linear	1.27408
	6	9 x 9	361	Quadratic	1.27392
	7	9 x 9	784	Cubic	1.27400
	8	18 x 9	100	Triangular	1.27340

convergence criterion on k_{eff} was 10^{-7} for the CD results and 10^{-5} for the FELTRAN results while no mention was made in the other results.

As can be seen the values of k_{eff} obtained from the various codes agree very well with each other, the difference lying in the order of up to 0.2%. In the FELTRAN results the k_{eff}'s from the unhomogenised system are larger than those from the homogenised system. Also the results for the quadratic and cubic elements are almost identical indicating that quadratic elements are suitable for such analyses and that there is no necessity in using higher ordered elements.

Table 5.4 shows the execution times and the number of outer iterations for the FELTRAN results. In all the runs the initial guess was 1.0 for k_{eff} and the fluxes. This is also the starting guess for all the subsequent FELTRAN results in the sections to come where eigenvalue problems are discussed. The number of outer iterations is quite high, being higher for the homogenised baffle/water results. Naturally if the initial guess on k_{eff} was nearer 1.274 rather than unity the number of iterations would be considerably lower. Also, in the outer iterations no attempt was made to accelerate the convergence on k_{eff} like, for example, in the CD results. Greenstadt reported that by using the method of dominance ratio to speed up the convergence in the outer iterations an improvement of 2 to 3 times was obtained. However none of the other results (other

than FELTRAN) quoted the number of outer iterations.

The FELTRAN results in Table 5.4 are quoted in CDC 6600 seconds. Only Run 3 was achieved by using the AMDAHL computer. A conversion factor of 8 was used in converting the AMDAHL time to equivalent CDC 6600 seconds. This factor was made by comparing the run times by running an identical case on both machines. No attempt was made to optimise the compilation in the FELTRAN results (except for the AMDAHL run). A factor of 3 to 4 times increase in speed [43] can be reported if an optimisation compiler such as FTN5, was used.

None of the other reports quoted their execution times except for Greenstadt who ran the CD results on an IBM 370/158. For comparison purposes, Greenstadt has quoted an approximate execution time of 10 sec when two (100 x 100) matrices are multiplied. The equivalent time for this matrix multiplication on the CDC 6600 is approximately 5 sec. Therefore basing on this factor of 2 in favour for the speed on the CDC 6600, Table 5.5 tabulates the execution times for the CD results in both IBM 370 and CDC 6600 seconds. It can be mentioned that basing on the number of unknowns per energy group FELTRAN performs better than CD. However the comparison cannot be taken at face value because of the following reasons: (i) FELTRAN execution times are reported with a non-optimising compiler while CD results were obtained with an optimising compiler; (ii) the convergence criterion

TABLE 5.4

EXECUTION TIMES AND NUMBER OF OUTER ITERATIONS

FOR FELTRAN RESULTS

Run No.	Number of Iterations	Execution Time (CDC 6600 sec)	Time per Iteration (CDC 6600 sec)
1	32	9.39	0.29
2	44	114.45	2.60
3	42	440.96*	10.50
4	32	10.37	0.32
5	61	8.06	0.13
6	59	59.41	1.01
7	59	95.57	1.62
8	60	7.50	0.13

*55.12 sec on the AMDAHL

TABLE 5.5

COMPARISON OF EQUIVALENT EXECUTION TIMES

FROM CD AND FELTRAN RUNS

Run No.	Execution Time (IBM 370/158 sec)	Execution Time (CDC 6600 sec)
1	152	76
2	420	210
3	1106	553
4	1293	646.5
5	3442	1721
6	537	268.5

on k_{eff} was finer in CD (being 10^{-7} against 10^{-5} in FELTRAN; (iii) convergence technique was used to accelerate the outer iterations in CD; (iv) a direct elimination algorithm (BANSOL) was used in solving the set of equations in FELTRAN while CD utilised the generalised conjugate gradient (GCG) method which is an iterative technique.

Deppe and Hansen performed power calculations. Rather, the region-averaged to core-averaged power ratios were calculated. Fig.5.5 is a reproduction of their results for the (10 x 10) mesh compared against CITATION (75 x 75) and PDQ-5 (44 x 44) results.

The power in a region of volume V_k is given by the expression:

$$P_k = \alpha \int_{V_k} \sum_{g=1}^{G} \omega \Sigma_{f_g} \phi_g \, dV \qquad (5.1)$$

where,

α = conversion factor from fission rate into equivalent power units.

Since,

$$\phi_g = \sum_{i=1}^{L} N_i u_{g_i} \qquad (5.2)$$

$$\therefore P_k = \alpha \int_{V_k} \sum_{g=1}^{G} \omega \Sigma_{f_g} \sum_{i=1}^{L} N_i u_{g_i} \, dV \qquad (5.3)$$

or,

$$P_k = \alpha \int_0^{x_k} \int_0^{y_k} \sum_{g=1}^{G} \omega \Sigma_{f_g} \sum_{i=1}^{L} N_i u_{g_i} \, dx \, dy \qquad (5.4)$$

where,

x_k, y_k being the dimensions of the region .

Finally,

$$P_k = \alpha \sum_{g=1}^{G} \omega \Sigma_{f_g} \sum_{i=1}^{L} U_i u_{g_i} \qquad (5.5)$$

where,

$$U_i = \int_0^{x_k} \int_0^{y_k} N_i \, dx \, dy \qquad (5.6)$$

$$\therefore \bar{P}_{core} = \sum_{k=1}^{R} P_k / V_{core} \qquad (5.7)$$

where,

R = no. of regions in the core

Hence,

$$\bar{P}_k = \frac{P_k}{V_k \bar{P}_{core}} \qquad (5.8)$$

will give the region averaged to core-averaged power ratio.

	1	2	3	4	5	6	7	8
1	1.6271 1.6361 1.6524	1.7590 1.8002 1.8108	1.5320 1.5387 1.5524	1.5519 1.5856 1.5918	1.2537 1.2560 1.2623	1.1587 1.1758 1.1742	0.8039 0.7904 0.7896	0.5115 0.4954 0.4871
2		1.5800 1.5873 1.6025	1.6563 1.6951 1.7038	1.3945 1.3990 1.4087	1.3556 1.3818 1.3841	1.0372 1.0318 1.0339	0.9166 0.9200 0.9186	0.4970 0.4786 0.4705
3			1.4452 1.4490 1.4603	1.4664 1.4966 1.5023	1.1831 1.1813 1.1859	1.0779 1.0903 1.0878	0.7262 0.7092 0.7078	0.4455 0.4285 0.4206
4				1.2447 1.2439 1.2493	1.2123 1.2255 1.2257	0.9001 0.8872 0.8869	0.7216 0.7123 0.7067	0.3233 0.3013 0.2911
5					1.0777 1.0749 1.0747	0.8526 0.8401 0.8379	0.5340 0.5104 0.5019	
6						0.6682 0.6516 0.6462	0.3277 0.3042 0.2947	
7								
8								

KEY

CITAT.	(75 x 75)
PDQ-5	(44 x 44)
CHD	(10 x 10)

Fig.5.5 Deppe and Hansen's results for region-averaged to core-averaged power ratios

1.6503	1.8873	1.5446	1.6849	1.2622	1.2344	0.7446	0.4422
1.5923	1.7512	1.5155	1.5755	1.2654	1.1877	0.7954	0.4822
1.5834	1.7387	1.5076	1.5670	1.2619	1.1863	0.7993	0.4883
	1.5907	1.7927	1.4037	1.4645	1.0170	0.9364	0.4125
	1.5545	1.6687	1.3972	1.3904	0.0460	0.9271	0.4671
	1.5460	1.6587	1.3913	1.3863	1.0467	0.9293	0.4719
		1.4553	1.5918	1.1853	1.1332	0.6570	0.3784
		1.4424	1.5009	1.1975	1.1054	0.7133	0.4157
		1.4355	1.4947	1.1958	1.1059	0.7180	0.4223
			1.2399	1.2783	0.8540	0.6864	0.2431
			1.2607	1.2476	0.9021	0.7120	0.2890
			1.2573	1.2467	0.9057	0.7172	0.2942
				1.0836	0.8111	0.4529	
				1.1008	0.8531	0.5054	
				1.1004	0.8580	0.5115	
					0.5933	0.2389	
					0.6548	0.2943	
					0.6577	0.2999	

Key

LINEAR
QUAD.
CUBIC

Fig.5.6 FELTRAN's results for region-averaged to core-averaged power ratios

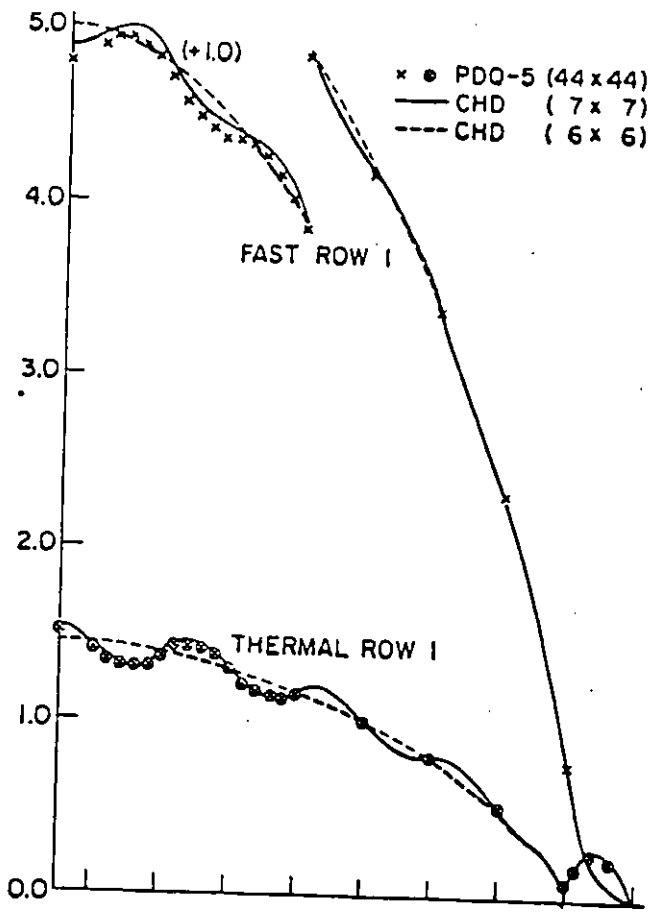

Fig.5.7 Flux plots from Deppe and Hansen

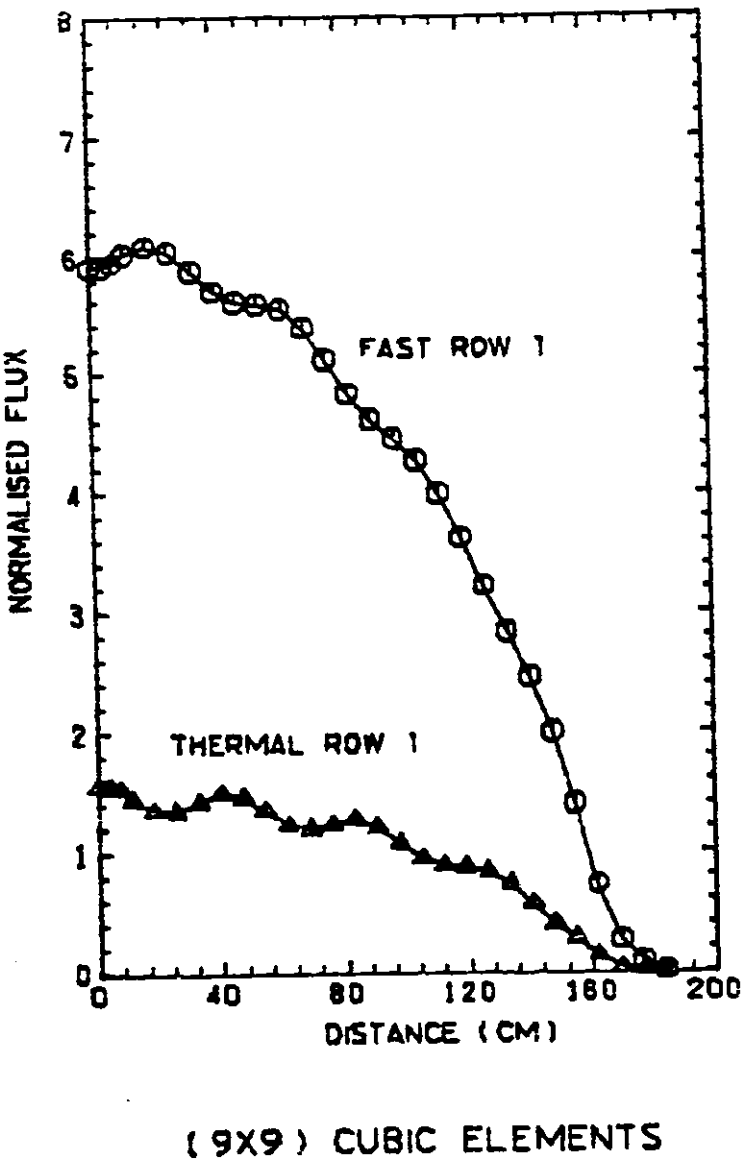

Fig.5.8 Flux plots from FELTRAN

Fig.5.6 shows the values of $\bar{P}_k$ for the homogenised baffle/water system from FELTRAN. As can be seen closer agreement was obtained for quadratic and cubic elements as contrasted against linear elements. Comparing Figs.5.5 and 5.6 it can be seen that the FELTRAN results for both quadratic and cubic elements agree well with the results quoted by Deppe and Hansen. In particular the PDQ-5 and CHD results show closer agreement with FELTRAN higher ordered elements. Any differences between these two sets of results can be attributed to the different methods of homogenising the baffle/water arrangement.

To conclude this section Figs.5.7 and 5.8 show the plot of the fluxes from Deppe and Hansen's study and FELTRAN (Run 7) respectively. The similarity in the flux profiles reflect the excellent agreement.

5.3 A 4-Group Multiregion Diffusion Problem

This problem was first reported by Kaper, Leaf and Lindeman [51]. Fig.5.9 is a quarter-core representation of the geometry and material properties of the problem which is a mockup of a typical oxide-fuelled liquid metal fast breeder reactor. In all there are five different material regions whose cross-sections are represented by four energy groups which were obtained from the Argonne National Laboratory (ANL) data by averaging and collapsing techniques. The aim of this analysis is to determine the value of k_{eff} for the system shown in Fig.5.9. The interior boundaries are reflectors while vacuum conditions are considered for the exterior boundaries.

Material legend:

1 - Core 1
2 - Blanket 1
3 - Reflector
4 - Core 2
5 - Blanket 2

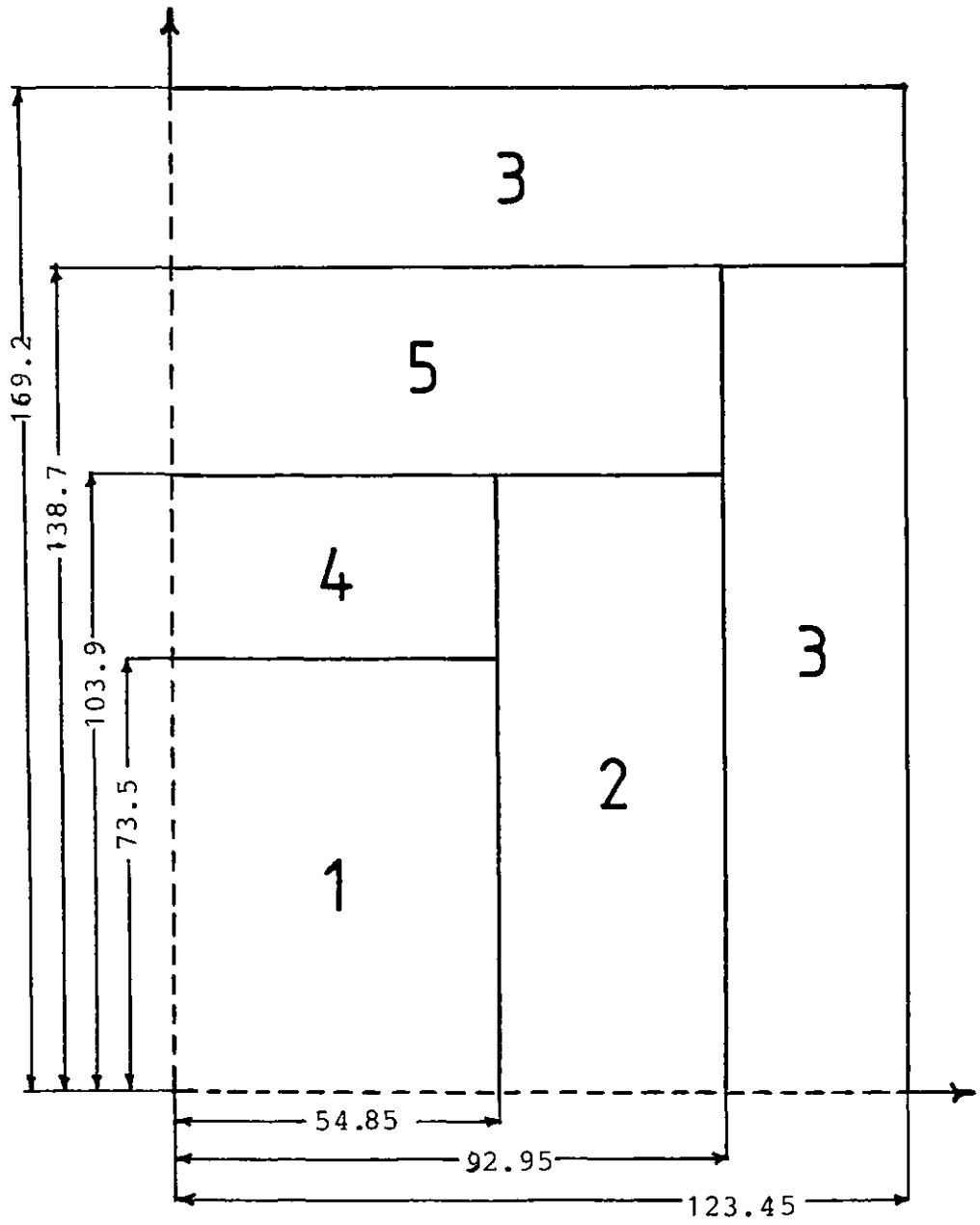

Fig.5.9 Typical quarter-core oxide-fuelled LMFBR configuration (dimensions in cm)

In the study by Kaper et al, results from low order finite difference approximations and high order finite element approximations were presented. The finite difference results were obtained from the DARC2D [48] code while the finite element results were produced by HOD, which is a two-dimensional multigroup high order diffusion program adapted from a finite element program originally written by George [35]. DARC2D was the production program in the Argonne Reactor Computation (ARC) System for two-dimensional diffusion calculations at the Argonne National Laboratory. The objective of the study by Kaper et al was to determine a timing comparison between low order finite difference approximations and high order finite element approximations. The low order finite difference approximation in DARC2D was achieved by using a five-point difference approximation while in the high order finite element approximations triangular elements of up to quintic polynomial representations were used. In all seven sets of results were reported for DARC2D ranging from 48 to 1452 mesh cells. Six sets of results were quoted for HOD using quadratic to quintic triangular elements and two meshes of 17 and 24 elements. In all runs the convergence criterion on k_{eff} was 10^{-5} except in the case of the quintic elements where it was 10^{-10}. Kaper et al considered the quintic result using 24 elements as their benchmark value.

Greenstadt [38], whose Cell Discretization method was described in the previous section, has also reported the values of k_{eff} for this problem. He only used one type of mesh, i.e. one of (3 x 4) cells, but with interface

conditions ranging from 1 to 5. The convergence criterion on k_{eff} was, as in the previous example, 10^{-7}.

When FELTRAN was used to analyse this problem the linear, quadratic and cubic elements were used as well as the triangular elements. Three meshes of (3 x 4), (6 x 8) and (12 x 16) were used for the rectangular elements while the corresponding elemental mesh for the triangular elements were (6 x 4), (12 x 8) and (24 x 16). The (3 x 4) mesh is depicted in Fig.5.10. The finer meshes are built up in a proportionate manner from this basic mesh. The reason for attempting such a fine mesh refinement for this problem was that since this particular problem is especially suited for mesh refinement in a "doubling" manner, it was desirable to see the manner in which k_{eff} was behaving when such mesh refinements were carried out. The convergence criterion on k_{eff} was 10^{-5} and in all runs the initial guess for k_{eff} was 1.0.

Table 5.6 shows the cross-sections associated with this problem.

Table 5.7 shows the values of k_{eff} reported from the various codes. As can be seen FELTRAN results for quadratic and cubic elements agree very well with the CD and HOD values while the k_{eff} for the linear elements (for both rectangular and triangular) are approaching a higher value with increasing mesh refinement. This indicates the accuracy afforded by higher order elements even with a very coarse mesh. If one were to accept Kaper et al's value of 1.056992 as the benchmark value then Table 5.8 indicates the percentage deviation of the FELTRAN values for k_{eff} from the benchmark.

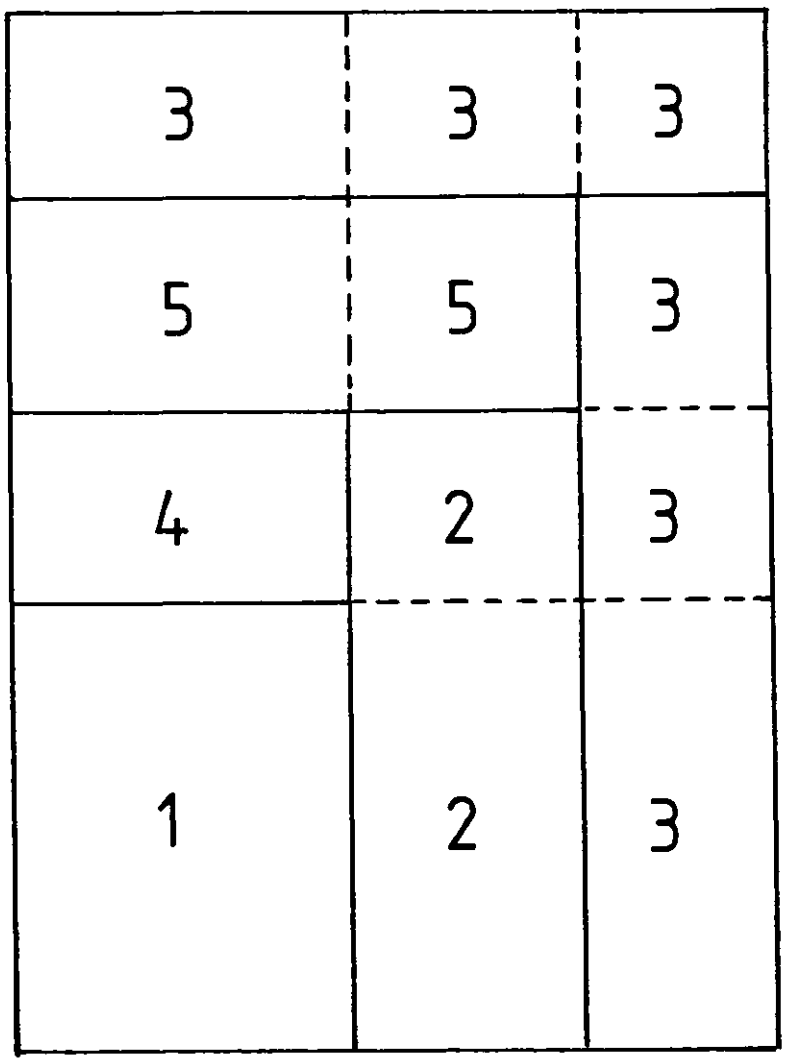

Fig.5.10 The (3 x 4) mesh of rectangular elements used in FELTRAN

TABLE 5.6

CROSS-SECTIONAL DATA FOR THE 4-GROUP

DIFFUSION PROBLEM

CROSS-SECTIONS

REGION NO 1

POS	GROUP 1	GROUP 2	GROUP 3	GROUP 4
1	1.7811E-02	4.7769E-03	6.3202E-03	2.4478E-02
2	1.1676E-01	2.2193E-01	3.4858E-01	3.5097E-01
3	7.2352E-02	2.1436E-01	3.3785E-01	3.2258E-01
4	0	3.7673E-02	4.1582E-03	1.8005E-03
5	0	0	1.9084E-04	3.0708E-07
6	0	0	0	1.3105E-08

REGION NO 2

POS	GROUP 1	GROUP 2	GROUP 3	GROUP 4
1	1.4126E-02	8.3826E-04	1.0735E-03	4.2049E-03
2	1.2268E-01	2.3409E-01	3.6316E-01	3.4522E-01
3	7.4933E-02	2.2764E-01	3.5444E-01	3.2905E-01
4	0	4.1965E-02	4.3170E-03	1.7933E-03
5	0	0	2.2105E-04	1.7578E-07
6	0	0	0	0

REGION NO 3

POS	GROUP 1	GROUP 2	GROUP 3	GROUP 4
1	0	0	0	0
2	1.1317E-01	1.7762E-01	3.6705E-01	4.1154E-01
3	8.2292E-02	1.7456E-01	3.6420E-01	4.0703E-01
4	0	3.0282E-02	2.8252E-03	1.6299E-03
5	0	0	7.2047E-05	0
6	0	0	0	0

REGION NO 4

POS	GROUP 1	GROUP 2	GROUP 3	GROUP 4
1	1.9505E-02	6.1077E-03	8.0891E-03	3.1306E-02
2	1.1670E-01	2.2178E-01	3.4887E-01	3.5633E-01
3	7.2383E-02	2.1376E-01	3.3741E-01	3.2424E-01
4	0	3.7094E-02	4.1507E-03	1.8030E-03
5	0	0	1.8535E-04	3.0817E-07
6	0	0	0	1.3648E-08

REGION NO 5

POS	GROUP 1	GROUP 2	GROUP 3	GROUP 4
1	1.7301E-02	1.3584E-03	1.7672E-03	6.9204E-03
2	1.3259E-01	2.5603E-01	3.8695E-01	3.6959E-01
3	7.9093E-02	2.4868E-01	3.7668E-01	3.4972E-01
4	0	4.6522E-02	4.6940E-03	1.9052E-03
5	0	0	2.5647E-04	2.0861E-07
6	0	0	0	0

FISSION SPECTRUM

GROUP 1	GROUP 2	GROUP 3	GROUP 4
5.8815E-01	4.0819E-01	3.6383E-03	1.9472E-05

TABLE 5.7

COMPARISON OF k_{eff} FROM VARIOUS CODES

Code	Run No.	Mesh	No. of Unknowns Per Group	Element Type	k_{eff}
DARC2D	1	6 x 8	48	-	1.067176
	2	10 x 14	140	-	1.064142
	3	14 x 20	280	-	1.058874
	4	20 x 28	560	-	1.057842
	5	25 x 36	900	-	1.057838
	6	29 x 40	1160	-	1.057414
	7	33 x 44	1452	-	1.057298
HOD	1	17	46	Quad.Tri.	1.056700
	2	24	63	Quad.Tri.	1.056851
	3	17	94	Cubic Tri.	1.057007
	4	17	159	Quartic.Tri.	1.056995
	5	17	241	Quintic.Tri.	1.056992
	6	24	336	Quintic.Tri.	1.056992
CD	1	3 x 4	17	-	1.059819
	2	3 x 4	34	-	1.057063
	3	3 x 4	51	-	1.057005
	4	3 x 4	68	-	1.056995
	5	3 x 4	85	-	1.056995
FELTRAN	1	3 x 4	20	Linear Rect.	1.036018
	2	3 x 4	63	Quad.Rect.	1.057073
	3	3 x 4	130	Cubic Rect.	1.057156
	4	6 x 4	20	Linear Tri.	1.032673
	5	6 x 8	63	Linear Rect.	1.052499
	6	6 x 8	221	Quad.Rect.	1.057139
	7	6 x 8	475	Cubic Rect.	1.057106
	8	12 x 8	63	Linear Tri.	1.051338
	9	12 x 16	221	Linear Rect.	1.055927
	10	12 x 16	825	Quad.Rect.	1.057108
	11	12 x 16	1813	Cubic Rect.	1.057094
	12	12 x 16	221	Linear Tri.	1.055559

TABLE 5.8

PERCENTAGE DEVIATION OF k_{eff} FROM BENCHMARK FOR FELTRAN RESULTS

FELTRAN Run	Element Type	Δk_{eff} %
1	Linear Rect.	- 1.9846
2	Quad.Rect.	0.0074
3	Cubic Rect.	0.0152
4	Linear Triang.	- 2.3011
5	Linear Rect.	- 0.4254
6	Quad.Rect.	- 0.0136
7	Cubic Rect.	0.0105
8	Linear Triang.	- 0.5352
9	Linear Rect.	- 0.1010
10	Quad.Rect.	- 0.0107
11	Cubic Rect.	- 0.0094
12	Linear Triang.	- 0.1359

TABLE 5.9

VALUES OF k_{eff} FROM FELTRAN USING LINEAR ELEMENTS WITH MESH REFINEMENT

Run No.	Mesh	Number of Unknowns Per Group	Element Type	k_{eff}	Δk_{eff}
13	24 x 32	825	Linear Rect.	1.056815	- 0.0167
14	48 x 32	825	Linear Tri.	1.056718	- 0.0259

The deviation is calculated as

$$\Delta k_{eff} = \frac{k_{eff} - k^*}{k^*} \times 100 \qquad (5.9)$$

where,

k^* = benchmark value of Kaper et al.

As can be seen the deviations for the linear rectangular and triangular elements drop when the mesh is refined. For the quadratic elements there is an increase followed by a decrease but in the case of the cubic elements the drop is steady but not appreciable. What can therefore be deduced is that higher order elements provide reasonable and accurate answers even on a coarse mesh and improved accuracy is not matched by an increase in mesh refinement owing to the already excellent estimate on a coarse mesh. As for linear elements, mesh refinement serves to bring about an increasing order of accuracy which can be seen to be approaching the benchmark value. Actually the k_{eff} for the linear elements do not seem to have attained the "equilibrium state". Therefore it was decided to further refine these meshes for the linear elements and see how the values of k_{eff} turn out. Table 5.9 shows these values and their corresponding k_{eff}. The approach to "equilibrium" is maintained. Indeed, the values of k_{eff} are now closer to those for the coarsest mesh with quadratic and cubic elements (Runs 2 and 3) but still not as small. Therefore one can infer that the higher order elements are definitely to be used in preference over the linear elements. This observation agrees with that of Biswas et al [13] who showed

that quadratic elements provide the same trend when compared against linear rectangular and triangular elements.

One important feature to bear in mind is that the results from HOD and CD do not show an attempt at mesh refinement. It is almost certain that if mesh refinement had been carried out as well then the pattern turned out by FELTRAN would be followed. That means to say the values of k_{eff} from HOD and CD would not necessarily turn out to be 1.056992 but some values around there. Hence on an equal footing comparison basis the FELTRAN Runs 1 to 4 when compared with those results from HOD and CD demonstrate the accuracy of higher order finite elements for diffusion problems using coarse mesh analysis. On the other hand finite difference methods do not demonstrate this feature as can be seen from the DARC2D results where the values of k_{eff} are still varying to some extent even with mesh refinement.

The execution times, number of outer iterations and time per iteration for the FELTRAN results are shown in Table 5.10. All the results are quoted in CDC 6600 sec. Run 11 was made on the AMDAHL and the result quoted in equivalent CDC 6600 sec by using a conversion factor of 8 (as in the previous section). As can be seen the time per iteration for the linear elements agree very well with each other when compared on the basis of equivalent mesh sizes. The time per iteration for Runs 5 and 8 are very close to those for Runs 9 and 12 although the latter runs have more unknowns. This can be attributed to the fact

TABLE 5.10

EXECUTION TIMES AND NUMBER OF OUTER ITERATIONS

FOR FELTRAN RESULTS

Run No.	Number of Iterations	Execution Time (CDC 6600 sec.)	Time Per Iteration (CDC 6600 sec.)
1	22	7.60	0.35
2	25	9.40	0.38
3	26	23.71	0.91
4	18	4.58	0.25
5	9	10.01	1.11
6	26	30.81	1.19
7	26	155.16	5.97
8	8	9.15	1.14
9	24	22.02	0.92
10	26	229.66	8.83
11	26	724.32*	27.86
12	24	24.47	1.02
13	25	124.84	4.99
14	25	132.18	5.29

*90.54 sec. on the AMDAHL

that Runs 5 and 8 require a surprisingly low number of iterations and hence the time per iteration for these runs include a significant portion due to initialisation and assembly of the global matrix.

The times for the other codes are reproduced in Table 5.11 together with their number of unknowns per group. DARC2D and HOD were run on an IBM 360 Model 50/75 while CD was fun on IBM 370/158 which is, of course, a faster machine than the IBM 360. However comparison times between these two machines are unavailable and therefore no conclusion can be made about the HOD or CD results, but nevertheless the times quoted by Kaper et al for both codes are quite impressive since one can surmise that the IBM 370/158 must be at least 3 or 4 times faster than the IBM 360. The relation between the speed of the IBM 370/158 and CDC 6600 is two in favour of the latter as was shown in the previous section. To provide a not unreasonable comparison consider CD/5 and FELTRAN/3. The time for CD/5 in CDC 6600 time would be about 65 sec. while it is about 24 secs. for FELTRAN/3. Although the number of unknowns are more for FELTRAN/3 the time taken is about $2\frac{1}{2}$ times faster. However, in the end, no firm conclusion can be drawn up as regards the execution times of these various codes. The reasons have already been expounded in the previous section.

To conclude it can be said that FELTRAN do provide excellent results especially with quadratic and cubic elements. No firm conclusion can be drawn as regards the speed when compared with the other published results.

TABLE 5.11

EXECUTION TIMES FOR DARC2D, HOD AND CD RESULTS

Code	Run No.	No.Unknowns Per Group	Execution Time (sec.)	
DARC2D	1	48	30.7	A
	2	140	36.4	
	3	280	50.6	
	4	560	87.4	
	5	900	176.5	
	6	1160	284.7	
	7	1452	317.4	
HOD	1	47	16.5	
	2	63	23.0	
	3	94	46.2	
	4	159	110.8	
	5	241	246.1	
	6	336	370.5	
CD	1	17	20.0	B
	2	34	50.0	
	3	51	52.0	
	4	68	127.0	
	5	85	130.0	

A- IBM 360 Model 50/75

B- IBM 370/158

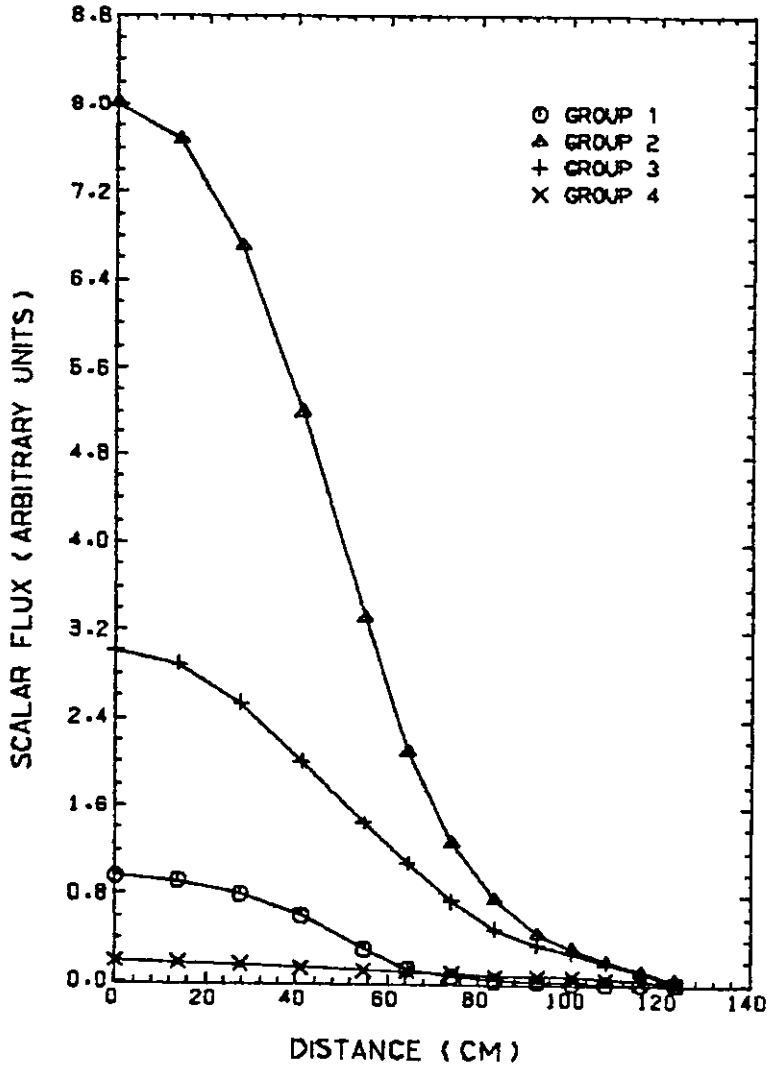

Fig.5.11 Flux plots along x = 0.0 cm for FELTRAN using cubic elements (Run 11)

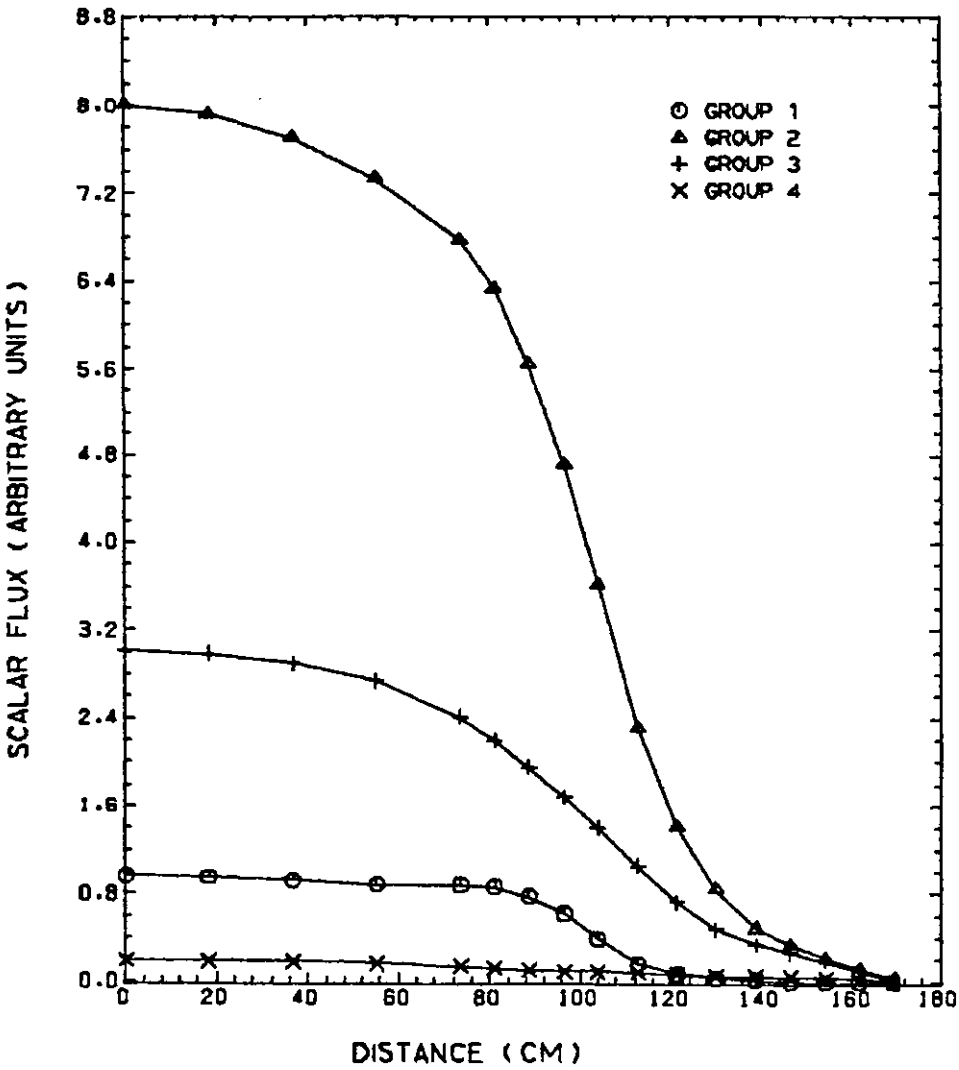

Fig.5.12 Flux plots along y = 0.0 cm for FELTRAN using cubic elements (Run 11)

None of the other results have shown any flux profiles. However Figs.5.11 and 5.12 show the scalar flux profiles along x = 0.0 cm and y = 0.0 cm respectively for FELTRAN/11. Both exhibit a downwards trend for all four group fluxes as the exterior boundaries are approached. Besides the relative distributions of the four groups behave in a similar manner to that shown by a typical four group model representation of a LMFBR [97]. This further confirms the accuracy afforded by FELTRAN in analysing diffusion problems.

5.4 A 5-Group Eigenvalue Problem

After witnessing the ability of FELTRAN to cope with diffusion problems our attention is now focussed on a transport problem. This 5-group problem was first analysed by Lillie and Robinson [65] who incidentally also provided the data set by private communication. Fig.5.13 shows this 7-region problem which is a one-dimensional representation of the ZPR-9 reactor at the Argonne National Laboratory. In the FELTRAN analysis the vertical dimension was chosen as 1 cm with reflective boundary conditions on all sides except the right hand end where bare surface conditions were considered. Table 5.12 lists the cross-sections for this problem.

In their study, Lillie and Robinson employed three different methods to solve this problem. Firstly, the problem was to validate their own finite element code called DAFE. This code is based on a variational approach to the finite element method. Lillie and Robinson used a second-order form of a discretized Boltzmann transport equation. The

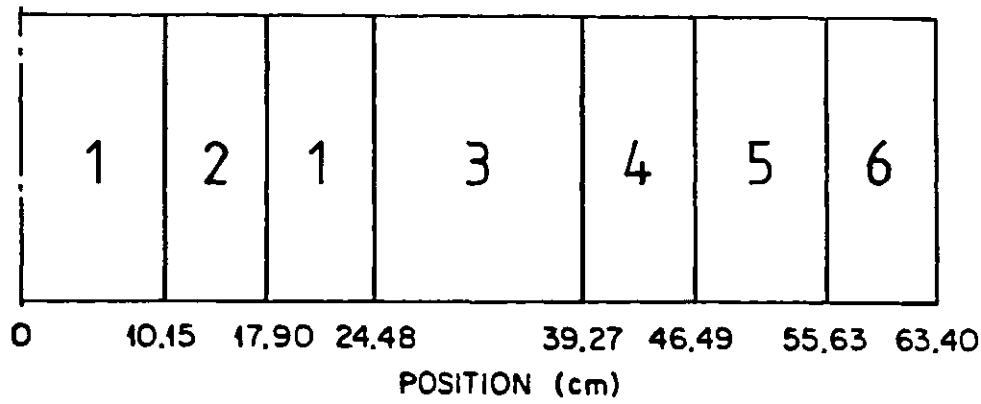

1 - Core Zone 1
2 - Core Zone 1 + Loops
3 - Core Zone 2
4 - Reflector + Control Material
5 - Reflector
6 - Shield

Fig.5.13 Geometrical and materials representation of the ZPR-9 Reactor (dimensions in cm.)

TABLE 5.12

CROSS-SECTIONAL DATA FOR THE 5-GROUP EIGENVALUE PROBLEM

CROSS-SECTIONS

REGION NO 1

POS	GROUP 1	GROUP 2	GROUP 3	GROUP 4	GROUP 5
1	9.7992E-03	4.5500E-03	5.2237E-03	1.0838E-02	2.8846E-02
2	1.6066E-01	2.2063E-01	3.3302E-01	4.8904E-01	4.0986E-01
3	1.3150E-01	2.1314E-01	3.2307E-01	4.7319E-01	3.8785E-01
4	0	2.4734E-02	4.8741E-03	4.8484E-03	4.0625E-03
5	0	0	4.6832E-04	3.3638E-06	1.8872E-06
6	0	0	0	3.2206E-05	2.5020E-08
7	0	0	0	0	2.2738E-06

REGION NO 2

POS	GROUP 1	GROUP 2	GROUP 3	GROUP 4	GROUP 5
1	4.8937E-03	2.3048E-03	2.6484E-03	5.5096E-03	1.4600E-02
2	1.5550E-01	2.1197E-01	3.6560E-01	5.3636E-01	4.5972E-01
3	1.3116E-01	2.0642E-01	3.5752E-01	5.2438E-01	4.4673E-01
4	0	2.1572E-02	4.1072E-03	5.0840E-03	4.2189E-03
5	0	0	5.1596E-04	3.4157E-06	9.2929E-07
6	0	0	0	4.5138E-05	1.2800E-08
7	0	0	0	0	3.5972E-06

REGION NO 3

POS	GROUP 1	GROUP 2	GROUP 3	GROUP 4	GROUP 5
1	1.3318E-02	6.4095E-03	7.3151E-03	1.5141E-02	4.3267E-02
2	1.7866E-01	2.4663E-01	3.7242E-01	5.2955E-01	4.8259E-01
3	1.4504E-01	2.3804E-01	3.6049E-01	5.0886E-01	4.4722E-01
4	0	2.7838E-02	5.0683E-03	5.2531E-03	4.3213E-03
5	0	0	5.6095E-04	4.0382E-06	2.3035E-06
6	0	0	0	3.8268E-05	3.8704E-08
7	0	0	0	0	2.7030E-06

REGION NO 4

POS	GROUP 1	GROUP 2	GROUP 3	GROUP 4	GROUP 5
1	9.6410E-15	7.8964E-15	1.0621E-14	2.5050E-14	1.3919E-13
2	2.1552E-01	3.0209E-01	8.0108E-01	1.0055E+00	1.0172E+00
3	1.9195E-01	2.9452E-01	7.8399E-01	9.8534E-01	9.6472E-01
4	0	2.0265E-02	6.3811E-03	1.4353E-02	1.1711E-02
5	0	0	7.2145E-04	1.9033E-06	4.7415E-19
6	0	0	0	4.6683E-05	1.8779E-10
7	0	0	0	0	2.2371E-06

REGION NO 5

POS	GROUP 1	GROUP 2	GROUP 3	GROUP 4	GROUP 5
1	9.3336E-15	7.9002E-15	1.0516E-14	2.5826E-14	1.5231E-13
2	2.1443E-01	3.0054E-01	7.7351E-01	9.9200E-01	9.7055E-01
3	1.9117E-01	2.9363E-01	7.5948E-01	9.7617E-01	9.6331E-01
4	0	2.0889E-02	6.3567E-03	1.3025E-02	1.3361E-02
5	0	0	6.8633E-04	2.0028E-06	4.9815E-19
6	0	0	0	4.8504E-05	1.7994E-10
7	0	0	0	0	2.5907E-06

REGION NO 6

POS	GROUP 1	GROUP 2	GROUP 3	GROUP 4	GROUP 5
1	9.2172E-15	7.9143E-15	1.0401E-14	2.6142E-14	1.6235E-13
2	1.8704E-01	2.6449E-01	5.7203E-01	7.1268E-01	6.5780E-01
3	1.5724E-01	2.6039E-01	5.6501E-01	6.9749E-01	6.5120E-01
4	0	2.7967E-02	3.7636E-03	5.8470E-03	9.4752E-03
5	0	0	1.2987E-03	5.1880E-06	5.3743E-19
6	0	0	0	1.4652E-04	7.7887E-10
7	0	0	0	0	1.2748E-05

FISSION SPECTRUM

GROUP 1	GROUP 2	GROUP 3	GROUP 4	GROUP 5
7.5504E-01	2.3803E-01	6.9300E-03	0	0

angular dependence is discretised using the discrete coordinates method. Secondly, DOT-III [82], a discrete ordinates code, was used to analyse the problem in order to provide comparative results for DAFE. Being of a more established nature the DOT-III results were held as the representative solutions. Finally, a Monte Carlo simulation was carried out with the KENO [98] code to provide a further check.

A distinction should be made between DAFE and FELTRAN as regards the application of the variational method. In DAFE, the variational is applied after angular discretization of the Boltzmann equation, whereas in FELTRAN the variational method is applied directly to the second-order Boltzmann Equation.

Two sets of DOT-III results were presented. Both used the same spatial mesh of 72 rectangles and were S_2 and S_4 calculations using 6 and 16 angular directions respectively. The DAFE results utilised 144 linear triangles and were labelled E_2 and E_4 in the angular representation. However these only used 2 and 6 angular directions respectively although both DOT-III and DAFE used the same quadrature sets. Lillie and Robinson attributed this to the fact that they only used those discrete angles having positive and non-zero direction cosines owing to symmetry in their canonical form of the transport equation. The KENO results were obtained by tracking 30,000 particulate histories. In both the DOT-III and DAFE results a convergence criteria of 10^{-4} was imposed on

the value of k_{eff}. DAFE uses a direct elimination solver while DOT-III, with an iterative solver, used a convergence criteria of 10^{-3} on the pointwise flux.

Table 5.13 presents the results of Lillie and Robinson together with those from FELTRAN using 72 elements for all but one case. The allocation of elements was 8 for all the regions except Region 3 where 24 were used. In the 144 elements run the elements per region were doubled.

The symbols NOM refer to the number of moments in the trial function while NORD refers to the order of the element employed ranging from 1 for linear elements to 3 for cubic elements. Since Lillie and Robinson have chosen to compare their results with those of DOT-III as the standard owing to the established nature of that code the same policy was adopted here. In particular the DOT-III S_4 case was chosen to be the yardstick in Table 5.13 and the Δk_{eff} is calculated as in Eq.(5.9). From the figures for k_{eff} it can be seen that they agree very well with the DOT-III S_4 result. In fact, the results are better than those from DAFE or KENO. However this is assuming that the DOT-III S_4 result is accurate.

In the remaining problems to be discussed and including this one no FELTRAN results using linear triangles are presented. The diffusion results in the previous two sections had already shown that both linear triangles and rectangles are of nearly the same accuracy but with linear rectangles being better off. And when compared against the higher order elements these linear elements are not

TABLE 5.13

COMPARISON OF k_{eff} FROM VARIOUS CODES

Code	No. of Elements	Angle/ NOM	NORD	k_{eff}	Δk_{eff}
DOT-III	72	S_2	-	1.1496	- .17
	72	S_4	-	1.1515	-
DAFE	144	E_2	-	1.1551	+ .31
	144	E_4	-	1.1576	+ .53
FELTRAN	72	2	1	1.15245	+ .095
	72	3	1	1.15257	+ .093
	72	4	1	1.15259	+ .095
	72	2	2	1.15208	+ .050
	72	3	2	1.15222	+ .063
	72	2	3	1.15204	+ .047
	144	2	2	1.15199	+ .043

KENO, using 30,000 particulate histories, predict

$k_{eff} = 1.1649 \pm .0078$

Note:

(i) DAFE use linear triangles
(ii) NOM = number of moments
(iii) NORD = order of element

quite as accurate. Hence it is not surprising that the DAFE results are not as accurate as FELTRAN for this problem since only linear triangles are used in DAFE.

On the other hand the FELTRAN results agree very well with each other and in all the runs 10 outer iterations were required to satisfy the convergence criterion on k_{eff} of 10^{-5}. When the NOM = 2, NORD = 2 case was compared with the NOM = 2, NORD = 3 case the k_{eff} are very nearly identical. Therefore it was decided to run a finer mesh case using 144 elements for NOM = 2 and NORD = 2 to see if any significant change in k_{eff} would result and the result is that no significant change was noticed. Therefore in this study the mesh of 72 elements was adequate for the problem.

No mention was made about computing times and number of outer iterations by Lillie and Robinson. Therefore the FELTRAN times are not mentioned here except that in the 72 elements runs with NOM = 2 the times on the AMDAHL computer were 21.45 sec for NORD = 2 and 134.91 sec for NORD = 3. The ratio of the global matrices in these two cases was 1:3.55.

Fig.5.14 shows the 5 group fluxes for the NOM = 2, NORD = 2 case with 72 elements. No flux profiles were provided by Lillie and Robinson and therefore no comparison could be made. Nevertheless the profiles are representative of such a system. In particular Groups 4 and 5 do exhibit the humps in the reflector region and all the fast groups show a gradual descent from the centre to the bare surface.

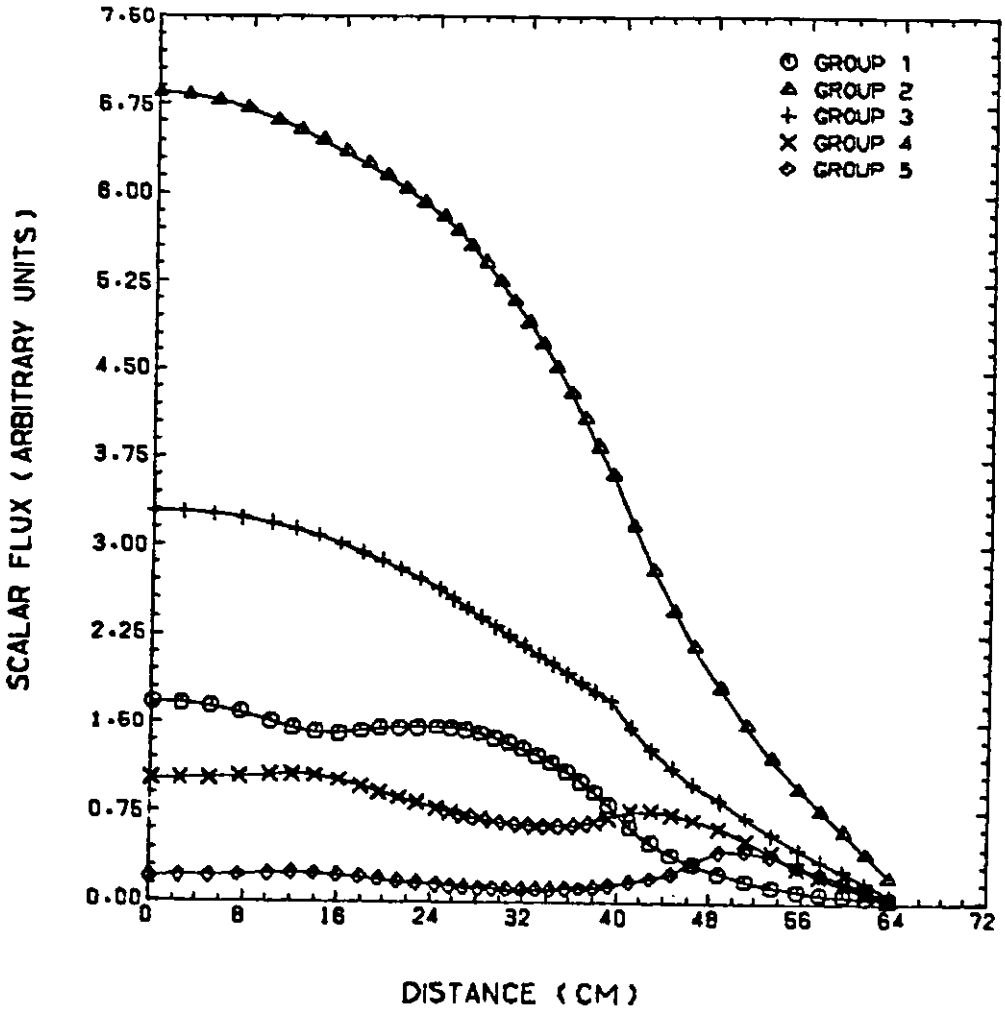

Fig.5.14 Flux plots from FELTRAN using 72 quadratic elements and a 2-moment trial function

To conclude, this multigroup, multi-region problem has confirmed that FELTRAN can predict accurate results for transport problems, although the problem is essentially one-dimensional in aspect. However in the next sections more rigorous studies will be made to examine the transport aspects.

5.5 A High Leakage Problem

A high leakage situation arises when all four boundaries are bare surfaces as in this problem. Also because the angular flux is highly anisotropic it would be difficult to analyse such problems without high angular resolution.

Fig.5.15 shows the geometry and material distribution of this problem which was first posed by Kaper et al [53]. Of the eight different materials present only material 4 is non-fissile. The cross-sections for these eight materials appear in Table 5.14.

Kaper et al had met with considerable success in applying the finite element method to solve the multigroup diffusion problems [52]. In solving this problem they were extending their earlier work to solve transport problems. Their finite element approach is based on a variational formulation of the self-adjoint form of the one-group transport equation. Lagrangian triangular elements ranging in polynomial order from 1 to 5 were used to span the spatial domain while three types of angular approximations were tried, namely, piecewise polynomial functions, surface harmonic functions and cubature formulae

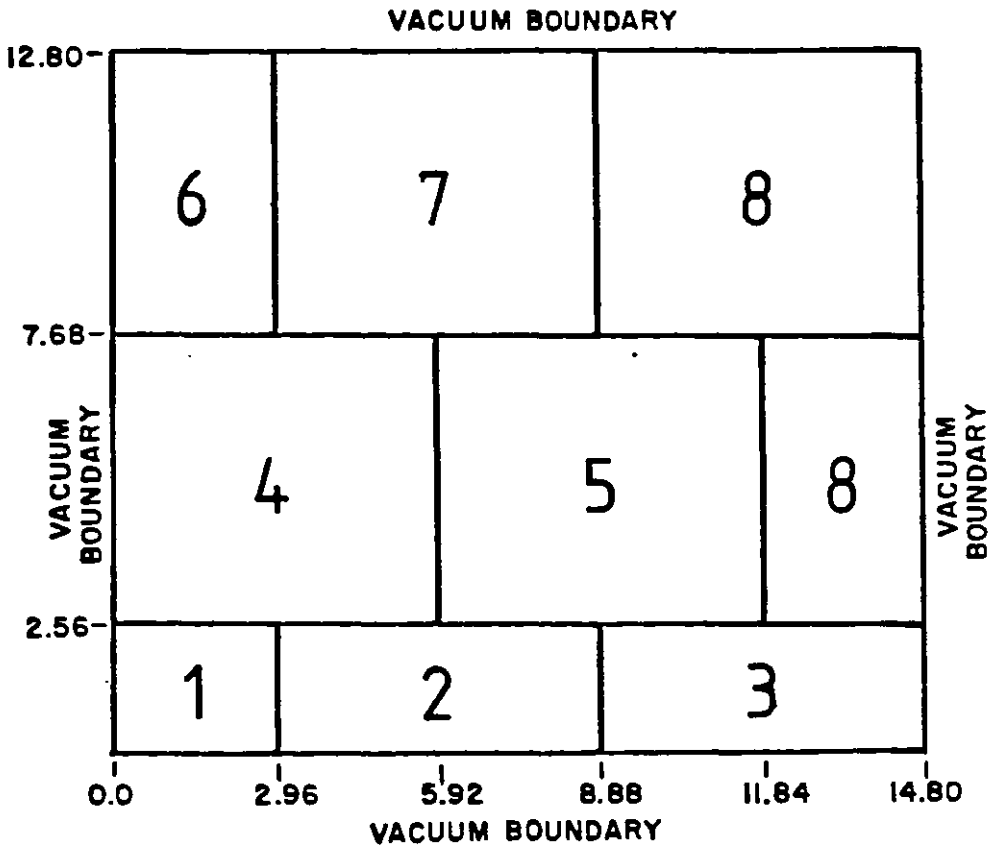

Materials 1 to 8 are fissile except for material 4

Fig.5.15 Geometry and materials representation in the high leakage problem

TABLE 5.14

CROSS-SECTIONAL DATA FOR THE HIGH LEAKAGE PROBLEM

CROSS-SECTIONS

REGION NO 1

POS	GROUP 1	GROUP 2	GROUP 3	GROUP 4	GROUP 5	GROUP 6
1	3.6322E-02	2.5739E-02	2.0361E-02	2.3840E-02	3.0038E-02	4.9114E-02
2	1.2419E-01	1.3482E-01	1.9215E-01	2.2708E-01	2.9296E-01	3.2381E-01
3	4.8547E-02	8.7926E-02	1.5516E-01	2.0231E-01	2.6489E-01	2.9480E-01
4	0	3.3980E-02	2.3374E-02	1.1597E-02	7.9482E-03	6.9954E-03
5	0	0	1.6332E-02	5.2657E-03	6.9205E-04	2.6528E-04
6	0	0	0	4.5529E-03	9.2922E-04	9.9946E-05
7	0	0	0	0	8.1354E-04	1.5581E-04
8	0	0	0	0	0	1.3829E-04

REGION NO 2

POS	GROUP 1	GROUP 2	GROUP 3	GROUP 4	GROUP 5	GROUP 6
1	3.6469E-02	2.5837E-02	2.0476E-02	2.3976E-02	3.0212E-02	4.9399E-02
2	1.2436E-01	1.3500E-01	1.8241E-01	2.2746E-01	2.9347E-01	3.2944E-01
3	4.8515E-02	8.8029E-02	1.5534E-01	2.0262E-01	2.6530E-01	2.9527E-01
4	0	3.4006E-02	2.3396E-02	1.1617E-02	7.9597E-03	7.0032E-03
5	0	0	1.6349E-02	5.2726E-03	6.9478E-04	2.6669E-04
6	0	0	0	4.5573E-03	9.3046E-04	1.0026E-04
7	0	0	0	0	8.1429E-04	1.5609E-04
8	0	0	0	0	0	1.3041E-04

REGION NO 3

POS	GROUP 1	GROUP 2	GROUP 3	GROUP 4	GROUP 5	GROUP 6
1	2.4500E-02	1.7377E-02	1.3784E-02	1.6143E-02	2.0346E-02	3.3272E-02
2	1.0779E-01	1.1879E-01	1.6295E-01	1.9456E-01	2.4301E-01	2.7379E-01
3	4.3406E-02	7.9120E-02	1.3966E-01	1.7399E-01	2.2667E-01	2.4956E-01
4	0	3.0665E-02	2.0612E-02	1.0775E-02	7.4770E-03	6.7083E-03
5	0	0	1.2765E-02	3.0574E-03	5.0574E-04	1.7950E-04
6	0	0	0	3.4713E-03	6.8638E-04	7.3119E-05
7	0	0	0	0	5.1390E-04	1.1495E-04
8	0	0	0	0	0	9.6267E-05

REGION NO 4

POS	GROUP 1	GROUP 2	GROUP 3	GROUP 4	GROUP 5	GROUP 6
1	0	0	0	0	0	0
2	1.8524E-01	1.8007E-01	2.4514E-01	2.7390E-01	3.5323E-01	4.1299E-01
3	7.7636E-02	1.3544E-01	2.2366E-01	2.5678E-01	3.4866E-01	4.0624E-01
4	0	5.5925E-02	3.0240E-02	1.4240E-02	1.0561E-02	1.1648E-02
5	0	0	1.4077E-02	3.9634E-03	1.9784E-04	2.0540E-05
6	0	0	0	3.6630E-03	7.9636E-04	2.5991E-05
7	0	0	0	0	6.3594E-04	1.3748E-04
8	0	0	0	0	0	8.5505E-05

REGION NO 5

POS	GROUP 1	GROUP 2	GROUP 3	GROUP 4	GROUP 5	GROUP 6
1	1.6524E-02	9.9711E-03	6.2237E-03	5.8829E-03	5.7275E-03	7.6073E-03
2	9.3382E-02	1.1856E-01	1.5573E-01	1.7519E-01	2.1101E-01	2.2713E-01
3	4.3391E-02	8.0195E-02	1.3247E-01	1.5847E-01	1.9475E-01	2.1759E-01
4	0	2.4218E-02	2.4519E-02	1.5009E-02	8.9717E-03	8.7565E-03
5	0	0	9.0254E-03	2.5947E-03	1.6246E-04	1.7432E-05
6	0	0	0	2.4745E-03	4.3596E-04	2.6089E-05
7	0	0	0	0	4.3965E-04	7.1080E-05
8	0	0	0	0	0	6.8622E-05

REGION NO 6

POS	GROUP 1	GROUP 2	GROUP 3	GROUP 4	GROUP 5	GROUP 6
1	3.3369E-02	2.5397E-02	2.1097E-02	2.4703E-02	3.1123E-02	5.0886E-02
2	1.3511E-01	1.2501E-01	1.6814E-01	2.0721E-01	2.6746E-01	2.9967E-01
3	4.5648E-02	8.1130E-02	1.4167E-01	1.8288E-01	2.3984E-01	2.6574E-01
4	0	3.1548E-02	2.1437E-02	1.1022E-02	7.4165E-03	6.5714E-03
5	0	0	1.4333E-02	4.6073E-03	6.6566E-04	2.6673E-04
6	0	0	0	3.9733E-03	8.3651E-04	9.5847E-05
7	0	0	0	0	7.0850E-04	1.4037E-04
8	0	0	0	0	0	1.1258E-04

REGION NO 7

POS	GROUP 1	GROUP 2	GROUP 3	GROUP 4	GROUP 5	GROUP 6
1	3.6560E-02	2.6134E-02	2.0723E-02	2.4266E-02	3.0580E-02	5.0004E-02
2	1.2497E-01	1.3565E-01	1.8330E-01	2.2874E-01	2.9511E-01	3.3142E-01
3	4.8930E-02	8.8402E-02	1.5604E-01	2.0370E-01	2.6571E-01	2.9690E-01
4	0	3.4131E-02	2.3502E-02	1.1677E-02	7.9361E-03	7.0293E-03
5	0	0	1.6448E-02	5.3182E-03	6.3149E-04	2.6985E-04
6	0	0	0	4.5853E-03	9.3655E-04	1.0216E-04
7	0	0	0	0	8.1933E-04	1.5719E-04
8	0	0	0	0	0	1.3126E-04

REGION NO 8

POS	GROUP 1	GROUP 2	GROUP 3	GROUP 4	GROUP 5	GROUP 6
1	4.4474E-02	8.8421E-03	3.0705E-04	3.0350E-04	3.5658E-04	6.2063E-04
2	1.6322E-01	1.7905E-01	2.4699E-01	3.2970E-01	4.3929E-01	4.8855E-01
3	5.8516E-02	1.2273E-01	2.2497E-01	3.1064E-01	4.0969E-01	4.7209E-01
4	0	4.6934E-02	3.3663E-02	1.4707E-02	1.1779E-02	1.0075E-02
5	0	0	3.8413E-02	9.9162E-03	3.5478E-04	9.3839E-05
6	0	0	0	8.7301E-03	1.3708E-03	6.5550E-05
7	0	0	0	0	1.5773E-03	2.2638E-04
8	0	0	0	0	0	2.6114E-04

FISSION SPECTRUM

GROUP 1	GROUP 2	GROUP 3	GROUP 4	GROUP 5	GROUP 6
3.4124E-01	4.1164E-01	1.7971E-01	5.1222E-02	1.2666E-02	3.7214E-03

with positive weights. In assessing their own results Kaper et al used TRIPLET [81] to obtain benchmarking data. In their conclusion the cubature method showed the most promising results but on the whole they were not very enthusiastic about the extension of the finite element method to transport problems.

Lillie and Robinson [65] had another look at this problem when they were validating DAFE against DOT-III and Keno (as shown in the previous section). They made comparative studies using the aforementioned codes and their own TRIPLET results. The TRIPLET computer code solves two-dimensional transport problems using regular triangular elements which are based on Lagrangian polynomials up to quadratic order. The finite element approach is based on the method of weighted residuals. For the angular domain a discrete ordinates' approximation is used and an iterative, rather than direct, solver was used to solve the system of equations.

In this presentation the work of Lillie and Robinson will be referred to for comparative results since they have quoted many different results. The work of Kaper et al has concentrated mainly on the choice of the angular discretization for their code and as such is not so easily presentable for comparative studies without delving into a lot of subsidiary material.

Convergence criteria of 10^{-3} and 10^{-4} on the pointwise scalar flux and eigenvalues were observed in the

DOT-III and TRIPLET results. For DAFE the eigenvalue criterion was 10^{-4} while in FELTRAN it was 10^{-5} as usual.

The KENO result, based on 30,000 particulate histories, was chosen to be the benchmark value when working out the percentage deviation of the values of k_{eff} as in Eq.(5.9). No reason was given as to why the KENO result was taken as the benchmark but nevertheless the FELTRAN results are judged by the same benchmark. The DOT-III results were based on a rectangular mesh while triangular elements were used in both TRIPLET and DAFE. Although TRIDENT can provide results for quadratic triangular elements no mention was made by Lillie and Robinson as to whether a linear or a quadratic element was used in their analysis. DAFE can only handle linear trianges but two types of triangulation were used. Fig.5.16 depicts these arrangements which have been referred to as the regular and crossed triangle arrangement. The regular arrangement is similar to the mesh used in the TRIDENT analyses.

Table 5.15 shows the results obtained by Lillie and Robinson. In the angular approximation the S_2, S_4 and S_6 denote the use of 6, 16 and 30 angles in the DOT-III calculations whereas for these calculations 4, 12 and 24 angles were used by TRIPLET. In DAFE the corresponding number of angles were 2, 6 and 12. Fig.5.17 (a) shows the msh for the 30 triangular elements used in DAFE and TRIPLET and the 15 rectangular cells in DOT-III while Fig.5.17 (b) shows the corresponding 50 triangular elements and 25 rectangular cells. A refinement of this second

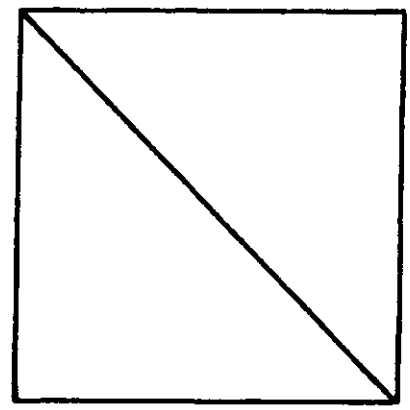

(a)

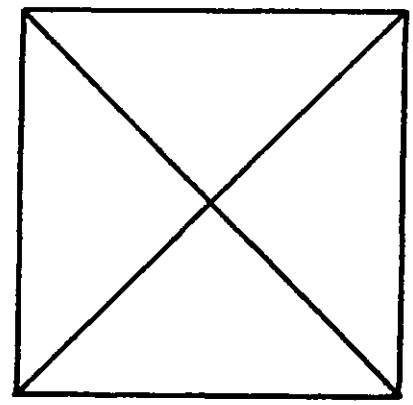

(b)

Fig.5.16 Triangular arrangements used by Lillie and Robinson in DAFE

(a) Regular triangle arrangement
(b) Crossed triangle arrangement

TABLE 5.15

VALUES OF k_{eff} QUOTED BY LILLIE AND ROBINSON

FOR THE HIGH LEAKAGE PROBLEM

%

Code	No. of Elements	Angular Approx.	k_{eff}	Δk_{eff}
DOT-III	15	S_2	0.1462	- 18.19
	25	S_2	0.1556	- 12.93
	100	S_2	0.1600	- 10.46
	15	S_4	0.1586	- 11.25
	25	S_4	0.1711	- 4.25
	100	S_4	0.1754	- 1.85
	15	S_6	0.1588	- 11.13
	25	S_6	0.1716	- 3.97
TRIPLET	30	S_2	0.1526	- 14.60
	50	S_2	0.1578	- 11.70
	200	S_2	0.1607	- 10.07
	30	S_4	0.1651	- 7.61
	50	S_4	0.1725	- 3.47
	200	S_4	0.1760	- 1.51
	30	S_6	0.1654	- 7.44
	50	S_6	0.1730	- 3.19
DAFE (with regular triangles)	30	E_2	0.1440	- 19.42
	50	E_2	0.1540	- 13.82
	200	E_2	0.1590	- 11.02
	30	E_4	0.1560	- 12.70
	50	E_4	0.1662	- 6.99
	200	E_4	0.1734	- 2.97
	30	E_6	0.1549	- 13.32
	50	E_6	0.1664	- 6.88
DAFE (with crossed triangles)	60	E_2	0.1484	- 16.96
	100	E_2	0.1581	- 11.53
	60	E_4	0.1560	- 12.70
	100	E_4	0.1710	- 4.31

KENO, based on 30,000 particulate histories and used as benchmark for problem, predicts $k_{eff} = 0.1787 \pm 0.0012$

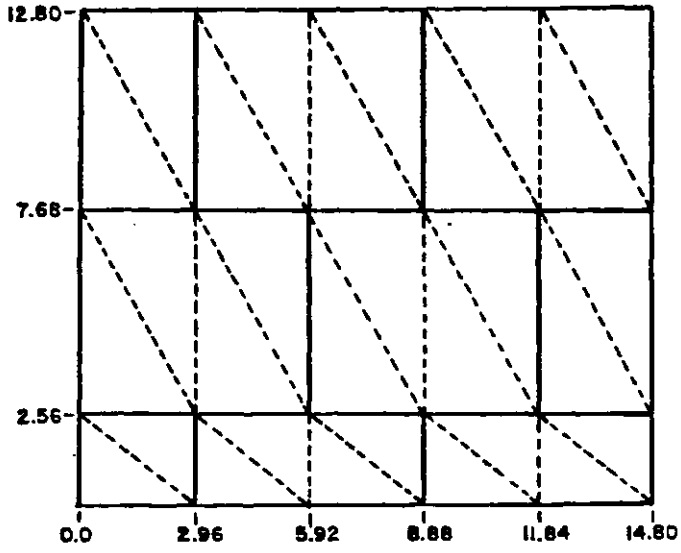

Fig.5.17(a) Mesh of 30 triangles used in DAFE and TRIPLET and 15 rectangles used in DOT-III

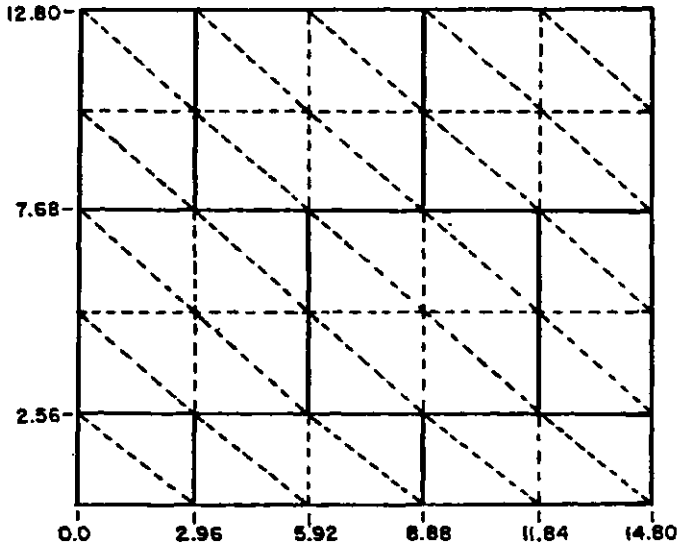

Fig.5.17(b) Mesh of 50 triangles used in DAFE and TRIPLET and 25 rectangles in DOT-III

mesh yields the case for 200 triangles and 100 triangles. In DAFE, the upper right and lower left triangles are reversed because DAFE requires the use of two triangles at the intersection of two vacuum boundaries. By replacing the two regular triangles per box in Fig.5.17 (a) and (b) by the four crossed triangles (as shown in Fig.5.16) the resultant meshes correspond to the cases for the 60 and 100 crossed triangular elements used in DAFE.

A quick glance at the figures for Δk_{eff} in Table 5.15 shows that the percentage errors are relatively high, but this is not unexpected for a system with a low multiplication. The values of k_{eff} improve to a higher value when the angular approximation gets better or when the mesh is refined.

Table 5.16 gives the FELTRAN results. The notation for NOM and NORD is as in the previous section. The mesh for the 25 elements is the same as the array of rectangular elements shown in Fig.5.17 (b) while the 100 elements is a refinement of this mesh. Only Run Number 13 was performed using 15 elements and this mesh corresponds to the rectangular array in Fig.5.17 (a). A run with 25 elements could not be made in this case because the resultant global matrix alone would occupy more space than is available on the AMDAHL computer. Runs 1 to 10 were achieved with 1 and 2 moments trial function respectively and with mesh refinement except for the cubic elements. A saturation value of nearly 0.15 was reached for the 1 moment results while in the 2 moment results this appears to around 0.173. The value of k_{eff} increases as the angular

TABLE 5.16

VALUES OF k_{eff} AND PERCENTAGE DEVIATIONS FROM FELTRAN FOR THE HIGH LEAKAGE PROBLEM

Run	No. of Elements	NOM	NORD	k_{eff}	Δk_{eff}
1	25	1	1	0.14688	- 17.81
2	100	1	1	0.14906	- 16.59
3	25	1	2	0.14978	- 16.18
4	100	1	2	0.14979	- 16.18
5	25	1	3	0.14979	- 16.18
6	25	2	1	0.16617	- 7.01
7	100	2	1	0.17043	- 4.63
8	25	2	2	0.17188	- 3.82
9	100	2	2	0.17194	- 3.78
10	25	2	3	0.17214	- 3.67
11	25	3	1	0.16952	- 5.14
12	25	3	2	0.17651	- 1.23
13	15	3	3	0.17657	- 1.19
14	25	4	1	0.17058	- 4.54
15	25	4	2	0.17819	- 0.29

approximation improves as borne out by the 3 and 4 moment results. In particular the 3 and 4 moment results for the higher order elements are encouraging. This suggests that better spatial and angular approximation would give higher values of k_{eff}. Tests of this kind would have been attempted had the out-of-core solver been available for eigenvalue problems. Nevertheless this would hopefully be exploited in the next phase of the finite element development being done at Imperial College.

Table 5.17 gives the computing times, number of outer iterations and the size of the global matrix for the FELTRAN results. The size of the global matrix is an indication of the size of the problem which is often the limitation factor, rather than execution time, for most practical problems. Conversion between the two different computer times could be taken as a factor of 8 in favour of the AMDAHL as mentioned in Section 5.2. No comparison in computing times could be made with the results provided by Lillie and Robinson since they did not provide any results on computing resources.

To conclude this discussion our attention is now focussed on the flux profiles for the six groups. Fig.5.18 shows the horizontal profiles at the location of 5.76 cm. (when referred to Fig.5.15) from the results of TRIPLET and DAFE as reported by Lillie and Robinson from their S_4 and E_4 results with 200 triangular elements. The FELTRAN results with 4 moments and quadratic elements (Run 15) are shown in Fig.5.19 and agree very well with the results of Lillie and Robinson.

TABLE 5.17

COMPUTATION DATA ON THE FELTRAN RUNS

FOR THE HIGH LEAKAGE PROBLEM

Run No.	No. of Iterations	Time (CDC 6600 sec.)	Time (AMDAHL sec.)	Size of Global Matrix
1	10	6.3		288
2	10	9.9		1573
3	10	16.2		3025
4	10	74.3		19845
5	10	50.4		13312
6	13	16.4		4608
7	13	111.5		25168
8	13	258.5		48400
9	13		285.5	317520
10	4		257.7	212992
11	14	107.0		23328
12	14		240.6	245025
13	15		702.4	440640
14	14		59.6	73728
15	14		1457.4	774400

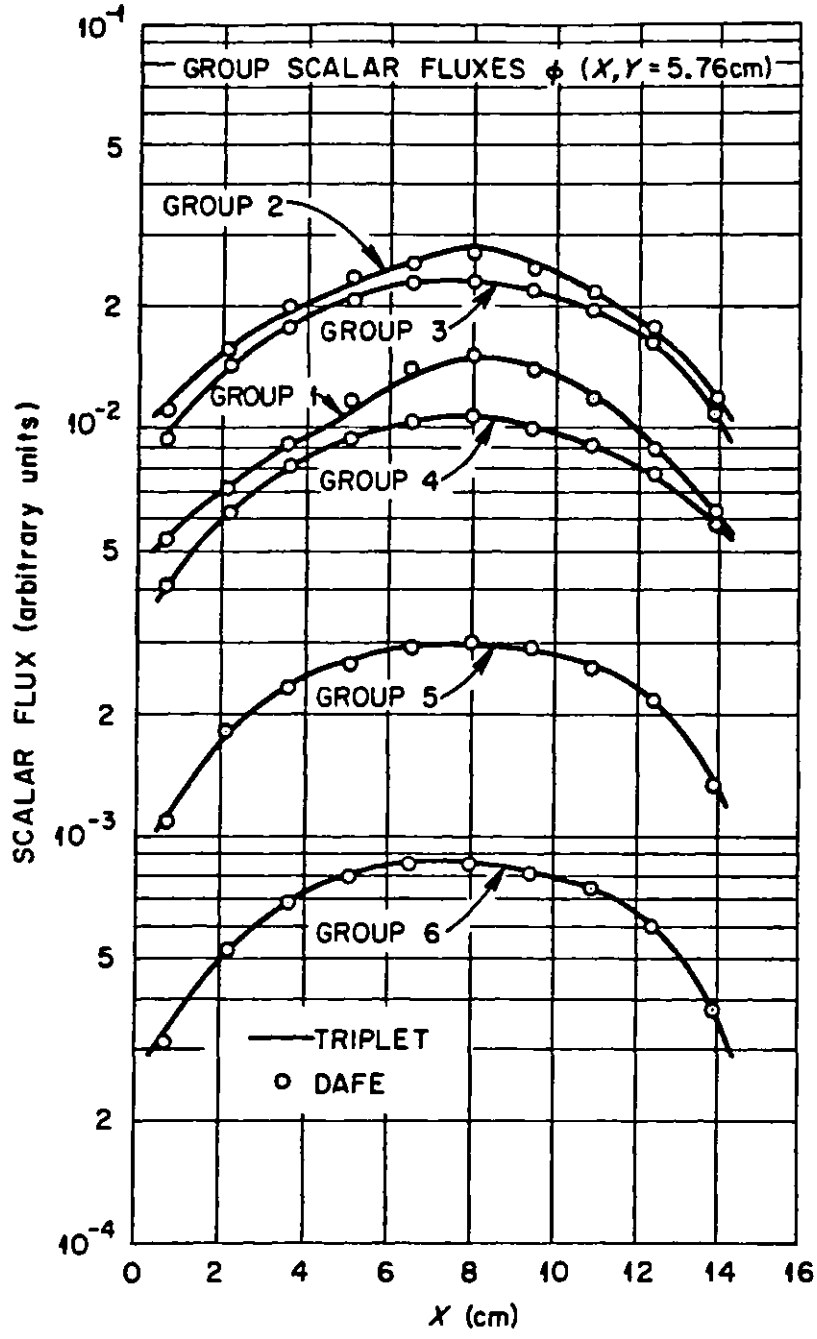

Fig.5.18 Flux plots for the high leakage problem as reported by Lillie and Robinson

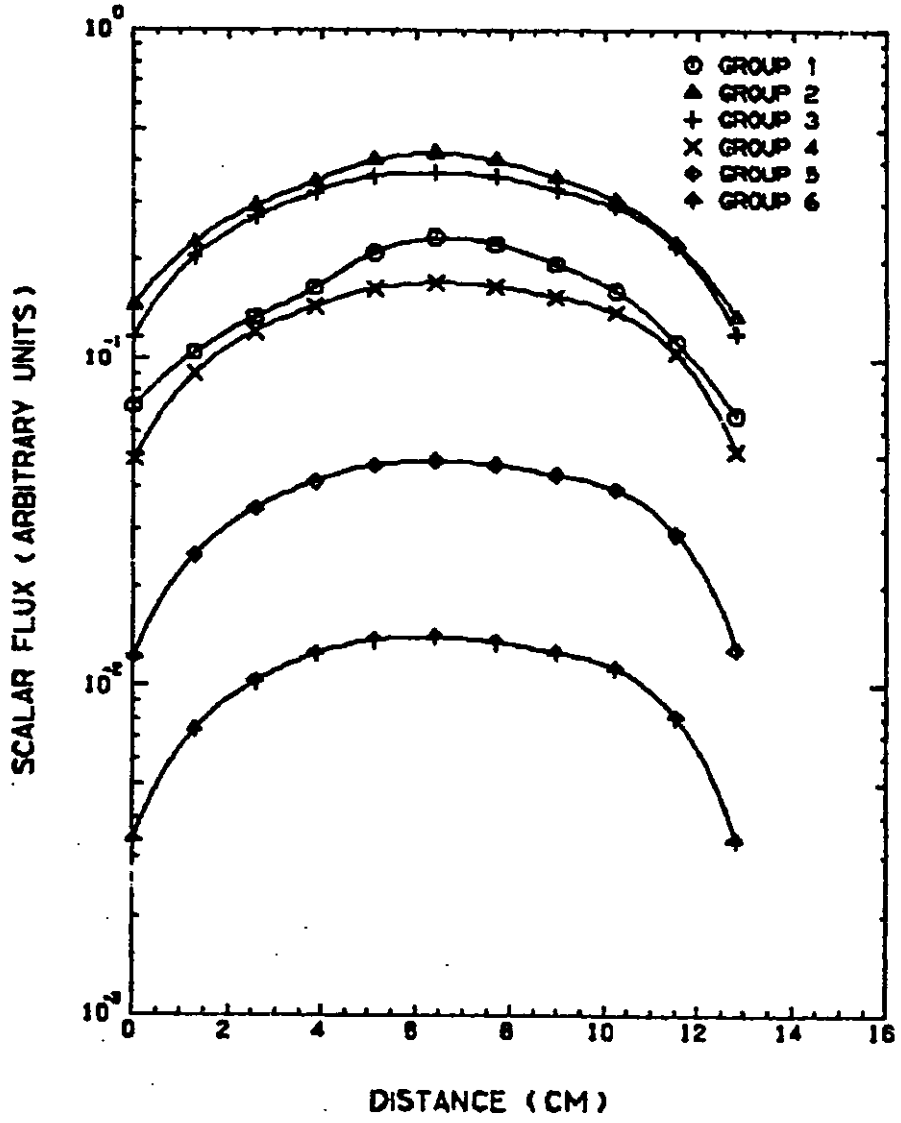

Fig.5.19 Flux plots for the high leakage problem from FELTRAN (Run 15)

Table 5.19 presents the results from DOT-III, TWOTRAN-II and FELTRAN. To start with both DOT-III and TWOTRAN-II imposed a convergence criteria of 2×10^{-5} on the value of k_{eff} and since both are discrete ordinates codes it is not surprising that the values of k_{eff} are close to each other in the similar cases. When compared to the $(48 \times 48)/S_8$ results the $(12 \times 12)/S_8$ and $(24 \times 24)/S_2$ results in these two sets of results do not agree so well as would be expected. On the other hand, no more than 5 transport results could be obtained from FELTRAN owing to computer storage requirements exceeding available resources. This is so because FELTRAN for k_{eff} problems is restricted to an in-core solver which uses a direct solution algorithm. The whole of the global matrix is stored for FELTRAN whereas in the discrete ordinates codes no such problem arises because the iterative methods of solution allow the coefficients to be assembled during each point of the solution cycles. As an idea of the size encountered, consider the case of (12 x 12) mesh using cubic elements and a two-moment trial function. The global matrix requires 2,518,960 storage locations and in double precision format this far exceeds the available memory on the AMDAHL computer. In order to run larger size jobs using FELTRAN the out-of-core solver, which can only handle source problems presently, would have to be modified in order to solve eigenvalue problems. This would be one of the proposals for future work and it is hoped then that more analysis on this problem would be attempted using FELTRAN.

To conclude, the results obtained by FELTRAN for this difficult problem are excellent when compared against the reported results from other codes. Nevertheless the available computing resources place a constraint on the achievement of high levels of accuracy by all the methods considered above.

5.6 BWR Fuel Bundle Benchmark Problem

This is a standard benchmark problem which first appeared in the ANL Benchmark Problem Book [7] and was first proposed by B.A. Zolotar of EPRI. From the finite element point of view the interesting aspect of this problem is the manner in which computing resources are constrained.

Fig.5.20 shows the layout of this problem which represents a (7 x 7) fuel assembly in a BWR rod bundle. The dimensions and composition numbers are shown in Fig.5.21 with the basic mesh of (12 x 12) elements. Being a rod bundle inside a BWR perfect reflector conditions exist on all four sides. Table 5.18 gives the cross-sections for theseven different materials which are characterised by two energy groups.

Both transport and diffusion results to this problem were presented separately. The transport results would be discussed first. Zolotar and Zahn of EPRI presented their results obtained with the DOT-III code [82] while Mallen of SRL used TWOTRAN-II [61] for his results. Both are discrete ordinates codes.

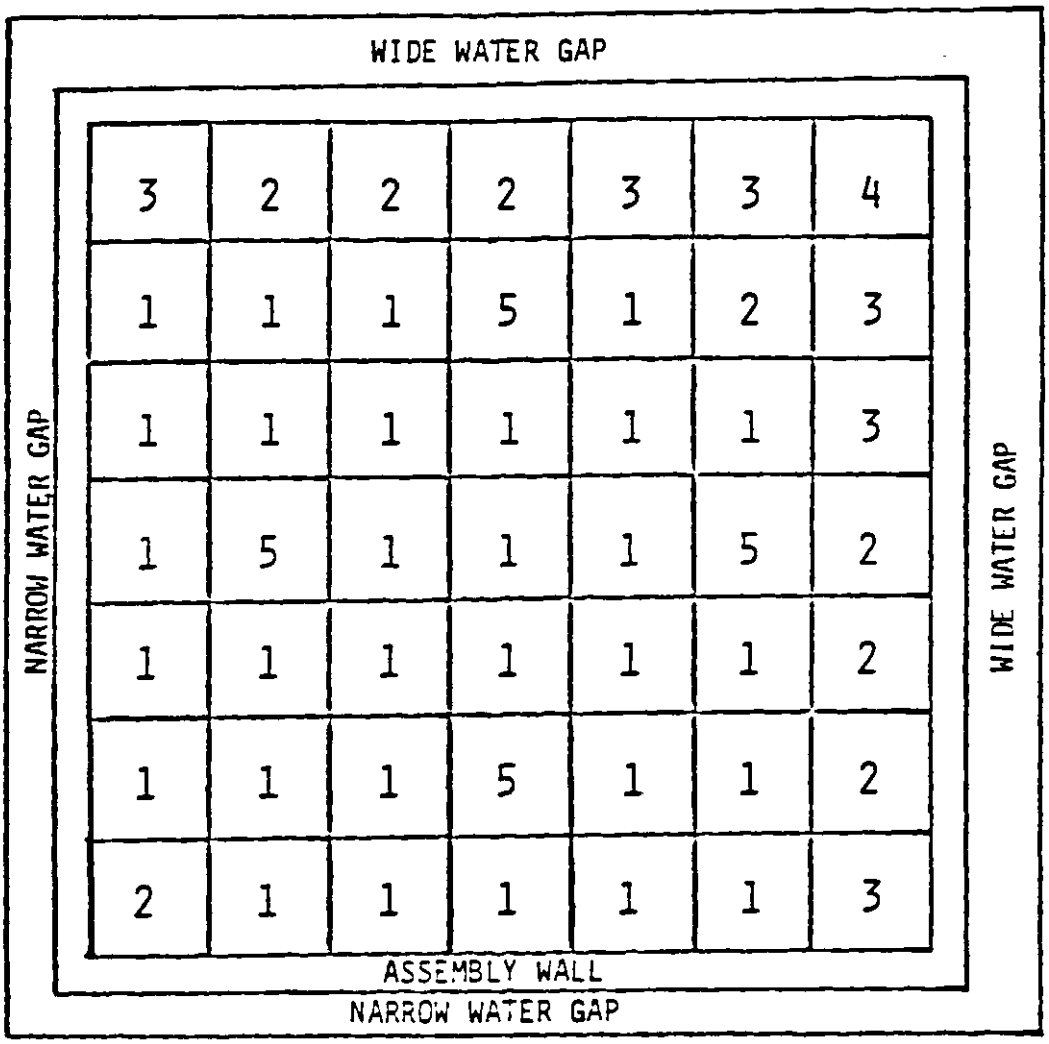

Fig.5.20 Layout of the BWR rod bundle

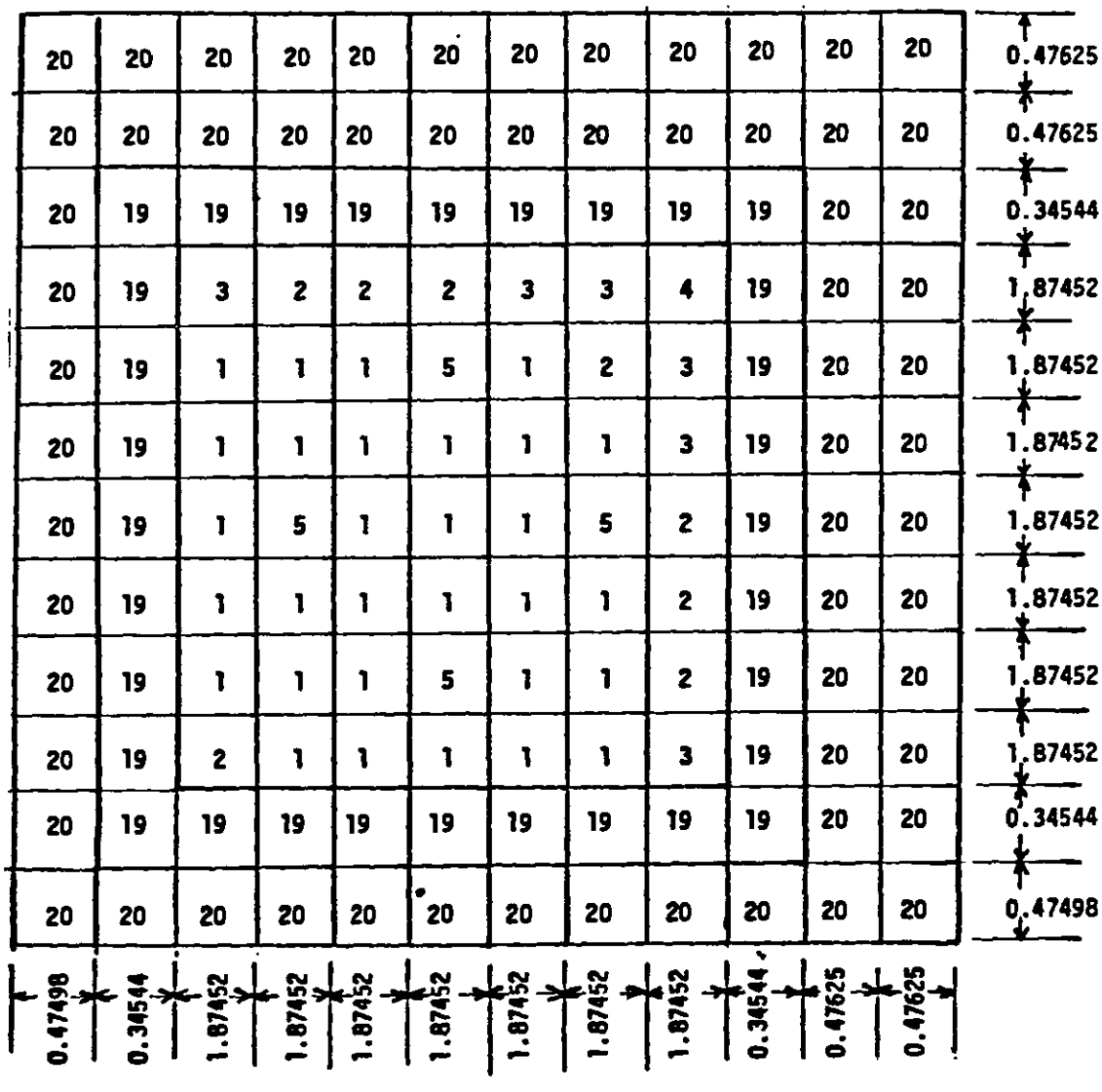

NOTE: All dimensions in centimeters.

Material 1,2,3,4 - fissile material
19 - Assembly wall
20 - Water
5 - Poison Pins

Fig.5.21 A (12 x 12) mesh showing the geometry and material configuration of the BWR rod bundle

TABLE 5.18

CROSS-SECTIONAL DATA FOR THE BWR ROD BUNDLE

CROSS-SECTIONS

REGION NO 1

POS	GROUP 1	GROUP 2
1	5.9250E-03	9.8178E-02
2	2.5310E-01	5.7320E-01
3	2.3343E-01	5.1428E-01
4	0	1.0690E-02

REGION NO 2

POS	GROUP 1	GROUP 2
1	5.2420E-03	8.2260E-02
2	2.5360E-01	5.7670E-01
3	2.3392E-01	5.2496E-01
4	0	1.0950E-02

REGION NO 3

POS	GROUP 1	GROUP 2
1	4.8208E-03	7.2000E-02
2	2.5358E-01	5.7970E-01
3	2.3379E-01	5.3253E-01
4	0	1.1120E-02

REGION NO 4

POS	GROUP 1	GROUP 2
1	4.3370E-03	5.9000E-02
2	2.5330E-01	5.8370E-01
3	2.3369E-01	5.4230E-01
4	0	1.1130E-02

REGION NO 5

POS	GROUP 1	GROUP 2
1	5.6050E-03	2.4240E-02
2	2.5060E-01	5.8530E-01
3	2.3085E-01	4.2270E-01
4	0	1.0160E-02

REGION NO 19

POS	GROUP 1	GROUP 2
1	0	0
2	2.1720E-01	4.7480E-01
3	2.0706E-01	4.7041E-01
4	0	9.0950E-03

REGION NO 20

POS	GROUP 1	GROUP 2
1	0	0
2	2.4760E-01	1.1230E+00
3	2.1058E-01	1.1152E+00
4	0	3.6820E-02

FISSION SPECTRUM

GROUP 1	GROUP 2
1.0000E+00	0

TABLE 5.19

COMPARISON OF k_{eff} FROM VARIOUS CODES FOR THE TRANSPORT ASPECTS OF THE ROD BUNDLE PROBLEM

Code	Mesh	ANGLE/NOM	NORD	k_{eff}
DOT-III	48 x 48	S_8	-	1.08714
	24 x 24	S_8	-	1.08709
	12 x 12	S_8	-	1.08441
	24 x 24	S_4	-	1.08724
	24 x 24	S_2	-	1.09195
TWOTRAN-II	48 x 48	S_8	-	1.08727
	24 x 24	S_8	-	1.08712
	12 x 12	S_8	-	1.08427
	24 x 24	S_4	-	1.08708
	24 x 24	S_2	-	1.09214
FELTRAN	12 x 12	2	1	1.08116
	12 x 12	3	1	1.08068
	12 x 12	2	2	1.08663
	24 x 24	2	1	1.08525

The FELTRAN results for the (12 x 12) linear elements are very poor as would be expected from using linear eements. When the mesh was refined to (24 x 24) in the case for 2-moments and linear elements there is quite an increase in the value of k_{eff} thereby emphasising that with mesh refinement better accuracy can be expected even with linear elements. The (12 x 12) mesh using quadratic elements and a 2-moment trial function produces an excellent k_{eff} which is not too far from the DOT-III or TWOTRAN-II benchmark value. To summarise it is expected that FELTRAN can produce excellent values of k_{eff} for this problem when higher spatial and angular resolutions can be attempted.

In the diffusion mode, Fowler and Vandy of ORNL used the VENTURE and VANCER codes to obtain their results. VENTURE is a mesh-centred finite difference code while VANCER is mesh-edged. The VANCER code was also able to produce results using linear finite elements. In these results the convergence criterion on k_{eff} was 5×10^{-5}. In the same vein, Zolotov and Rahn used the CITATION [30] code (described in Section 5.2) with a convergence criterion of 10^{-4}. The results of these diffusion codes and FELTRAN are presented in Table 5.20.

The entries for the mesh sizes in all the codes refer to number of mesh points except in CITATION and FELTRAN, where the elemental concept has always applied. Therefore the mesh sizes quoted for the VANCER finite element results and FELTRAN for NORD = 1 refer to the same element and meshes. The most striking thing about the results in Table 5.20 is the identical values for k_{eff} from the

TABLE 5.20

COMPARISON OF k_{eff} FROM VARIOUS CODES FOR DIFFUSION ASPECTS OF THE ROD BUNDLE PROBLEMS

Code	Mesh	NORD	k_{eff}
VENTURE	12 x 12	-	1.09238
	24 x 24	-	1.08759
	48 x 48	-	1.08606
	96 x 96	-	1.08565
VANCER (finite difference)	13 x 13	-	1.08061
	25 x 25	-	1.08389
	49 x 49	-	1.08525
VANCER (finite element)	13 x 13	-	1.08185
	25 x 25	-	1.08454
	49 x 49	-	1.08525
FELTRAN	12 x 12	1	1.08185
	12 x 12	2	1.08544
	12 x 12	3	1.08642
	24 x 24	1	1.08454
	24 x 24	2	1.08548
	48 x 48	1	1.08525
CITATION	48 x 48	-	1.087575

VANCER finite element and FELTRAN with NORD = 1 for the coarse, medium and fine meshes. Also the finest mesh VANCER finite difference result attained the same value as the linear finite elements results. For this fine mesh the CITATION code produced a higher value of k_{eff} than the VANCER and FELTRAN results. In both VANCER and FELTRAN the values of k_{eff} increase with mesh refinement while the reverse was observed for VENTURE. Of particular interest is the fact that the k_{eff} from the (24 x 24) quadratic elements of FELTRAN do not show an appreciable improvement over that of the (12 x 12) mesh. The trend observed in Section 5.3, viz. that higher order elements do produce excellent results even with a coarse mesh, is confirmed by these results.

In conclusion it is seen that FELTRAN can achieve excellent results for benchmark problems. This problem in particular demands considerable computer storage requirements and consequently the use of FELTRAN is not feasible at present for eigenvalue problems with very high spatial and angular resolutions. Even with a coarse mesh of quadratic elements and a 2 moment trial function the k_{eff} obtained was very close to the benchmark value.

5.7 A 1-Group Scattering Problem

In this problem the aim is to show that FELTRAN can produce results that are free from ray effects and at the same time accurate. It was mentioned in Section 1.5 that one of the aims of the FEM in solving the Boltzmann transport equation was to eliminate ray effect which is a

major defect of the discrete ordinates method. According to Lathrop [59], the ray effect, peculiar to discrete ordinates method, is due to the discretization of the angular variable of the leakage operator in the transport equation especially in problems with isolated sources. This discretization restricting the particles to travel or stream in straight lines between collisions produces the flux distortions.

Several remedies have been proposed for the elimination or mitigation of the ray effect in the discrete ordinates method [62,54,65,59]. Lathrop [59] has suggested a method whereby the discrete ordinates equations are altered in order that they have the desirable properties of spherical harmonics equations. In addition, Lathrop also provided evidence that using more angular directions in the discrete ordinates method (in this case the code used was TWOTRAN [60]) do not remove ray effects. Examples for S_2, S_4 and S_{16}, involving 6, 16 and 144 angular directions respectively, were provided and it was shown that even in the S_{16} calculation "bumps" were still present.

A typical problem to illustrate ray effect was reported by Lillie and Robinson [65]. They used linear triangular elements in their finite element formulation called DAFE which included a discrete angle representation to compare with results from DOT-III [82], a discrete ordinates code. Both DAFE and DOT-III have already been discussed in Section 5.

Fig.5.22 shows the geometry and material composition of the problem which is completely bounded by bare surfaces. The basic mesh of (3 x 6) elements as analysed by FELTRAN is shown in Fig.5.23. Table 5.21 shows the cross-sections for the problem. In actuality materials 1 and 2 are identical except that material 1 also contains a fixed source. Since no value is quoted for the source it is assigned the arbitrary value of 1.Ø for FELTRAN calculations.

Lillie and Robinson undertook an S_4 calculation using 144 squares and an S_{12} calculation using 576 squares on DOT-III while on DAFE they produced an E_4 calculation using 288 triangles. The S_4 and S_{12} calculations resulted in the use of 16 and 96 discrete angular directions respectively. The E_4 calculation required only 6 angular directions. The results from Lillie and Robinson are reproduced in Fig.5.24, in which the scalar flux in the y-direction at x = 2.875 cm are presented.

The situation should be contrasted to that of FELTRAN where only a coarse mesh of (3 x 6) elements were used. However the analysis was performed by using linear, quadratic and cubic elements and using a trial function of 2, 3 and 4 moments. It is to be expected that with a relatively coarser mesh when compared to those of DOT-III and DAFE the higher order elements would give the more accurate results.

Figs.5.25, 5.26, 5.27 show the FELTRAN results achieved with linear, quadratic and cubic elements respectively. In each case trial functions ranged from 2 to 4 moments.

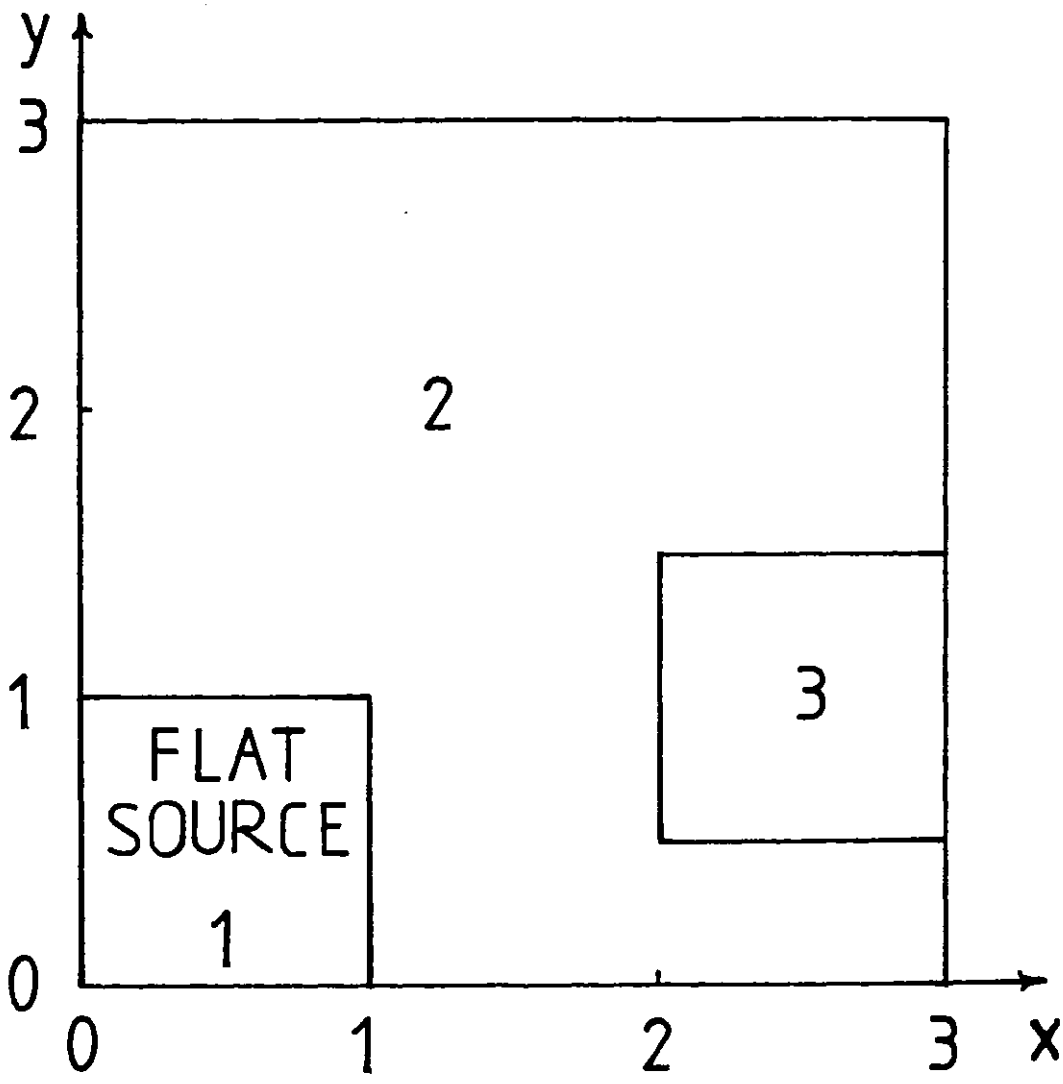

Fig.5.22 Geometry and material composition of the 1-group scattering problem (dimensions in cm)

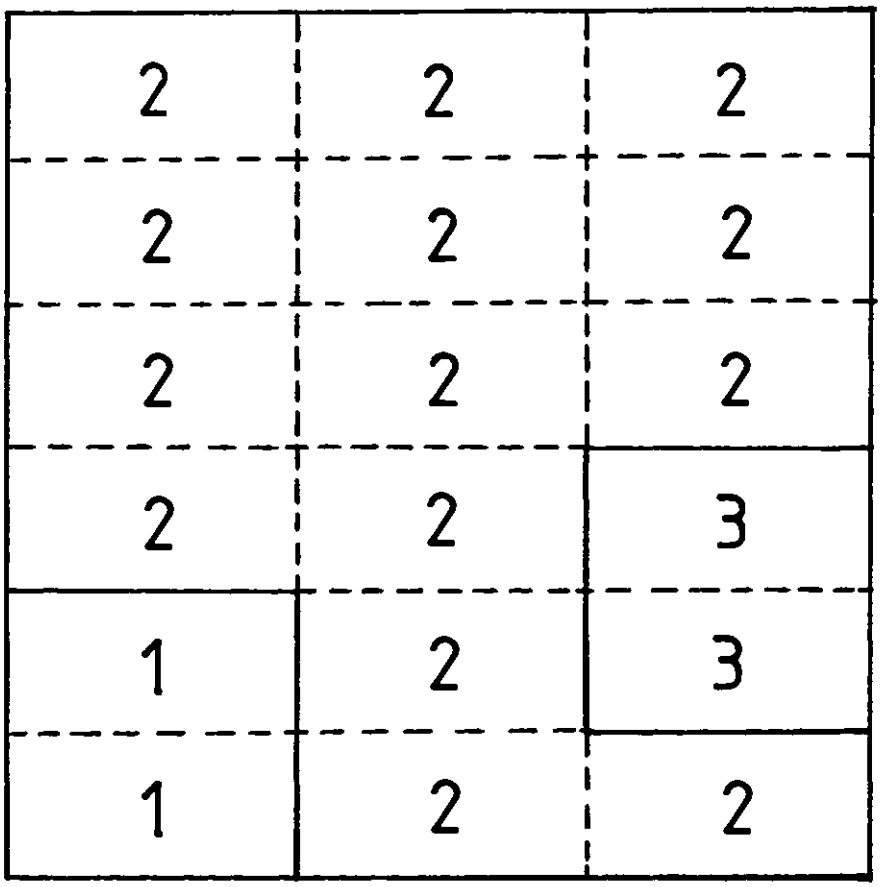

Fig.5.23 Basic mesh of (3 x 6) elements

TABLE 5.21

CROSS-SECTIONAL DATA FOR THE

1-GROUP SCATTERING PROBLEM

CROSS-SECTIONS

REGION NO 1

POS	GROUP 1
1	0
2	7.5000E-01
3	2.5000E-01

REGION NO 2

POS	GROUP 1
1	0
2	7.5000E-01
3	2.5000E-01

REGION NO 3

POS	GROUP 1
1	0
2	1.0000E+00
3	9.0000E-01

SOURCES

REG	GROUP 1
1	1.0000E+00

REG	GROUP 1
2	0

REG	GROUP 1
3	0

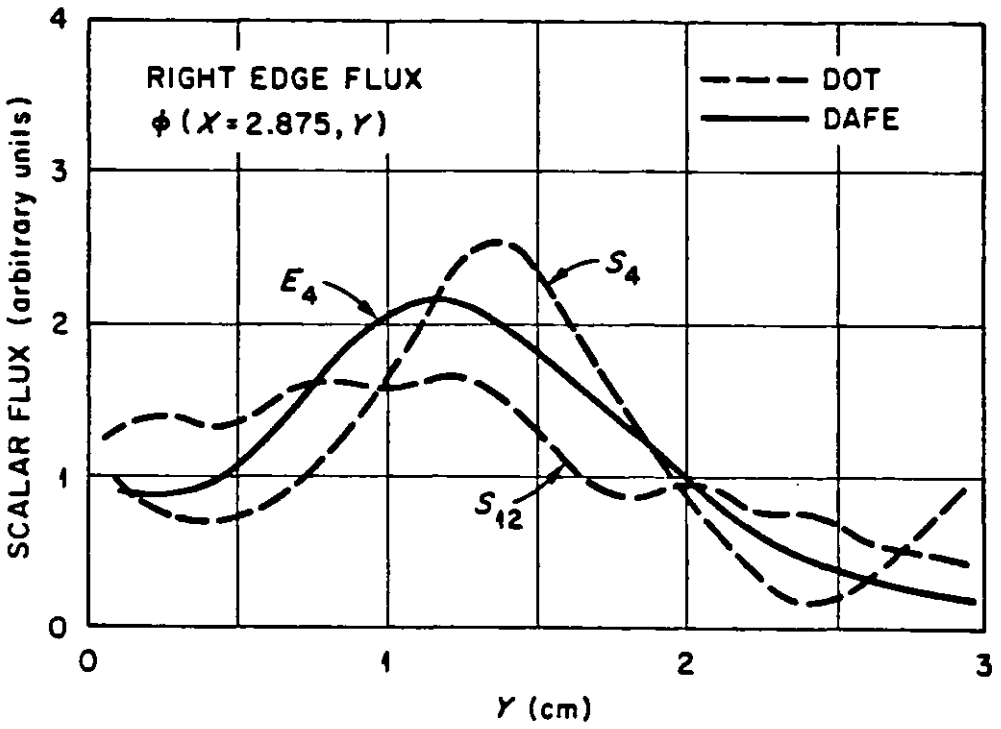

Fig.5.24 Lillie and Robinson's results for the 1-group scattering problem

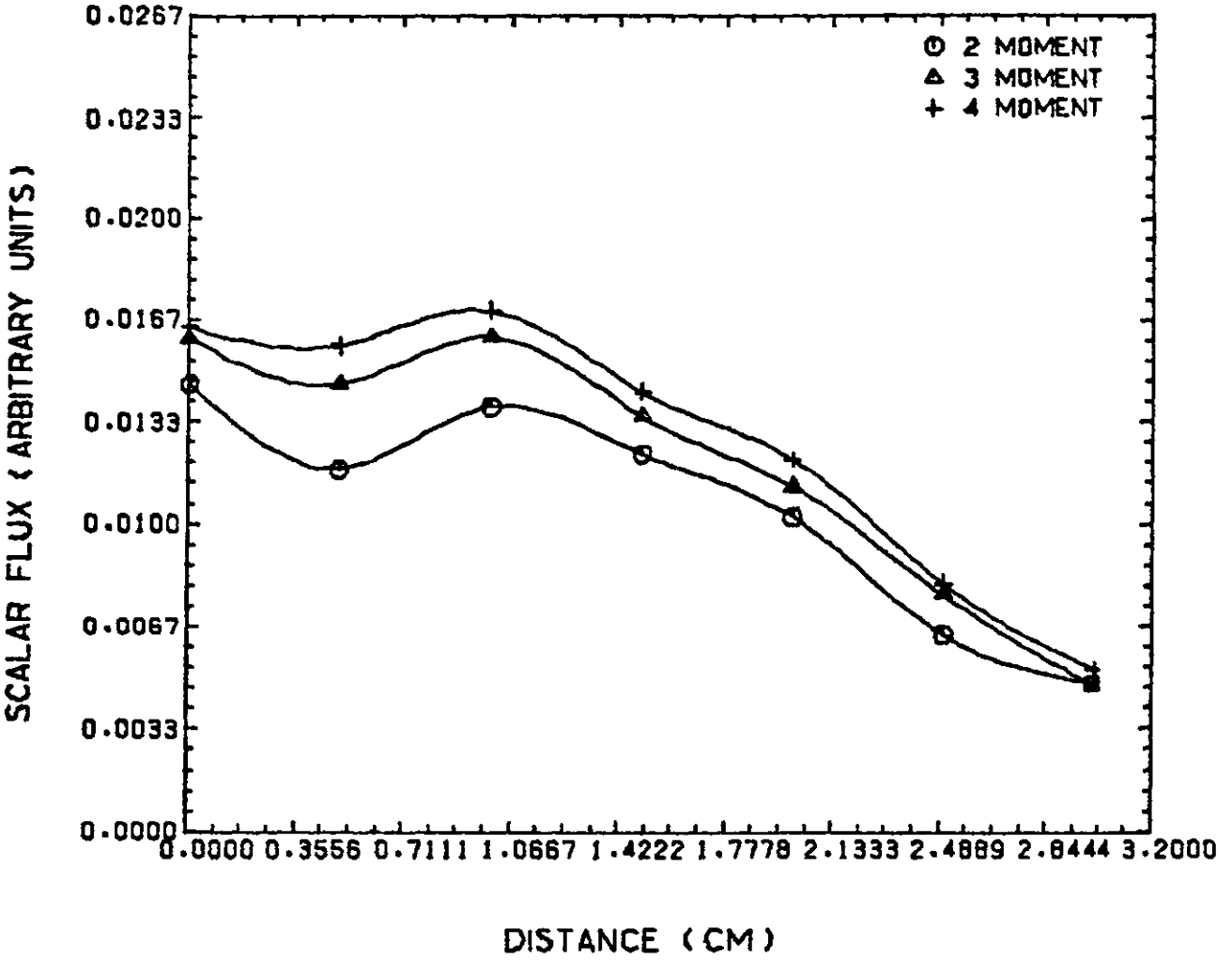

Fig.5.25 FELTRAN results for the 1-group scattering problem using linear elements

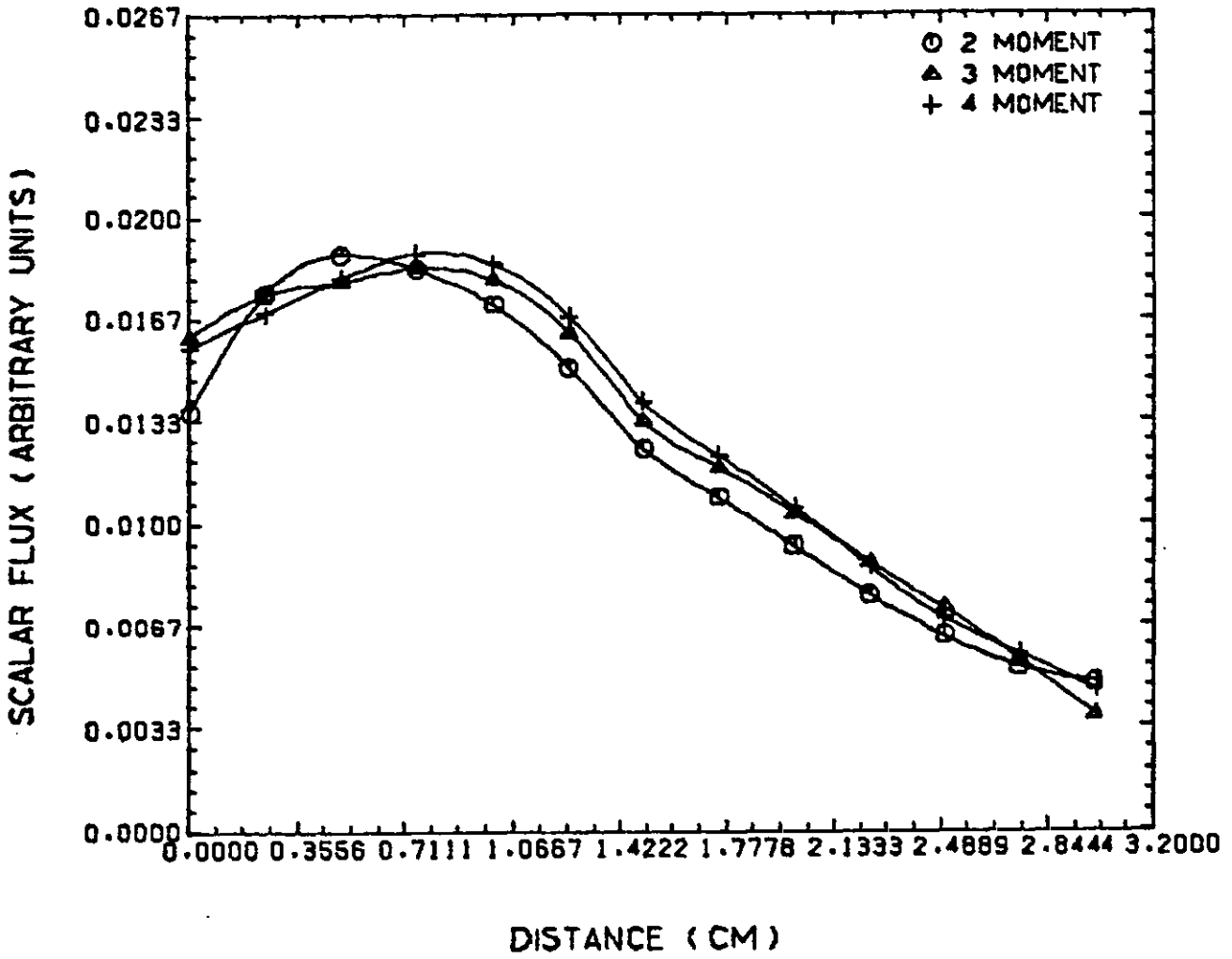

Fig.5.26 FELTRAN results for the 1-group scattering problem using quadratic elements

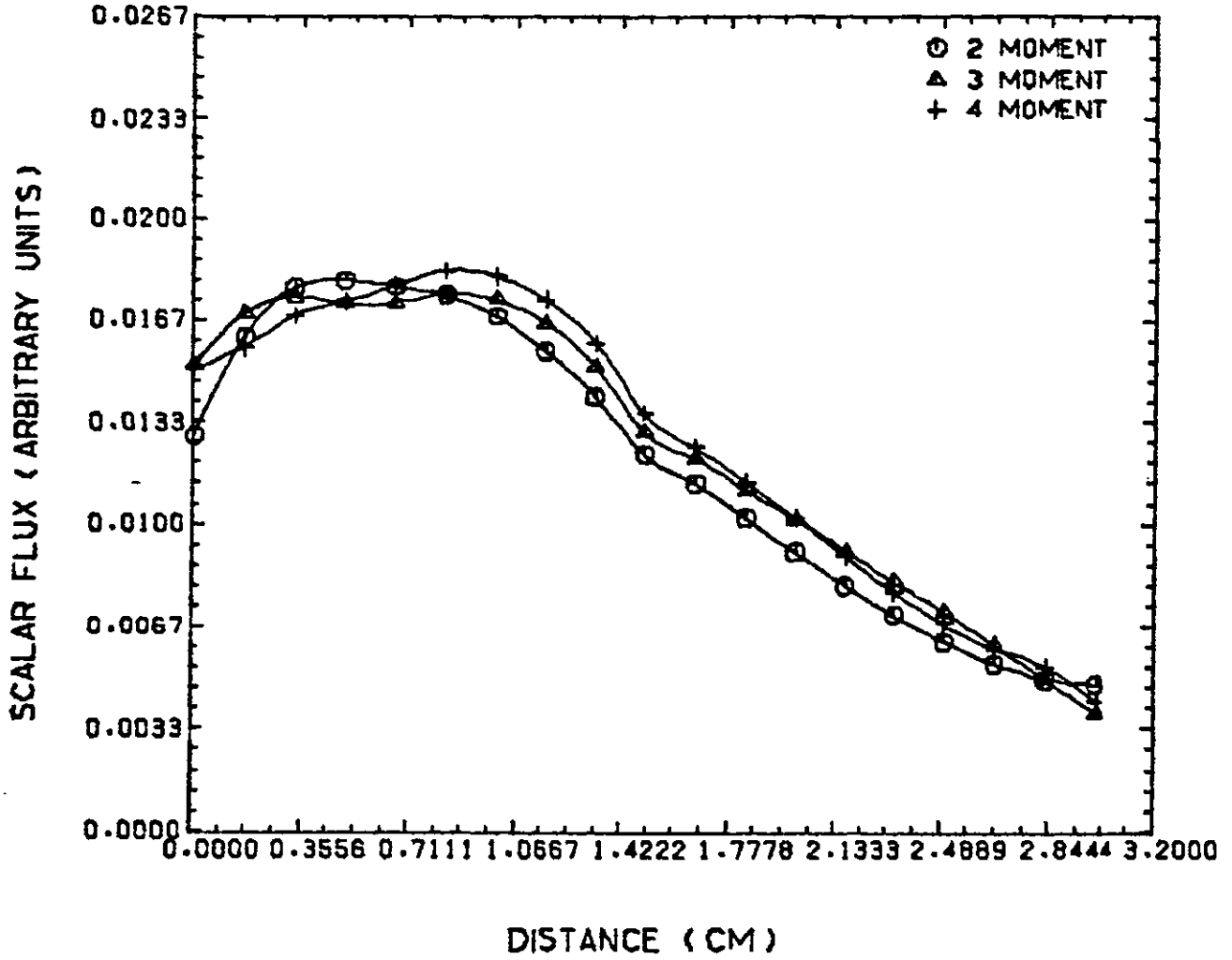

Fig.5.27 FELTRAN results for the 1-group scattering problem using cubic elements

To start with, Lillie and Robinson has criticised the DOT-III results as inaccurate on two counts. Firstly, the flux gradients for the S_4 calculations predicted an inward flow of neutrons. Secondly, the S_{12} results, while being more representative of the physics of the problem, display many oscillations due to the presence of ray effect. In contrast the DAFE E_4 results were free of ray effects thereby confirming that the finite element method does eliminate ray effects. However the large hump illustrated by the E_4 curve is subjected to uncertainty which the researchers could not resolve with another analysis with higher angular approximation owing to problems of computer storage on their local environment. Furthermore, the DAFE result indicates no leakage at the bare surface at y = 0 cm, a serious deficiency.

Turning our attention now to the FELTRAN results it must be mentioned that the FELTRAN results could not be compared with the results of Lillie and Robinson in terms of the scalar flux's magnitudes because no magnitude of the source (other than the fact that it is flat) was provided. Nevertheless from looking at Figs.5.25 to 5.27 it can be said that the linear element results of FELTRAN are inaccurate in the neighbourhood of y = 0.0 cm where there seems to be a flux inflow at the vacuum boundary. However this effect for the linear elements decreases when the trial function is increased. On the other hand no such discrepancy exists for the quadratic and cubic elements. Within the limits of the plotter precision the curves in Figs.5.26 and 5.27 can be said to

be smooth and display no oscillation. Hence this further confirms that finite elements do eliminate ray effects. It is to be expected that the linear elements would give better results with finer meshes but no attempt was made since the higher order elements already provide convincing evidence with a coarse mesh that ray effects do not exist in finite elements.

Fig.5.28 brings together the 4 moment results for the three types of elements. As can be seen the FELTRAN results for quadratic and cubic elements agree very closely.

The accuracy of the results was tested by calculating the ratios of the maximum flux to those at the vacuum boundaries. Table 5.22 gives these ratios for the DOT-III S_{12}, DAFE E_4 and FELTRAN cubic elements with a 4 moment trial function. These ratios for DOT-III and FELTRAN agree quite well with each other while the DAFE result is relatively misplaced. When the ray effect ripples in the DOT-III S_{12} fluxes are disregarded there is reasonable agreement with the FELTRAN flux. It is then reasonable to say that the FELTRAN and DOT-III S_{12} are the best available solutions, and the FELTRAN solution is to be preferred because it is not beset with the ray effect ripples.

Table 5.23 shows the computing aspects for the FELTRAN results. All the tabulated FELTRAN results were obtained with the out-of-core solver. No comparison can be made with the DOT-III and DAFE results since Lillie and Robinson did

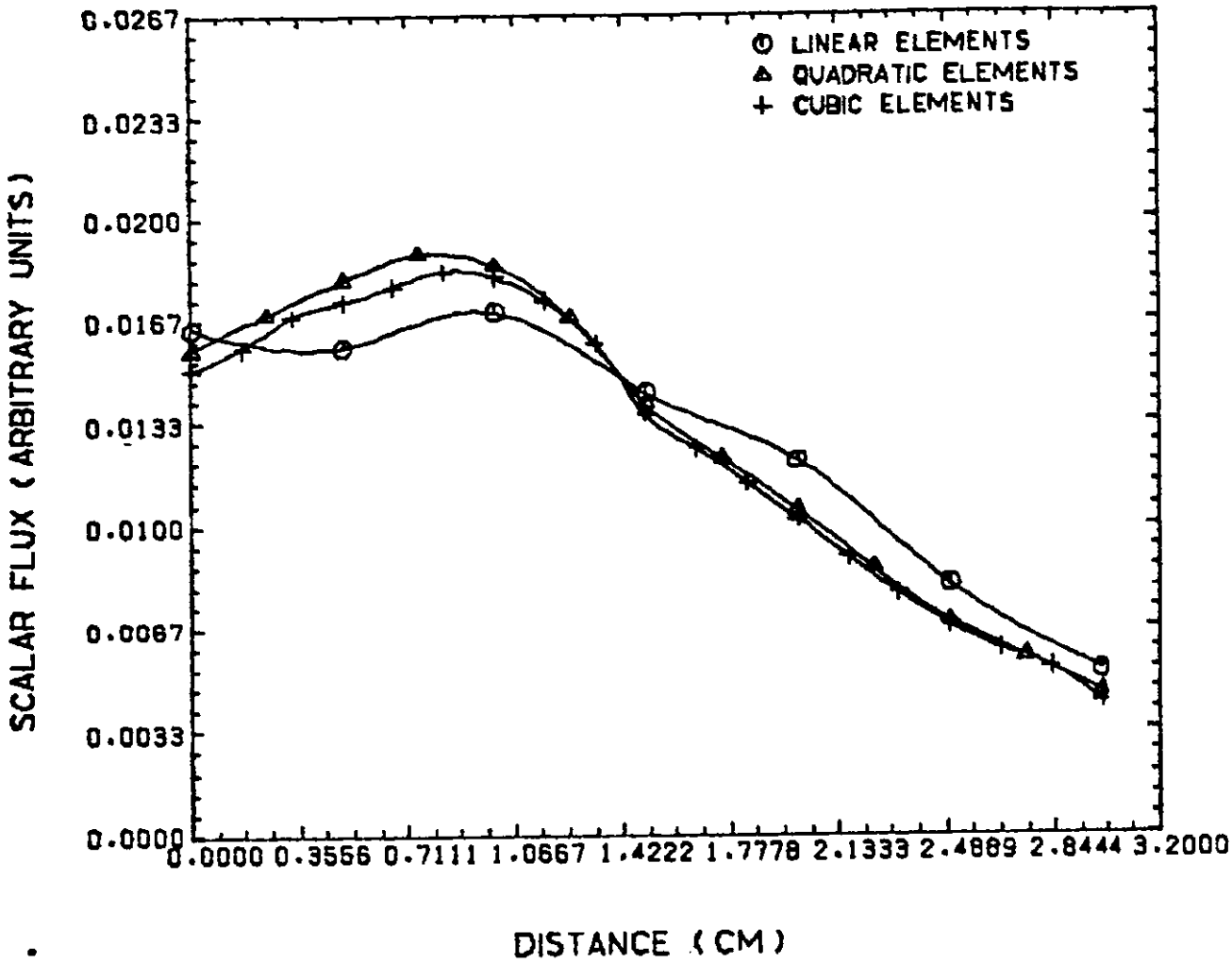

Fig.5.28 FELTRAN results for the 1-group scattering problem using a 4-moment trial function with linear, quadratic and cubic elements

TABLE 5.22

RATIOS OF MAXIMUM FLUX TO THOSE AT

THE VACCUM BOUNDARIES FROM THE VARIOUS CODES

CASE	$\phi_{max}/\phi_{0.0}$	$\phi_{max}/\phi_{3.0}$
DOT-III S_{12}	1.4	3.9
DAFE E_4	2.4	11.0
FELTRAN cubic elements 4 moment t.f.	1.2	4.3

$\phi_{0.0}$ = scalar flux at y = 0.0 cm

$\phi_{3.0}$ = scalar flux at y = 3.0 cm

TABLE 5.23

COMPUTATION DATA ON THE FELTRAN RESULTS

USING THE OUT-OF-CORE SOLVER WITH 7 BLOCKS

NOM	NORD	Time (CDC 6600 seconds)	Time (AMDAHL) seconds)	In-Core Storage of Global Matrix	Actual Size of Global Matrix
2	1	1.64	-	768	2688
2	2	6.12	-	7616	24752
2	3	29.06	-	32640	103360
3	1	3.99	-	3888	13608
3	2	38.93	-	38556	125307
3	3	-	31.03	165240	523260
4	1	-	1.97	12288	43008
4	2	-	23.68	121856	396032
4	3	-	157.11	522240	1653760

Computing resources for FELTRAN results using the Out-of-Core Solver with 7 blocks

TABLE 5.24

PERCENTILE IN-CORE OCCUPANCY OF THE GLOBAL MATRIX

WITH RESPECT TO ACTUAL SIZE

NORD	% In-Core Global Matrix to Actual Size
1	28.57
2	30.77
3	31.58

Number of blocks = 7

not report on this aspect at all. Nevertheless Table 5.23 is related to Table 5.24 where the percentage values for the in-core storage of the global matrix are presented. These percentages only differ in the order of the element with the same number of blocks (which is 7 in this case). The storage refers to the individual elements of the matrix. The AMDAHL results are single precision results. There is no loss of precision in using single precision computations for source problems. To bear this out Table 5.25 represents the single and double precision results for the cubic elements and 3 moment trial function at the element boundaries. The values are the scalar fluxes in the y-direction at x = 2.875 cm. Since the values only differ by no more than ± .00002 at the most therefore the single precision results are accurate enough for source problems. However the time taken to run the double precision case was 50.27 seconds, about 60% more than the time for the single precision results.

On the aspect of computing time, a run was also made for this case using the in-core solver on the AMDAHL computer and with single precision arithmetic. This was found to be 56.47 seconds. On this basis the in-core solver can be said to be slower than the out-of-core solver, even when double precision arithmetic was used. It is surprising that this should be so but when the internal mechanics of BANSOL and SESOL are examined the latter algorithm has a provision for leaving out unnecessary zero arithmetic operations. Therefore a large number of zero

TABLE 5.25

COMPARISON OF SINGLE AND DOUBLE PRECISION

RESULTS ON THE AMDAHL FOR THE CASE

USING CUBIC ELEMENTS AND A 3-MOMENT TRIAL FUNCTION

Y(cm)	Single Precision	Double Precision
0.0	0.01516	0.01517
0.5	0.01722	0.01723
1.0	0.01734	0.01736
1.5	0.01306	0.01307
2.0	0.01018	0.01019
2.5	0.00716	0.00717
3.0	0.00385	0.00386

arithmetic operations must have been encountered in this particular problem due to the nature of cubic elements such that even with the relatively time consuming I/O operations the out-of-core solver still managed to be more than 80% faster in this particular case.

On the other hand when a smaller problem was examined, for example the 2 moment linear element case, the time taken using the in-core solver was 1.28 seconds as contrasted to 1.61 seconds for the out-of-core solver (in this example both are CDC 6600 time). This reflects on the fact that the number of zero entries in this example is relatively less and the I/O time becomes the over-riding factor.

To conclude, the study of this problem has shown that FELTRAN can handle the problem of ray effects and yield accurate answers with the higher order elements even with a coarse mesh. The out-of-core solver has been shown to be reliable and in this example, albeit with only 7 blocks, can surpass the in-core solver in terms of speed.

5.8 A Shielding Problem

Much has been mentioned about the problem of ray effects in the discrete ordinates method due to the angular discretization. Turning to the spatial aspects of the discrete ordinates method, the diamond differencing (DD) scheme has been the traditionally adopted method. As of late, the linear characteristic method [6, 57] has been one of the recently proposed methods to represent the spatial discretization in the discrete ordinates method.

In brief the major difference between the DD and LC method is that in the LC method the boundary conditions and source term for a spatial cell are represented by linear functions and the cell transport problem solved analytically by integration along its characteristic lines from which linear representations are generated for use as boundary conditions for adjoining cells and for constructing a scattering source for the next iteration.

Larsen and Alcouffe [57] have chosen a 3-group shielding problem to compare the merits of the DD and LC schemes. In their conclusion the general concensus is that, using the same mesh, LC requires lengthier computation times, generally less than two times those for DD but it provides more accurate and stable results. Storage requirements are essentially the same for both methods.

The geometry and compositional layout for this 3-group problem is shown in Fig.5.29. This layout is a 90° rotation from that shown by Alcouffe and Larsen. The reason for analysing the problem in this manner for FELTRAN is that the bandwidth associated with this arrangement will be less. From this arrangement, the top and left sides are bare surfaces while the other two are perfect reflectors. Table 5.26 shows the cross-sections for this problem and the fixed source contributions by group. Alcouffe and Larsen did not provide the magnitude of this source (i.e. material 1) but a total of 1 over the groups is assumed in the FELTRAN calculations.

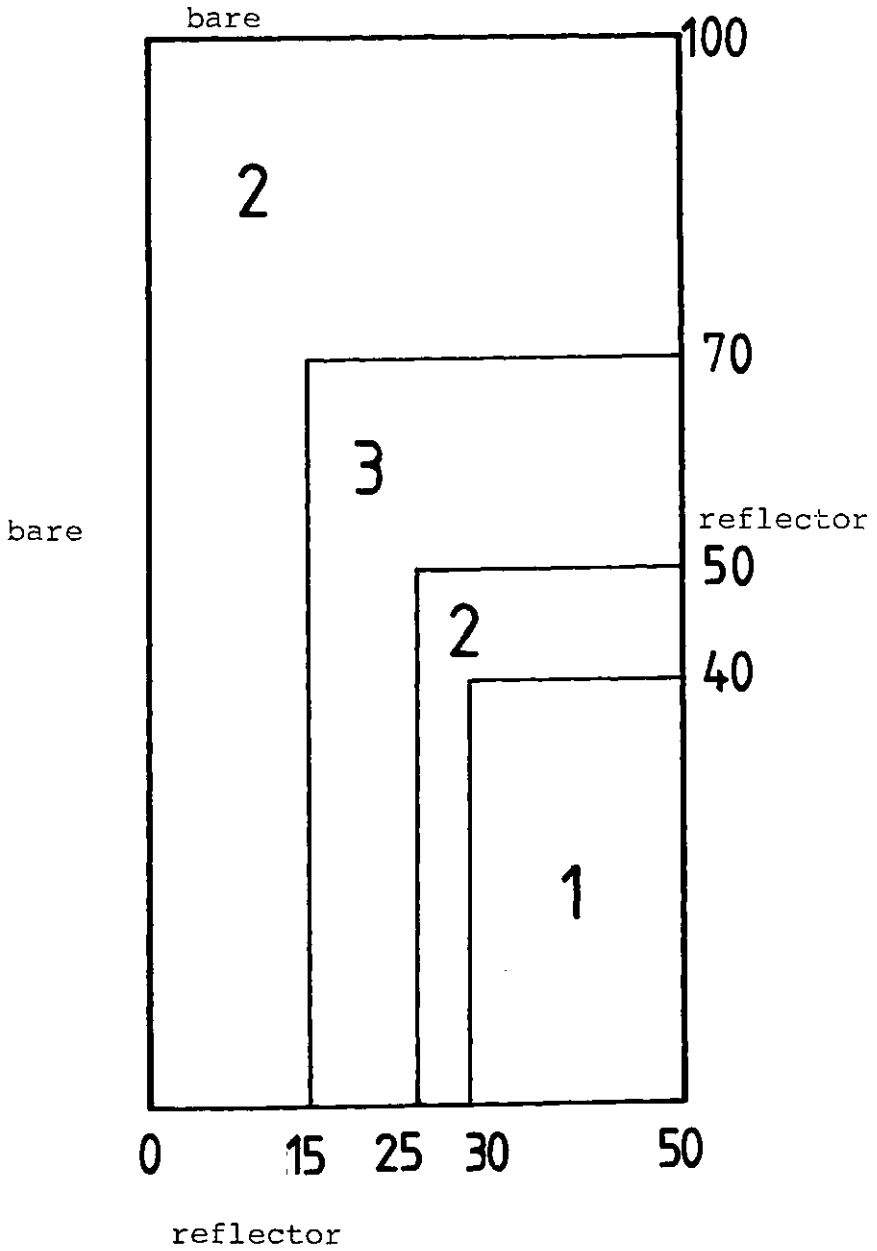

Fig.5.29 Geometry and composition of the 3-group shielding problem (dimensions in cm)

TABLE 5.26

CROSS-SECTIONAL DATA FOR THE 3-GROUP SHIELDING PROBLEM

CROSS-SECTIONS

REGION NO 1

POS	GROUP 1	GROUP 2	GROUP 3
1	0	0	0
2	2.6560E-01	1.1745E+00	3.2749E+00
3	1.6000E-01	1.1010E+00	3.2565E+00
4	0	1.0520E-01	7.3000E-02
5	0	0	0

REGION NO 2

POS	GROUP 1	GROUP 2	GROUP 3
1	0	0	0
2	2.6560E-01	1.1745E+00	3.2749E+00
3	1.6000E-01	1.1010E+00	3.2565E+00
4	0	1.0520E-01	7.3000E-02
5	0	0	0

REGION NO 3

POS	GROUP 1	GROUP 2	GROUP 3
1	0	0	0
2	2.1630E-01	3.2550E-01	1.1228E+00
3	1.7600E-01	3.2360E-01	9.3280E-01
4	0	3.9900E-02	9.8280E-01
5	0	0	0

SOURCES

REG	GROUP 1	GROUP 2	GROUP 3
1	7.3900E-01	2.6100E-01	0

REG	GROUP 1	GROUP 2	GROUP 3
2	0	0	0

REG	GROUP 1	GROUP 2	GROUP 3
3	0	0	0

Two sets of solutions were provided for both the DD and LC methods using spatial meshes of (27 x 27) and (55 x 55) spatial cells and an S_8 quadrature set with a convergence criterion of 10^{-4} on the pointwise flux. Full convergence was not achieved on the DD fine mesh and this behaviour by DD for fine meshes in general is one of the motivations for seeking a more stable and accurate differencing scheme. However the authors added that the coarse mesh case is about as coarse as it could be for both the methods to achieve full convergence. These two sets of results are shown in Fig.5.30. The distance at 0.0 cm and 50.0 cm corresponds to the horizontal distance of 50 cm and 0 cm in Fig.5.29. The cell-averaged fluxes are for those cells at the top face as seen in Fig.5.29. As can be seen the DD results do not show as smooth a variation as the LC results in both cases. Since cell-averaged fluxes were plotted it is possible that negative fluxes were the order of the day for the DD results especially since convergence was not achieved in the fine mesh run.

Fig.5.31 shows the (12 x 20) mesh used in FELTRAN. A mesh of (6 x 10) would have sufficed but negative values in the scalar flux were observed for some values in the lower groups. However no negative scalar fluxes resulted when the (12 x 20) mesh was used. As such the results reported here are for the (12 x 20) mesh.

The cell-averaged fluxes along the top face are also calculated from the FELTRAN results. These fluxes are the sum over the 3 groups, and are given by:

LC (——) and DD (x x x) Cell-Average Fluxes on Top Edge of Shielding Problem (Coarse Mesh).

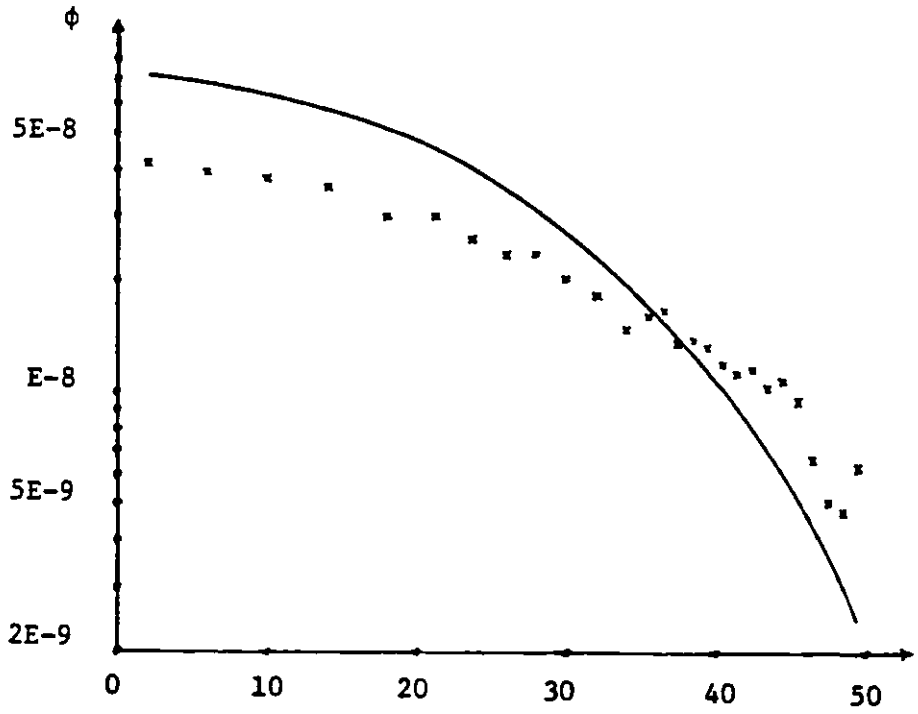

LC (——) and DD (x x x) Cell-Average Fluxes on Top Edge of Shielding Problem (Fine Mesh).

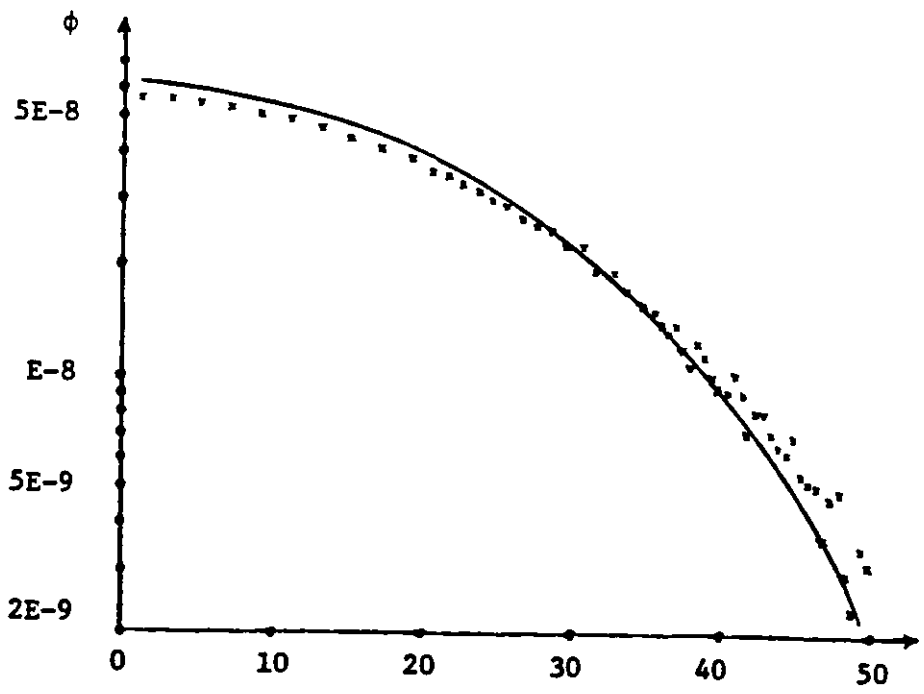

Fig.5.30 Results of Larsen and Alcouffe

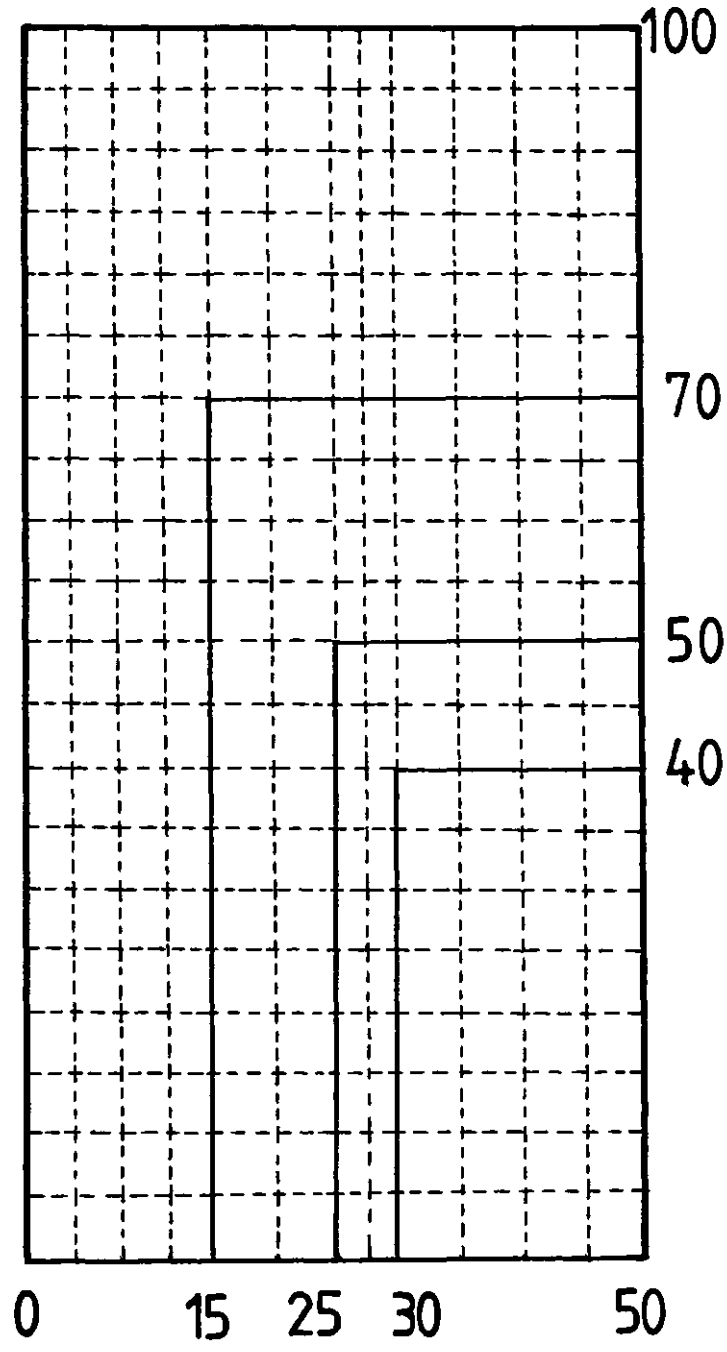

Fig.5.31 The (12 x 20) mesh used in FELTRAN for analysing the 3-group shielding problem

$$\bar{\phi} = \frac{\int_V \sum_{g=1}^{3} \phi_g \, dV}{\int_V dV} \qquad (5.10)$$

$$\bar{\phi} = \frac{\sum_{g=1}^{3} \sum_{i=1}^{L} \int_V N_i \, dV \cdot u_{gi}}{\int_V dV} \qquad (5.11)$$

where,

L = number of nodal points in the cell.

Figs.5.32, 5.33 show the FELTRAN results with a 2-moment trial function using quadratic and cubic elements respectively. Additionally Fig.5.34 shows the 3 moments case with quadratic elements. It is obvious that the FELTRAN results are excellent since no distortion in the cell-averaged fluxes is discernible. Besides when compared with the LC results the profiles are all in agreement. Also, in all the FELTRAN cases the ratio of the cell-fluxes at the ends is approximately 31. From Fig.5.31 it is estimated that in the LC results the number is approximately 30. Therefore good agreement is once more observed.

Fig.5.35 shows the 2-moments results for both quadratic and cubic elements. Agreement in both cases is excellent. In Fig.5.36 the quadratic elements results for 2 and 3 moments are shown. The results are nearly identical.

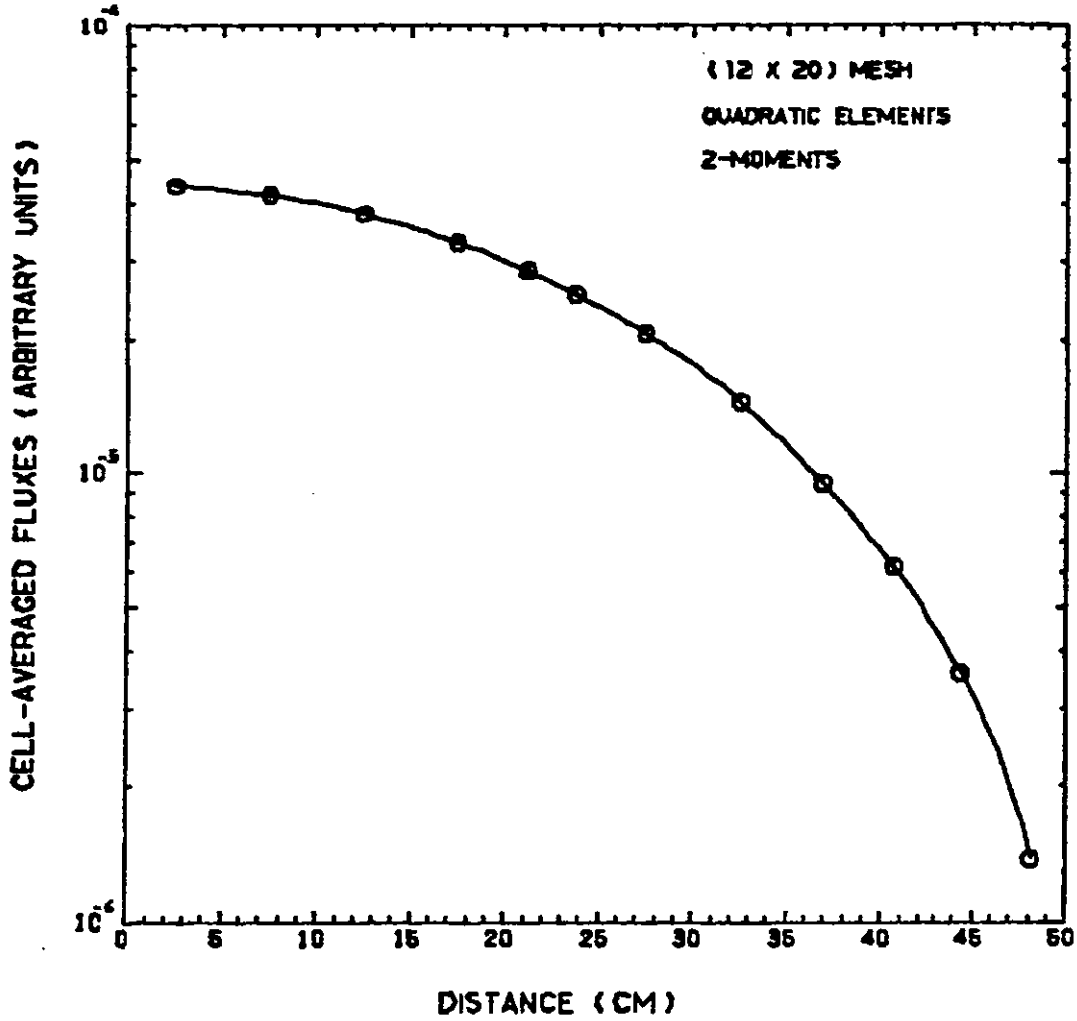

Fig.5.32 FELTRAN result for the 3-group shielding problem using (12 x 20) quadratic elements and a 2-moment trial function

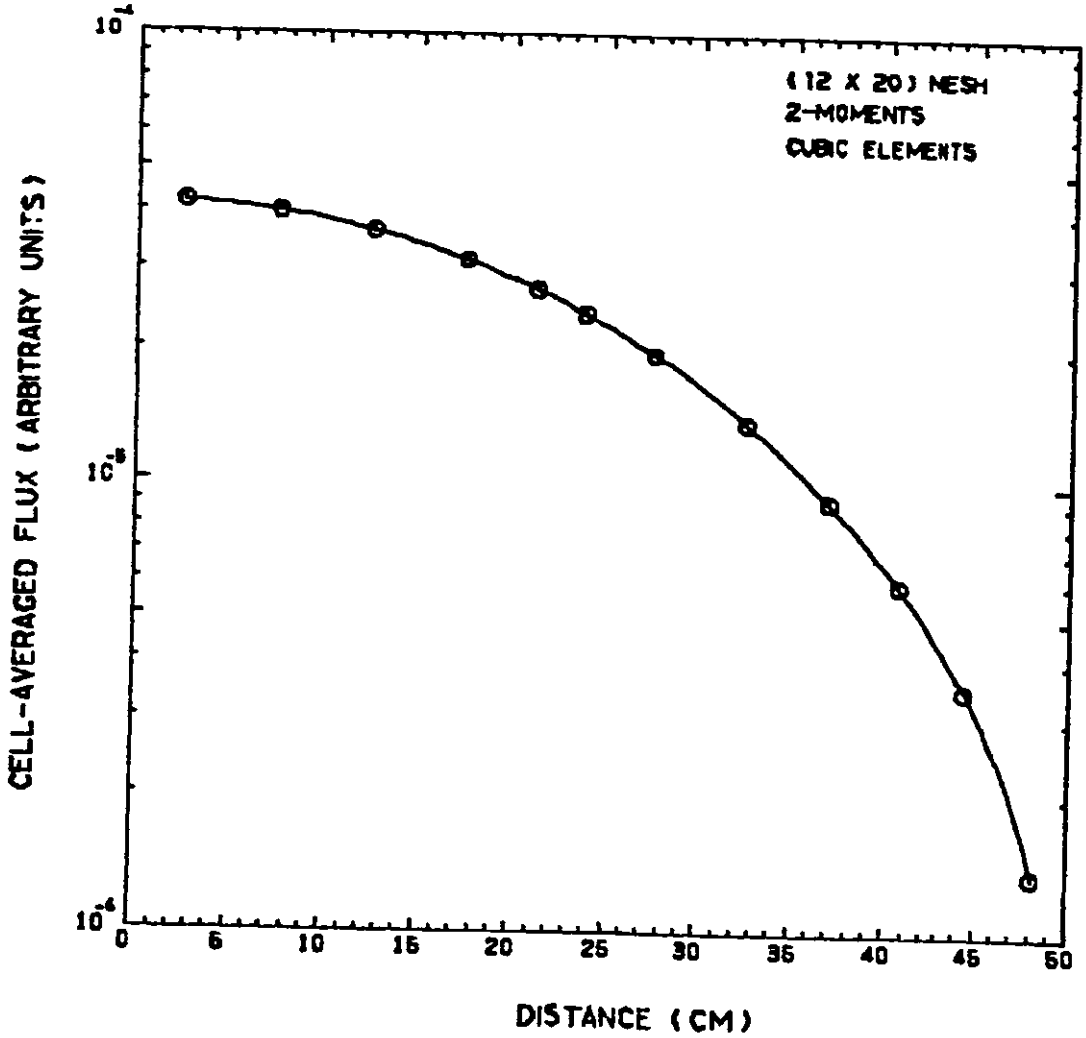

Fig.5.33 FELTRAN result for the 3-group shielding problem using (12 x 20) cubic elements and a 2-moment trial function

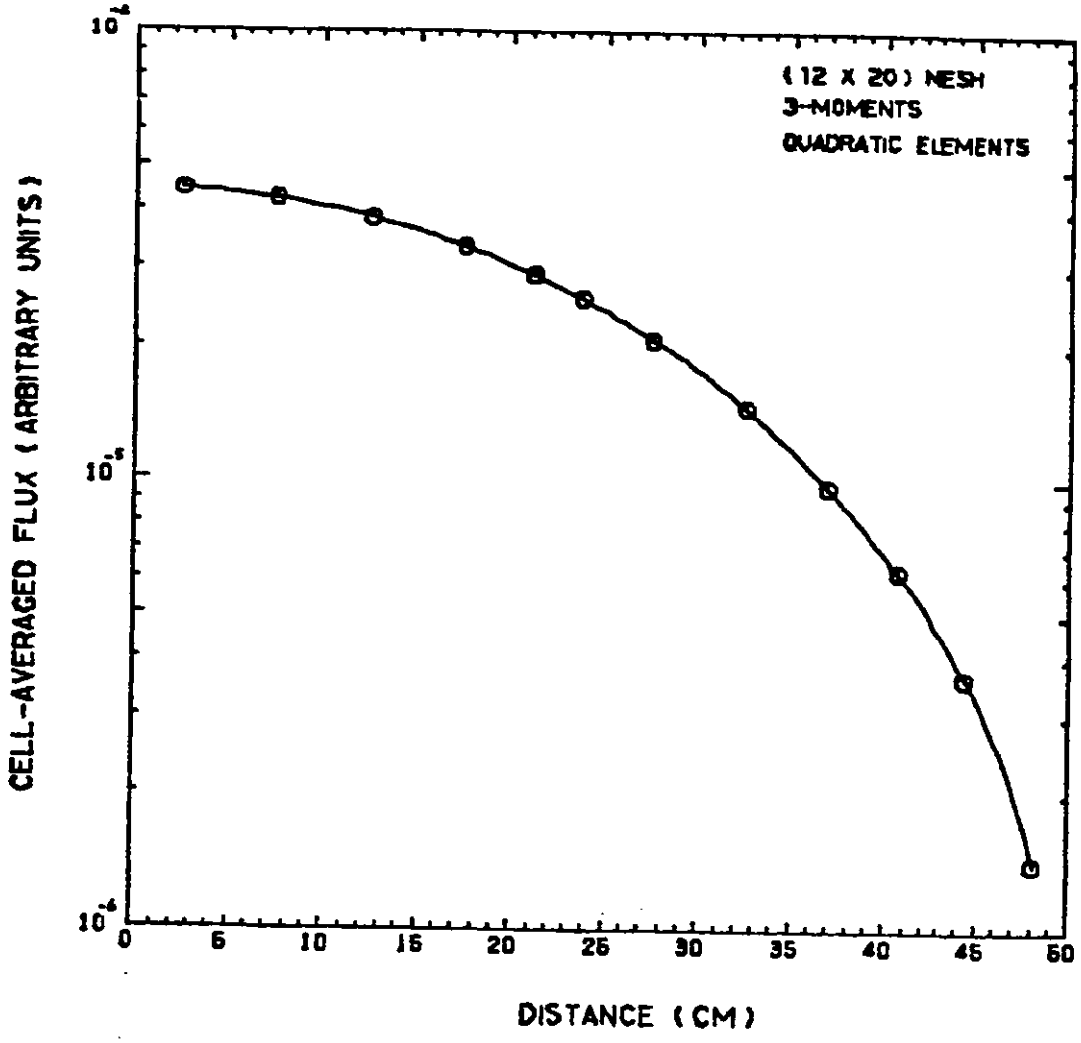

Fig.5.34 FELTRAN result for the 3-group shielding problem using (12 x 20) quadratic elements and a 3-moment trial function

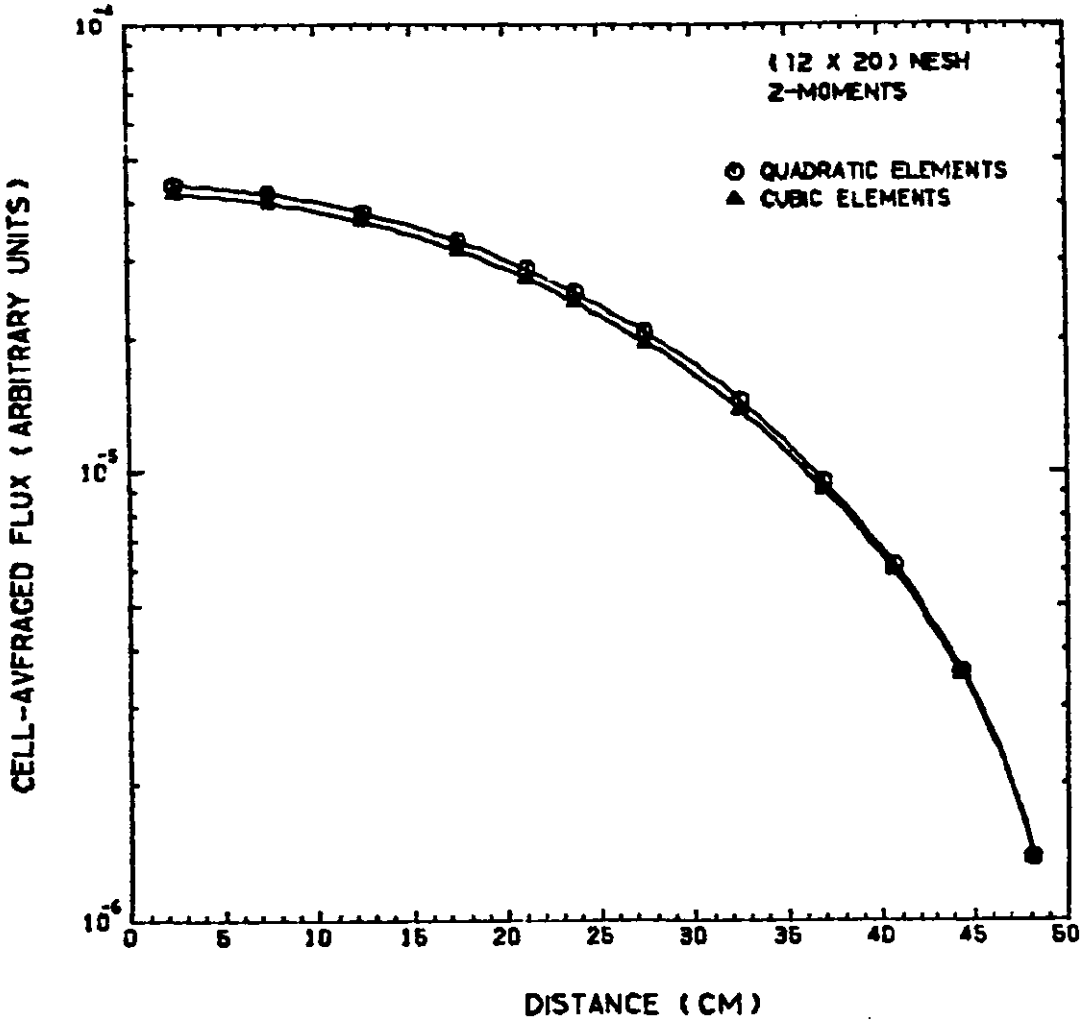

Fig.5.35 FELTRAN result for the 3-group shielding problem using (12 x 20) quadratic and cubic elements and a 2-moment trial function

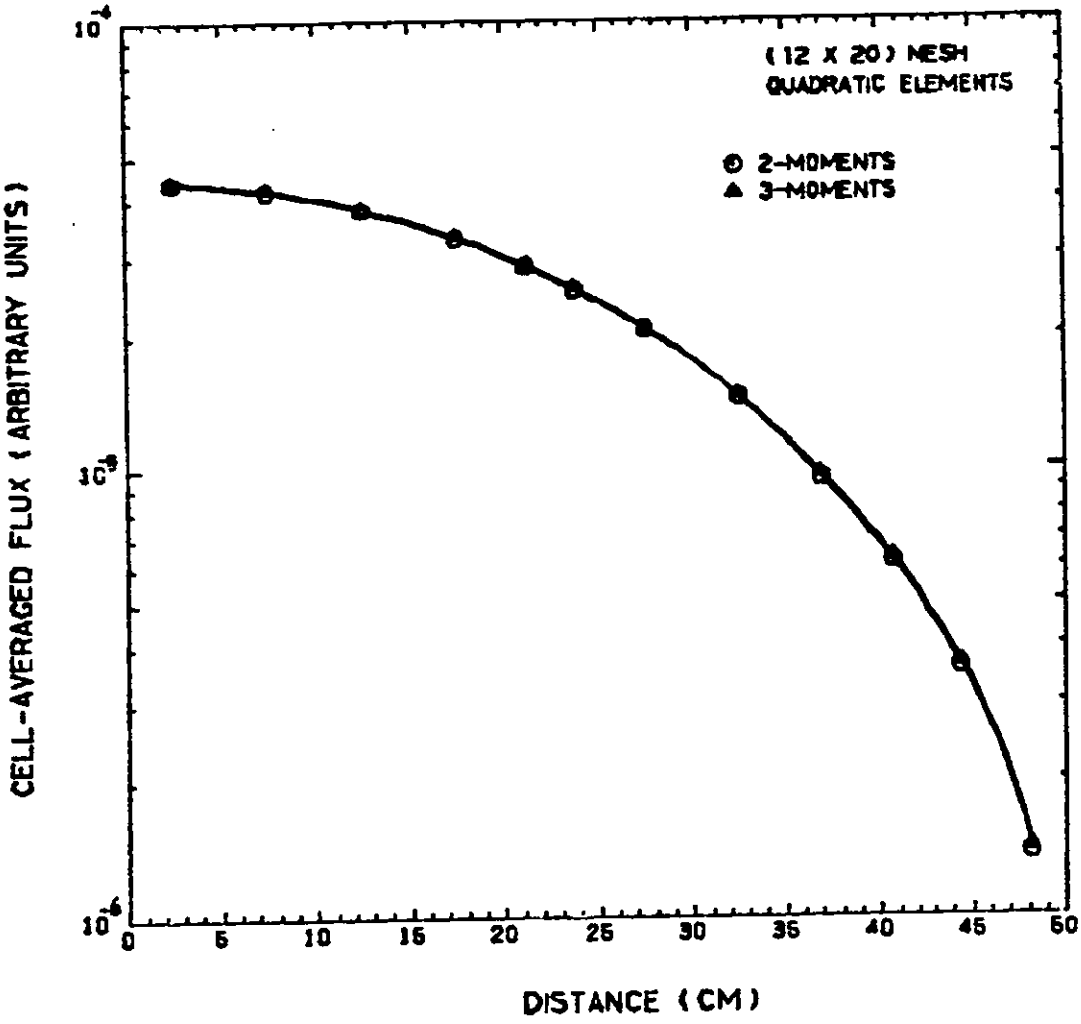

Fig.5.36 FELTRAN result for the 3-group shielding problem using (12 x 20) quadratic elements and a 2- and 3-moment trial function

Therefore, FELTRAN exhibits great potential for solving shielding problems. Taking this difficult problem as an exemplary case, in which two other finite difference codes showed difficulty in obtained convergence with a coarser mesh, FELTRAN has demonstrated its ability to produce accurate results with a relatively coarser mesh.

At this juncture our discussion will now be focussed on the out-of-core solver which was used to solve the 3 cases by FELTRAN. Table 5.27 shows the relevant parameters, storage requirements and times. Without the use of the out-of-core solver the last two problems would not have been solved even on the AMDAHL. For single precision arithmetic the maximum size of the global matrix would have to be less than 2 million storage locations. In the three cases the number of equations encountered were 4100, 9028 and 9225 respectively and 21 blocks were utilised each time. With the use of the out-of-core algorithm only slightly less than 10% of the actual storage for the global lmatrix was used which is very good savings indeed. However the execution times were lengthy, especially in the two larger jobs. This is to be expected because the number of equations to be solved has increased to more than 9000.

In the last section it was shown that BANSOL, the in-core solver, was slower than SESOL, the out-of-core solver when cubic elements were encountered. However it was added that there were only 7 blocks and 1 group. In this estimate the analysis was to be based on 21 blocks and 3 groups

TABLE 5.27

COMPUTATION DATA ON THE FELTRAN

RUNS FOR THE 3-GROUP SHIELDING PROBLEM

NOM	NORD	Time (AMDAHL seconds)	In-Core Storage of Global Matrix	Actual Size of Global Matrix	% In-Core of Global Matrix
2	2	157.98	84800	869200	9.76
2	3	1217.05	408480	4152880	9.84
3	2	1644.89	429300	4400325	9.76

and the same test was carried out. In executing a 1-moment linear element case on a (12 x 20) mesh the times taken were 0.41 seconds and 2.96 seconds on the AMDAHL for the in-core and out-of-core solvers respectively. When cubic elements were used the times were 37.13 and 26.97 seconds respectively. Therefore the evidence lends further conviction to the fact that the zero operations encountered in BANSOL, especially for cubic elements, are time consuming. Hence the introduction of a similar feature in BANSOL to eliminate the zero operations would speed up the computing time for the in-core solver.

In conclusion, FELTRAN has been successfully developed to a stage where practical shielding problems can be solved with relative ease. In practice there should not be any major problems with storage requirements since the out-of-core solver has been shown to be successfully implemented. Besides, it has been demonstrated that the out-of-core solver is not slow when compared with the in-core solver since it has the capability to avoid zero operations.

CHAPTER 6

DISCUSSION AND RECOMMENDATIONS

A journey of a thousand miles
begins with the first step.

Old Chinese saying

CHAPTER 6

The examples of the last chapter have shown that FELTRAN produces accurate results. Furthermore, wherever possible, it was shown that FELTRAN is fast. Also, with an out-of-core solver the problem of storage has been minimised, although only for source problems. All these pointers serve to indicate that FELTRAN could be developed into an alternative to S_N codes for commercial and academic work. To achieve this several recommendations are suggested. In putting forth these suggestions for future work it is not to be anticipated that they will be fulfilled in three man-years (the normal length of time taken to fulfill the requirements for a Ph.D. thesis). The length of time can only be guessed at when further progress has been made.

(1) Geometry and Mesh Specification

Perhaps this is the most important category for improvement. FELTRAN is at present limited to only x-y geometry. For two-dimensional analysis an alternative r-z capability is clearly needed. If successful this should be followed by an r-θ alternative. At present the CORFU package is available for generating the constants of the Reduced-Functional. This can be easily extended to produce the constants for r-z and r-θ geometries. In FELTRAN itself it would be the volume integrals and mesh generation where changes would have to be made to accommodate these capabilities.

Since the finite element method is most useful in applications with irregular geometries there is clearly a need to develop the modules to handle such situations. Naturally enough this is achieved by means of arbitrary triangulation. Therefore in this context an automatic mesh generator of the user-friendly kind now being produced commercially will also have to be integrated into the code together with the ability to use higher order triangles of arbitrary shapes in order to produce accurate results (it was shown throughout Chapter 5 that linear elements were inferior to the higher-ordered elements).

(2) Elements

The serendipity elements need to be investigated. The favourable aspect of serendipity elements is that they do not possess internal nodes and an arrangement of the higher-ordered serendipity elements will lead to a reduction in bandwidth when compared against Lagrangian elements under similar circumstances. Therefore if they can produce accurate results then they are clearly to be favoured because of the savings in storage. Extending the work, after including higher ordered arbitrary triangles (as mentioned above), would involve the use of iso-parametric elements which are most useful with curved boundaries and interfaces. For example a fast reactor shield often used consists of graphite filled iron cylinders stacked to form a circular annulus.

(3) Solution Algorithms

Clearly, the first task in this field is to modify the out-of-core solver for eigenvalue problems. Next, BANSOL needs modifications in order that the zero arithmetic operations be avoided. In Section 4.9 the frontal solution-technique was touched upon. Since it is in use in many practical finite element programs its use in FELTRAN needs to be investigated. However it does possess one major disadvantage when used on vector processing computers. Wilson [100] has shown that the increase in speed when used on parallel computers is not applicable for the frontal method. As regards iterative methods it is not anticipated that this would be necessary until three-dimensional work is considered.

(4) Additional Features

In this category we can consider anisotropicity and upscattering. Anisotropic scattering for example is important in the shields of reactors. The phenomenon of forward scattering is pronounced for the collisions of high energy neutrons with light nuclei. Upscattering occurs in the thermal energy range and so will be important in the analysis of thermal reactors.

(5) Computational Aspects

Presently the power method is used for calculating the values of k_{eff} in eigenvalue problems and no acceleration technique is used. The method of dominance ratio is one of the methods for achieving this acceleration and Greenstadt [38] has reported improvement in convergence of the outer iteration cycle by a factor of 2 to 3 times when using this method. Therefore the method of dominance ratio should be a potential candidate for the acceleration of the outer iteration cycle.

APPENDICES

APPENDIX A

THE SPHERICAL HARMONICS

The Spherical Harmonics, $Y_{\ell m}(\mu,\omega)$, are defined by

$$Y_{\ell m}(\mu,\omega) = \sqrt{\frac{2\ell+1}{4\pi}\cdot\frac{(\ell-m)!}{(\ell+m)!}}\, P_\ell^m(\mu)\, e^{im\omega} \qquad (A.1)$$

in which μ and ω are referred to in Fig.2.1 and $P_\ell^m(\mu)$ are the Associated Legendre Polynomials, defined as

$$P_\ell^m(\mu) = (-1)^m (1-\mu^2)^{\frac{m}{2}} \frac{d^m P_\ell(\mu)}{d\mu^m} \qquad (A.2)$$

for integral values of $m = 0, 1, 2, \ldots \ell$; $P_\ell(\mu)$ are the Legendre Polynomials where

$$P_\ell(\mu) = \frac{1}{2^\ell \ell!}\frac{d^\ell}{d\mu^\ell}(\mu^2-1)^\ell \qquad (A.3)$$

for $\ell = 0, 1, \ldots$

From Eq.(A.1) it can be seen that $Y^*_{\ell m}(\mu,\omega)$, the complex conjugate of $Y_{\ell m}(\mu,\omega)$ is related via

$$Y_{\ell,-m}(\mu,\omega) = (-1)^m Y^*_{\ell m}(\mu,\omega) \qquad (A.4)$$

APPENDIX B

THE TRIAL FUNCTION

The trial function, in terms of Spherical Harmonics, is given by

$$\hat{\Phi}(\pm,\underline{\Omega}) = \sum_{l=0}^{\infty}\sum_{m=-l}^{l} \Phi_{lm}(\pm) Y_{lm}(\underline{\Omega}) \qquad (B.1)$$

where

$\Phi_{lm}(\pm)$ are the spatial components of the angular flux.

In transport calculations it is not usually necessary to use values of l greater than 4 or 5. Higher values of l are seldom called for in practical calculations but the use of high values of l enables very precise benchmarks to be obtained. Let M represent the number of moments of the trial function (i.e. the order of the trial function), and therefore

$$\hat{\Phi}(\pm,\underline{\Omega}) = \sum_{l=0}^{M-1}\sum_{m=-l}^{l} \Phi_{lm}(\pm) Y_{lm}(\underline{\Omega}) \qquad (B.2)$$

The Spherical Harmonics $Y_{lm}(\underline{\Omega})$ in terms of μ and ω are as represented in Eq.(A.1) in Appendix A. The integrals over μ for the odd Spherical Harmonics are zero. Therefore only the even Spherical Harmonics will yield non-zero terms and so

$$\hat{\Phi}(\pm,\underline{\Omega}) = \sum_{l=0}^{M-1}\sum_{m=-l}^{l} \Phi_{2l,2m}(\pm) Y_{2l,2m}(\underline{\Omega}) \qquad (B.3)$$

represents the trial function for even Spherical Harmonics.

Recalling Eq.(A.4) from Appendix A, for even moments the complex conjugate is now related as

$$Y_{2\ell,-2m}(\underline{\Omega}) = Y^{*}_{2\ell,2m}(\underline{\Omega}) \tag{B.4}$$

Upon expanding the inner summation of Eq.(B.3) and using Eq.(B.4) we have

$$\hat{\Phi}(\pm,\underline{\Omega}) = \sum_{\ell=0}^{M-1}\left\{ \Phi_{2\ell,0}(\pm) Y_{2\ell,0}(\underline{\Omega}) \right. \tag{B.5}$$

$$\left. + \sum_{m=1}^{\ell}\left[\Phi_{2\ell,2m}(\pm) Y_{2\ell,2m}(\underline{\Omega}) + \Phi_{2\ell,-2m}(\pm) Y^{*}_{2\ell,2m}(\underline{\Omega})\right]\right\}$$

Replacing $\underline{\Omega}$ by μ and ω ,

$$Y_{2\ell,0}(\mu,\omega) = \sqrt{\frac{4\ell+1}{4\pi}}\, P^{0}_{2\ell}(\mu) \tag{B.6}$$

$$Y_{2\ell,2m}(\mu,\omega) = \sqrt{\frac{4\ell+1}{4\pi}\cdot\frac{(2\ell-2m)!}{(2\ell+2m)!}}\, P^{2m}_{2\ell}(\mu) e^{i2m\omega} \tag{B.7}$$

$$Y^{*}_{2\ell,2m}(\mu,\omega) = \sqrt{\frac{4\ell+1}{4\pi}\cdot\frac{(2\ell-2m)!}{(2\ell+2m)!}}\, P^{2m}_{2\ell}(\mu) e^{-i2m\omega} \tag{B.8}$$

Using these relations in Eq.(B.5)

$$\hat{\Phi}(\pm,\mu,\omega) = \sum_{\ell=0}^{M-1} \left\{ \sqrt{\frac{4\ell+1}{4\pi}}\, P_{2\ell}^{\circ}(\mu)\, \Phi_{2\ell,0}(\pm) \right.$$

$$\left. + \sum_{m=1}^{\ell} \sqrt{\frac{4\ell+1}{4\pi} \cdot \frac{(2\ell-2m)!}{(2\ell+2m)!}}\, P_{2\ell}^{2m}(\mu) \left[e^{i2m\omega}\, \Phi_{2\ell,2m}(\pm) + e^{-i2m\omega}\, \Phi_{2\ell,-2m}(\pm) \right] \right\} \tag{B.9}$$

Let,

$$A = e^{i2m\omega}\, \Phi_{2\ell,2m}(\pm) + e^{-i2m\omega}\, \Phi_{2\ell,-2m}(\pm) \tag{B.10}$$

or,

$$\begin{aligned} A = {} & \Phi_{2\ell,2m}(\pm) \left\{ \cos 2m\omega + i \sin 2m\omega \right\} \\ & + \Phi_{2\ell,-2m}(\pm) \left\{ \cos 2m\omega - i \sin 2m\omega \right\} \end{aligned} \tag{B.11}$$

Further, if we represent

$$\left.\begin{aligned} \Phi_{2\ell,2m}(\pm) &= B_{2\ell,2m}(\pm) + i\, C_{2\ell,2m}(\pm) \\ \Phi_{2\ell,-2m}(\pm) &= B_{2\ell,2m}(\pm) - i\, C_{2\ell,2m}(\pm) \end{aligned}\right\} \tag{B.12}$$

Then upon substitution Eq.(B.12) into (B.11) we have

$$
\begin{aligned}
A = {} & B_{2\ell,2m}(\pm)\cos 2m\omega - C_{2\ell,2m}(\pm)\sin 2m\omega \\
& + B_{2\ell,2m}(\pm)\cos 2m\omega - C_{2\ell,2m}(\pm)\sin 2m\omega \\
& + i\Big\{ C_{2\ell,2m}(\pm)\cos 2m\omega + B_{2\ell,2m}(\pm)\sin 2m\omega \\
& \quad - C_{2\ell,2m}(\pm)\cos 2m\omega - B_{2\ell,2m}(\pm)\sin 2m\omega \Big\}
\end{aligned}
\tag{B.13}
$$

i.e.

$$
A = 2B_{2\ell,2m}(\pm)\cos 2m\omega - 2C_{2\ell,2m}(\pm)\sin 2m\omega \tag{B.14}
$$

Hence,

$$
\hat{\Phi}(\pm,\mu,\omega) = \sum_{\ell=0}^{M-1} \Bigg\{ \sqrt{\frac{4\ell+1}{4\pi}}\, P_{2\ell}^{0}(\mu)\, \Phi_{2\ell,0}(\pm) \tag{B.15}
$$

$$
+ \sum_{m=1}^{\ell} \sqrt{\frac{4\ell+1}{4\pi}\cdot\frac{(2\ell-2m)!}{(2\ell+2m)!}}\, P_{2\ell}^{2m}(\mu)\Big[2B_{2\ell,2m}\cos 2m\omega - 2C_{2\ell,2m}\sin 2m\omega \Big] \Bigg\}
$$

If we now denote

$$
\begin{aligned}
\Phi_{(\ell^2+1)}(\pm) &= \Phi_{2\ell,0}(\pm) \\
\Phi_{(\ell^2+2m)}(\pm) &= 2B_{2\ell,2m}(\pm) \\
\Phi_{(\ell^2+2m+1)}(\pm) &= -2C_{2\ell,2m}(\pm)
\end{aligned}
\tag{B.16}
$$

we arrive finally at

$$\hat{\phi}(\pm,\mu,\omega) = \sum_{\ell=0}^{M-1} \left\{ \sqrt{\frac{4\ell+1}{4\pi}}\, P_{2\ell}^{0}(\mu)\, \phi_{(\ell^2+1)}(\pm) \right.$$

$$+ \sum_{m=1}^{\ell} \sqrt{\frac{4\ell+1}{4\pi} \cdot \frac{(2\ell-2m)!}{(2\ell+2m)!}}\, P_{2\ell}^{2m}(\mu) \qquad \text{(B.17)}$$

$$\left. \times \left[\phi_{(\ell^2+2m)}(\pm) \cos 2m\omega + \phi_{(\ell^2+2m+1)}(\pm) \sin 2m\omega \right] \right\}$$

in which $\phi_k(\pm)$ represent an ascending numbering order for the moments of the spatial fluxes.

Examples of the expansion of the trial function:

(i) M = 1

$$\hat{\phi}(\pm,\mu,\omega) = \frac{1}{\sqrt{4\pi}}\, \phi_1(\pm)$$

(ii) M = 2

$$\hat{\phi}(\pm,\mu,\omega) = \frac{1}{\sqrt{4\pi}}\, \phi_1(\pm) + \sqrt{\frac{5}{4\pi}}\, P_2^0(\mu)\, \phi_2(\pm)$$

$$+ \sqrt{\frac{5}{96\pi}}\, P_2^2(\mu) \left\{ \phi_3(\pm) \cos 2\omega + \phi_4(\pm) \sin 2\omega \right\}$$

(iii) M = 3

$$\hat{\phi}(\pm,\mu,\omega) = \frac{1}{\sqrt{4\pi}}\,\phi_1(\pm) + \sqrt{\frac{5}{4\pi}}\,P_2^0(\mu)\,\phi_2(\pm)$$

$$+\sqrt{\frac{5}{96\pi}}\,P_2^2(\mu)\left\{\phi_3(\pm)\cos 2\omega + \phi_4(\pm)\sin 2\omega\right\}$$

$$+\sqrt{\frac{9}{4\pi}}\,P_4^0(\mu)\,\phi_5(\pm)$$

$$+\sqrt{\frac{3}{460\pi}}\,P_4^2(\mu)\left\{\phi_6(\pm)\cos 2\omega + \phi_7(\pm)\sin 2\omega\right\}$$

$$+\sqrt{\frac{1}{1920\pi}}\,P_4^4(\mu)\left\{\phi_8(\pm)\cos 4\omega + \phi_9(\pm)\sin 4\omega\right\}$$

Therefore, as can be seen from these examples the trial function gets more complicated and lengthy with increasing number of moments. In particular, the number of terms equal M^2.

APPENDIX C

SOLUTIONS OF THE INTEGRATION OF SOME TRIGONOMETRIC FUNCTIONS

The results presented in this Appendix refer to the expressions tabulated in Table 3.3. As can be seen from Table 3.3, the G's are trigonometric functions. It can be unity or it can represent $\cos N\omega$ or $\sin N\omega$ where N is an even number. Each of the six expressions in the table are dealt with in turn below, together with all the possible combinations of the G's.

The letters M and N refer to positive even numbers except in the last case where they can also be taken to be zero.

1. Evaluation of J_1

(i)

$$\int_0^{2\pi} \cos^2\omega \, d\omega = \pi$$

(ii)

$$\int_0^{2\pi} \cos^2\omega \begin{Bmatrix} \cos M\omega \cos N\omega \\ \sin M\omega \sin N\omega \end{Bmatrix} d\omega = \begin{cases} \frac{\pi}{2} & \text{for } M=N\geqslant 2 \\ \frac{\pi}{4} & \text{for } M-N=\pm 2 \\ 0 & \text{otherwise} \end{cases}$$

(iii)

$$\int_0^{2\pi} \cos^2\omega \sin M\omega \cos N\omega \, d\omega = 0$$

2. Evaluation of J_2

(i)

$$\int_0^{2\pi} \sin 2\omega \, d\omega = 0$$

(ii)

$$\int_0^{2\pi} \sin 2\omega \sin M\omega \, d\omega = \pi \quad \text{for} \quad M = 2$$

(iii)

$$\int_0^{2\pi} \sin 2\omega \left\{ \begin{matrix} \cos M\omega \cos N\omega \\ \sin M\omega \sin N\omega \end{matrix} \right\} d\omega = 0$$

(iv)

$$\int_0^{2\pi} \sin 2\omega \sin M\omega \cos N\omega \, d\omega = \begin{cases} \frac{\pi}{2} & \text{for} \quad M-N = 2 \\ -\frac{\pi}{2} & \text{for} \quad M-N = -2 \\ 0 & \text{otherwise} \end{cases}$$

3. Evaluation of J_3

(i)

$$\int_0^{2\pi} \sin^2\omega \, d\omega = \pi$$

(ii)

$$\int_0^{2\pi} \sin^2\omega \begin{Bmatrix} \cos M\omega \cos N\omega \\ \sin M\omega \sin N\omega \end{Bmatrix} d\omega = \begin{cases} \frac{\pi}{2} & \text{for} \quad M=N\geq 2 \\ -\frac{\pi}{4} & \text{for} \quad M-N=\pm 2 \\ 0 & \text{otherwise} \end{cases}$$

(iii)

$$\int_0^{2\pi} \sin^2\omega \sin M\omega \sin N\omega \, d\omega = 0$$

4. Evaluation of J_4

Since $\cos^2\omega + \sin^2\omega = 1$,

$$J_{4ij} = J_{1ij} + J_{3ij}$$

i.e. the constants represented by J_4 are obtained from the above relationship after J_1 and J_3 have been obtained.

5. Evaluation of J_5

(i)

$$\int_0^{2\pi} \cos M\omega \, d\omega = 0$$

(ii)

$$\int_0^{2\pi} \sin M\omega \, d\omega = 0$$

6. Evaluation of J_6

It can easily be shown [90] that

$$\int_0^{2\pi} \left|\sin(\alpha-\omega)\right| G_i G_j \, d\omega$$

$$= \int_0^{2\pi} \left|\sin(\alpha-\omega)\right| \begin{Bmatrix} \cos M\omega \cos N\omega \\ \cos M\omega \sin N\omega \\ \sin M\omega \cos N\omega \\ \sin M\omega \sin N\omega \end{Bmatrix} d\omega$$

$$= \begin{Bmatrix} e_{M-N}\cos(M-N)\alpha + e_{M+N}\cos(M+N)\alpha \\ e_{M+N}\sin(M+N)\alpha - e_{M-N}\sin(M-N)\alpha \\ e_{M+N}\sin(M+N)\alpha + e_{M-N}\sin(M-N)\alpha \\ e_{M-N}\cos(M-N)\alpha - e_{M+N}\cos(M+N)\alpha \end{Bmatrix}$$

where,

$$e_k = \frac{1}{1-k^2}$$

APPENDIX D

DERIVATION OF THE SHAPE FUNCTIONS FOR LANGRANGIAN ELEMENTS

The Lagrangian Multipliers, of order n, are given by the relation;

$$\mathcal{L}_i^n(z) = \prod_{\substack{j=0 \\ j\neq i}}^{n} \frac{(z - z_j)}{(z_i - z_j)} \qquad (D.1)$$

$$i = 0, 1, \ldots . n$$

Here z is a free coordinate. The z_i are the coordinates for the nodes of a one-dimensional element. $\mathcal{L}_i^n(z)$ is then the shape function associated with the node i . These multipliers are used directly in the derivation of the shape functions of the Lagrangian quadrilateral elements. The order n determines the order of the element. For bi-linear elements n is equal to 1, for bi-quadratic elements n is 2 and so on. The number of shape functions, and therefore the number of nodes, of the element concerned is equal to $(n+1)^2$.

In plane geometry, the shape functions for an element of order n are given by the products

$$N_k(x,y) = \mathcal{L}_i^n(x)\, \mathcal{L}_j(y) \qquad (D.2)$$

$$k = 1, 2, \ldots . , (n+1)^2$$

in which

$$k = j(n+1) + i + 1 \qquad (D.3)$$

$$i = 0, 1, \ldots . n$$

$$j = 0, 1, \ldots . n$$

The numbering of the shape functions embodied in (D.3) ensures that the first shape function corresponds to the bottom left-hand corner node whilst the last shape function corresponds to the top right-hand corner node. The intermediate shape functions correspond to the nodes passed through successively by a right-wards sweep followed by an upward step. Fig.D.1 serves to illustrate this point with the bi-quadratic element as an example.

The bi-quadratic element is chosen as the illustrative element whose shape functions are to be determined. Let the dimensions of the element be a and b in the x- and y-directions respectively. Further, the side nodes are mid-way along the sides as shown in Fig.D.2. The Lagrangian Multipliers of order 2, with $z_0 = 0$, $z_1 = \ell/2$ and $z_2 = \ell$ are given by

$$\left.\begin{aligned} \mathcal{L}_0^2(z) &= \left(1-\frac{z}{\ell}\right)\left(1-\frac{2z}{\ell}\right) \\ \mathcal{L}_1^2(z) &= 4\left(\frac{z}{\ell}\right)\left(1-\frac{z}{\ell}\right) \\ \mathcal{L}_2^2(z) &= -\left(\frac{z}{\ell}\right)\left(1-\frac{2z}{\ell}\right) \end{aligned}\right\} \qquad (D.4)$$

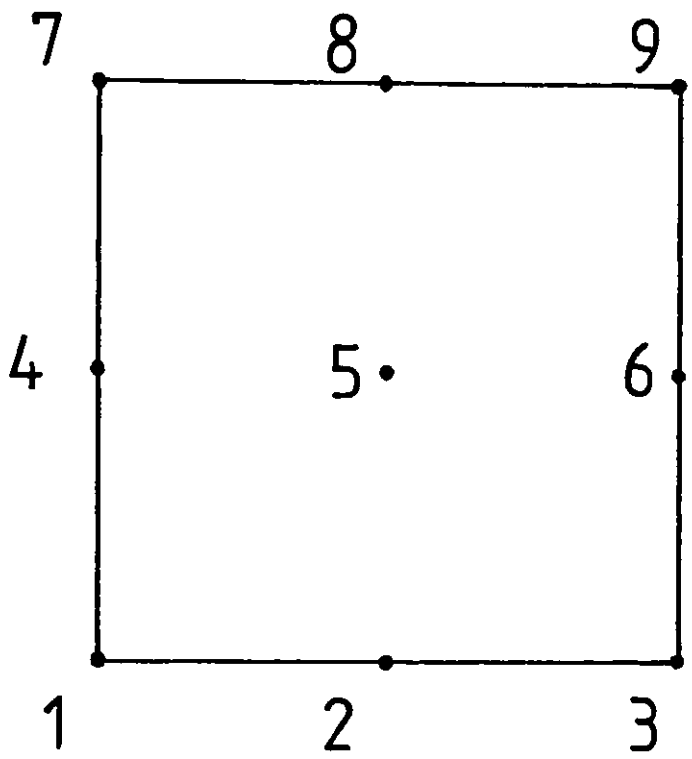

Fig.D.1 The numbering pattern for the nodes of a bi-quadratic element

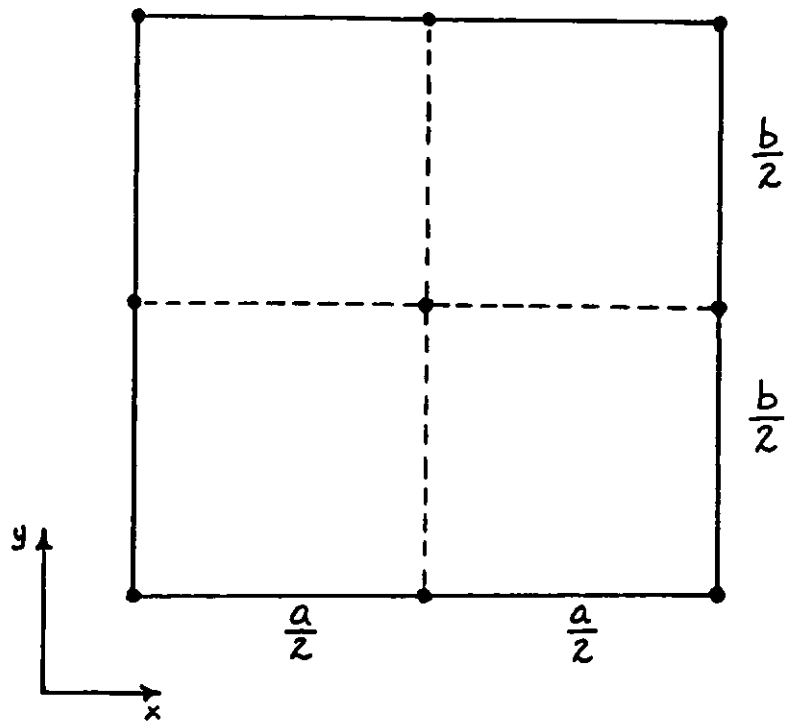

Fig.D.2 The dimensions of the bi-quadratic element

Therefore, from (D.2) and (D.3)

$$N_1(x,y) = \mathcal{L}_0^2(x)\,\mathcal{L}_1^2(y)$$

i.e.

$$N_1(x,y) = \left(1-\frac{x}{a}\right)\left(1-\frac{2x}{a}\right)\left(1-\frac{y}{b}\right)\left(1-\frac{2y}{b}\right)$$

with x, y, a and b replacing z and ℓ.

In this manner the other eight shape functions for the Lagrangian bi-quadratic element are arrived at. The nine shape functions are summarised in Table D.1.

It should be borne in mind that the coordinate system for the example could be shifted. In the example, the origin is at the bottom left-most node. Should the internal node be chosen as the origin then the Lagrangian Multipliers would produce different expressions, but as long as the coordinate system is monitored correctly results will be similar in the end.

TABLE D.1

THE SHAPE FUNCTIONS FOR THE

BI-QUADRATIC ELEMENT

N_1	$\left(1-\frac{x}{a}\right)\left(1-\frac{2x}{a}\right)\left(1-\frac{y}{b}\right)\left(1-\frac{2y}{b}\right)$
N_2	$4\left(\frac{x}{a}\right)\left(1-\frac{x}{a}\right)\left(1-\frac{y}{b}\right)\left(1-\frac{2y}{b}\right)$
N_3	$-\left(\frac{x}{a}\right)\left(1-\frac{2x}{a}\right)\left(1-\frac{y}{b}\right)\left(1-\frac{2y}{b}\right)$
N_4	$4\left(1-\frac{x}{a}\right)\left(1-\frac{2x}{a}\right)\left(\frac{y}{b}\right)\left(1-\frac{y}{b}\right)$
N_5	$16\left(\frac{x}{a}\right)\left(1-\frac{x}{a}\right)\left(\frac{y}{b}\right)\left(1-\frac{y}{b}\right)$
N_6	$-4\left(\frac{x}{a}\right)\left(1-\frac{2x}{a}\right)\left(\frac{y}{b}\right)\left(1-\frac{y}{b}\right)$
N_7	$-\left(1-\frac{x}{a}\right)\left(1-\frac{2x}{a}\right)\left(\frac{y}{b}\right)\left(1-\frac{2y}{b}\right)$
N_8	$-4\left(\frac{x}{a}\right)\left(1-\frac{x}{a}\right)\left(\frac{y}{b}\right)\left(1-\frac{2y}{b}\right)$
N_9	$\left(\frac{x}{a}\right)\left(1-\frac{2x}{a}\right)\left(\frac{y}{b}\right)\left(1-\frac{2y}{b}\right)$

REFERENCES

1. ACKROYD, R.T.
"The Finite Element Method for Neutron Transport. II. Boundary free minimum and maximum principles for for even-parity transport equation".
UKAEA TRG Rep. 2749 (R), 1975.

2. ACKROYD, R.T.
"A Finite Element Method for Neutron Transport. VII. Completely boundary-free maximum principle for the first-order Boltzmann equation".
Ann.Nucl.En., 10, No.5, 243-261, (1983).

3. ACKROYD, R.T.
"The Why and How of Finite Elements".
Ann.Nucl.En., 8, 539-566, (1981)

4. ACKROYD, R.T., BALL, J.M.
"Some Simple Mathematical Models for Criticality Problems".
Prog. in Nuc.En., 3, (1960).

5. ADAMS, C.H.
"Current Trends in Methods for Neutron Diffusion Calculations".
Nuc.Sc.Eng.,64, 552-562, (1977).

6. ALCOUFFE, R.E., LARSEN, E.W., MILLER, W.F. Jr., WIENKE, B.R.
"Computational Efficiency of Numerical Methods for the Multigroup Discrete-Ordinates Neutron Transport Equations: The Slab Geometry Case".
Nuc.Sc.Eng., 71, 111-127, (1979).

7. ARGONNE CODE CENTER: BENCHMARK PROBLEM BOOK.
ANL-7416, Supplement 2, Argonne National Laboratory, (1977).

8. ARGYRIS, J.H.
"Energy Theorems and Structural Analysis".
Aircraft Eng., 26, (1954).

9. ARGYRIS, J.H.
"Energy Theorems and Structural Analysis".
Aircraft Eng., 27, (1955).

10. BATHE, K-J., WILSON, E.L.
"Numerical Methods in Finite Element Analysis".
Prentice-Hall, (1976).

11. BELL, G.I., GLASSTONE, S.
"Nuclear Reactor Theory".
Van Nostrand Reinhold Co., New York, (1970).

12. BESSELING, J.F.
"The Complete Analogy between the Matrix Equations and the Continuous Field Equations of Structural Analysis".
Int.Symp. on Analogue and Digital Techniques Applied to Aeronautics, Liege, Belgium, (1963).

13. BISWAS, D., RAM, K.S., RAO, S.S.
"Application of Natural Coordinate System in the Finite Element Solution of Multigroup Neutron Diffusion Equation".
Ann.Nucl.En., 3, 465-469, (1976).

14. BLOMQUIST, R.N., LEWIS, E.E.
"A Rigorous Treatment of Transverse Buckling Effects in Two-Dimensional Neutron Transport Computations".
Nuc.Sci.Eng., 73, 125-139, (1980).

15. BRIGGS, L.L., MILLER, W.F., LEWIS, E.E.
"Ray-Effect Mitigation in Discrete Ordinate-like Angular Finite Element Approximations in Neutron Transport".
Nuc.Sci.Eng., 57, 205-217, (1975).

16. BUDD, C.
"An Outline Review of Numerical Transport Methods".
AEEW Report No. R1412, Winfrith, January 1981.

17. CARLSON, B.G.
"Solution of the Transport Equation by S_N Approximations".
LA-1599, Los Alamos Scientific Laboratory, (1953).

18. CARLSON, B.G., LATHROP, K.D.
"Transport Theory - The Method of Discrete Ordinates".
Computing Methods in Reactor Physics, H.Greenspan, C.N. Kelber, D. Okrent (Eds.)
Gordon & Breach, Science Publishers Inc., New York, (1968).

19. CARNAHAN, B., LUTHER, H.A., WILKES, J.O.
"Applied Numerical Methods".
John Wiley & Sons Inc., (1969).

20. CHEUNG, Y.K., YEO, M.F.
"A Practical Introduction to Finite Element Analysis".
Pitman, (1979).

21. CLOUGH, R.W.
"The Finite Element Method in Plane Stress Analysis".
Proc. of 2nd ASCE Conf. on Electronic Computation, Pittsburgh, (1960).

22. COURANT, R.
"Variational Methods for the Solution of Problems of Equilibrium and Vibrations".
Bull.Amer.Math.Soc., 49, 1-23, (1943).

23. COURANT, R., FRIEDRICH, K., LEWY, H.
"Uber die Partiellen Differengleichungen der Mathematischen Physik".
Mathematische Annalen, 100, 32-74, (1928).
"On the Partial Difference Equations of Mathematical Physics". (English Translation).
IBM Journal, 215-234, March 1967.

24. DAVISON, B.
"Neutron Transport Theory".
Oxford University Press, (1957).

25. DEPPE, L.O., HANSEN, K.F.
"Application of the Finite Element to Two-Dimensional Diffusion Problems".
Nuc.Sc.Eng., 54, 456-465, (1974).

26. DESAI, C.S., ABEL, J.F.
"Introduction to the Finite Element Method: A Numerical Method for Engineering Analysis".
Van Nostran Reinhold Co., (1972).

27. DOCTORS, L.J.
"An Application of the Finite Element Technique for Boundary Value Problems of Potential Flow".
Int.J.Num.Meth.Engng., 2, 243-252,(1970).

28. DUDERSTADT, J.J., HAMILTON, L.J.
"Nuclear Reactor Analysis".
John Wiley & Sons, (1976).

29. DUDERSTADT, J.J., MARTIN, W.R.
"Transport Theory".,
John Wiley & Sons, (1979).

30. FOWLER, T.B., VONDY, D.R., CUNNINGHAM, G.W.
"Nuclear Reactor Core Analysis Code: CITATION".
ORNL-TM-2496, Rev.2, Oak Ridge National
Laboratory, (July 1969).

31. FOX, L.
"An Introduction to Numerical Linear Algebra".
Oxford University Press, (1964).

32. FRAEIJIS DE BEUBEKE, B.M.
"Upper and Lower Bounds in Matrix Structural Analysis".
AGARD-ograph, 72, 165-203, (1964).

33. GALLIARA, J.S., WILLIAMS, M.M.R.
"A Finite Element Method for Neutron Transport.
II. Some Practical Considerations".
Ann.Nucl.En., 6, 205-223, (1979).

34. GALLIARA, J.S.
"The Finite Element Technique in Nuclear Reactor
Physics Calculations".
Ph.D. Thesis, University of London, (1978).

35. GEORGE, J.A.
"Computer Implementation of the Finite Element
Method".
STAN-CS-71-208, Stanford University, (1971).

36. GEORGE, J.A., LIU, J.W.H.
"Some Results on Fill-in for Sparse Matrices".
SIAM J.Numer.Anal., 12, 452-455, (1975).

37. GREENSTADT, J.
"On the Reduction of Continuous Problems to Discrete Form".
IBM J.Res.Dev., Vol.3, (1959).

38. GREENSTADT, J.
"The Application of Cell Discretization to Nuclear Reactor Problems".
Nuc.Sc.Eng., 82, 78-95, (1982).

39. GREENSTADT, J.
"Cell Discretization Algorithm with Numerical Examples".
G320-3405, IBM Palo Alto Scientific Center, (May 1980).

40. HAGEMAN, L., PFEIFER, C.J.
"The Utilisation of the Neutron Diffusion Program PDQ-5".
WAPD-TM-395, Bettis Atomic Power Laboratory, (January 1965).

41. HRENNIKOFF, A.
"Solution of Problems in Elasticity by the Framework Method".
J.App.Mech., 8, 169-175, (1941).

42. HUEBNER, K.H.
"The Finite Element Method for Engineers".
John Wiley & Sons, (1975).

43. IMPERIAL COLLEGE COMPUTER SERVICE.
Private Communication, (1983).

44. IRONS, B.
"A Frontal Solution Program for Finite Element Analysis".
Int.J.Num.Meth.Engng., 2, 5-32, (1970).

45. IRONS, B., AHMAD, S.
"Techniques of Finite Elements".
John Wiley & Sons, (1980).

46. ISSA, J.G.
Ph.D. Thesis, University of London, (1983).

47. JONES, R.E.
"A Generalization of the Direct Stiffness Method of Structural Analysis".
J.A.I.A.A., 2, 821-826,(1964).

48. JUST, L.C. et al.
"The System Aspects and Interface Data Sets of the Argonne Reactor Computation (ARC) System".
ANL-711, Argonne National Laboratory, (1971).

49. KALOS, M.H., NAKACHE, F.R., CELNIK, J.
"Monte Carlo Methods in Reactor Computations".
Computing Methods in Reactor Physics, H. Greenspan, C.N. Kelber, D. Okrent, (Eds.).
Gordon & Breach, Science Publishers Inc., New York, (1968).

50. KANG, C.M., HANSEN, K.F.
"Finite Element Methods for Reactor Analysis".
Nuc.Sci.Eng., 51, 456-495, (1973).

51. KAPER, H.G., LEAF, G.K., LINDEMAN, A.J.
"A Timing Comparison Study for some High Order Finite Element Approximation Procedures and a Low Order Finite Difference Approximation Procedure for the Numerical Solution of the Multigroup Neutron Diffusion Equation".
Nuc.Sc.Eng., 49, 27-48, (1972).

52. KAPER, H.G., LEAF, G.K., LINDEMAN, A.R.
"Applications of Finite Element Methods in Reactor Mathematics. Numerical Solution of the Neutron Diffusion Equation".
Argonne National Laboratory, ANL-7925, (April 1972).

53. KAPER, H.G., LEAF, G.K., LINDEMAN, A.R.
"Applications of Finite Element Methods in Reactor Mathematics. Numerical Solution of the Neutron Transport Equation".
Argonne National Laboratory, ANL-8126, (October 1974).

54. KAPLAN, S.
"A New Derivation of Discrete Ordinate Approximations".
Nuc.Sc.Eng., 34, 76, (1968).

55. KAPLAN, S., DAVIES, J.A.
"Canonical and Involuntary Transformations of the Variational Problems of Transport Theory".
Nuc.Sci.Eng., 28, 166-176, (1967).

56. KOMORIYA, H., WALTERS, W.F.
"The Energy-Dependent Finite Element Method for Two-Dimensional Diffusion Problems".
Nuc.Sci.Eng., 64, 576-581, (1977).

57. LARSEN, E.W., ALCOUFFE, R.E.
"The Linear Characteristic Method for Spatially Discretizing the Discrete Ordinates Equations in (x,y)-Geometry".
Proc.Int.Topical Mtg. on Advances in Mathematical Methods for the Solution of Nuclear Engineering Problems, Munich, (April 27-29, 1981).

58. LATHROP, K.D.
"Discrete-Ordinates Methods for the Numerical Solution of the Transport Equation".
Reactor Technology, 15, No.2, 107-135, (1972).

59. LATHROP, K.D.
"Remedies for Ray Effects".
Nuc.Sci.Eng., 45, 255-268, (1971).

60. LATHROP, K.D., BRINKLEY, F.W.
"Theory and Use of the General Geometry TWOTRAN Program".
LA-4432, Los Alamos Scientific Laboratory.

61. LATHROP, K.D., BRINKLEY, F.W.
"TWOTRAN II: An Interfaced, Exportable Version of the TWOTRAN Code for Two-Dimensional Transport".
LA-4848-MS, Los Alamos National Laboratory, (1973).

62. LATHROP, K.D.
"Ray Effects in Discrete Ordinates Equations".
Nuc.Sci.Eng., 32, 357, (1968).

63. LEWIS, E.E.
"Progress in Multidimensional Neutron Transport Computation".
Nuc.Sci.Eng., 64, 279-293, (1977).

64. LIEBMANN, H.
"Die Angenaherte Ermittebung Harmonischer Functionen und Konformer Abbildungen"".
Bayer.Akad.Wiss., Math-Phy.Klasse, Sitz., (1918).

65. LILLIE, R.A., ROBINSON, J.C.
"A Linear Triangle Finite Element Formulation for Multigroup Neutron Transport Analysis with Anisotropic Scattering".
ORNL-TM-5281, Oak Ridge National Laboratory, (1976).

66. MARTIN, W.R., DUDERSTADT, J.J.
"Finite Element Solutions of the Neutron Transport Equation with Applications to Strong Heterogeneities".
Nuc.Sci.Eng., 62, 371-390, (1977).

67. McGUIRE, W., GALLAGHER, R.H.
"Matrix Structural Analysis".
John Wiley & Sons, (1979).

68. McHENRY, D.
"A Lattice Analogy for the Solution of Plane Stress Problems".
J.Inst.Civ.Eng., 21, 59-82, (1943).

69. MELOSH, R.J.
"Basis for Derivation of Matrices for the Direct Stiffness Method".
J.A.I.A.A., 1, 1631-1637, (1973).

70. METCALF, M.
"Fortran Optimisation".
Academic Press, (1982).

71. MILLER, W.F., LEWIS, E.E., ROSSOW, E.C.
"The Application of the Phase-Space Finite Elements to the Two-Dimensional Neutron Transport Equation in x-y Geometry".
Nuc.Sci.Eng., 52, 12-22, (1973).

72. MONDKAR, D.P., POWELL, G.H.
"Towards Optimal In-Core Equation Solving".
Computers and Structures, 4, 531-548, (1974).

73. MORDANT, M.
"ZEPHYR: A Code for Solving Neutron Transport Problems on Irregular Meshes in Two-Dimensional Geometries".
IAEA Mtg., Bologna, Italy, (November 1975).

74. MYNATT, F.R., MUCKENTHALER, F.J., STEVENS, P.N.
"Development of Two-Dimensional Discrete Ordinates Transport Theory for Radiation Shielding".
CTC-INF-952, Oak Ridge Computing Technology Center, (August 1969).

75. NATELSON, M.
"Variational Derivation of Discrete Ordinate-Like Approx."
Nuc.Sci.Eng., 43, 131, (1971).

76. NORRIE, D.H., de VRIES, G.
"An Introduction to Finite Element Analysis".
Academic Press, (1978).

77. OHNISHI, T.
"Application of Finite Element Solution Technique to Neutron Diffusion and Transport Equations".
Proc.Conf. on New Developments in Reactor Mathematics and Applications, USAEC Rep. CONF-710302, 1971).

78. PITKARANTA, J., SILVENNOINEN, P.
"Finite Element Analysis of some Critical Fast Assemblies".
Nuc.Sci.Eng., 52, 447-453, (1973).

79. POLYA, G.
"How to Solve It".
Doubleday Anchor Books, (1957).

80. PRAGER, W., SYNGE, J.L.
"Approximation in Elasticity Based on the Concept of Function Space".
Quart.Appl.Math., 5, (1947).

81. REED, W.H., HILL, T.R., BRINKLEY, F.W., LATHROP, K.D.
"TRIPLET: A Two-Dimensional, Multigroup, Triangular Mesh, Planar Geometry, Explicit Transport Code".
LA-5428-MS, Los Alamos Scientific Laboratory, (1973).

82. RHOADES, W.A., MYNATT, F.R.
"The DOT-III Two-Dimensional Discrete Ordinates Transport Code".
ORNL-TM-4280, Oak Ridge National Laboratory, (1973).

83. RICHARDSON, L.F.
"The Approximate Arithmetical Solution by Finite Differences of Physical Problems Involving Differential Equations with an Application to the Stresses in a Masonry Dam".
Trans.Roy.Soc.Lond, Ser.A., 210, 307-357,(1910).

84. SANCHEZ, R., McCORMICK, N.J.
"A Review of Neutron Transport Approximations".
Nuc.Sci.Eng., 80, 481-535, (1982).

85. SCHMIDT, F.A.R., FRANKE, H.P.
"Power Reactor Calculations with the Finite Element Program FEM 2D".
Nuc.Sci.Eng., 56, 431-433, (1975).

86. SCHMIDT, F.A.R., FREMD, R., WÖRNER, D.
"DIFGEN-Ein Programmpaket Zur Lösung Der Diffusionsgleichung Nach Der Methode Der Finiten Elemente".
IKE4-75, Institut für Kernenergetik . Und Energiesyteme, Universität Stuttgart, (April 1979).

87. SEGERLIND, L.J.
"Applied Finite Element Analysis".
John Wiley & Sons, (1976).

88. SEMENZA, L.A., LEWIS, E.E., ROSSOW, E.C.
"The Application of the Finite Element Method to Multigroup Neutron Diffusion Equation".
Nuc.Sci.Eng., 47, 302-310, (1972).

89. SPANIER, J., GELBAND, E.M.
"Monte Carlo Principles and Neutron Transport".
Addison-Wesley, (1969).

90. SPLAWSKI, B.A.
Private Communication.

91. SPLAWSKI, B.A.
Ph.D. Thesis, University of London, (1982).

92. STRANG, G., FIX, G.J.
"An Analysis of the Finite Element Method".
Prentice-Hall, (1973).

93. SZABO, B.A., LEE, G.C.
"Derivation of Stiffness Matrices for Problems in Plane Elasticity by Galerkin's Method".
Int.J.Num.Meth.Engng., 1, 301-310,(1969).

94. TAYLOR, R.L.
"On Completeness of Shape Functions for Finite Element Analysis".
Int.J.Num.Meth.Engng., 4, 17-22, (1972).

95. TONG, P., ROSSETTOS, J.N.
"Finite-Element Method: Basic Technique and Implementation".
MIT Press, (1977).

96. TURNER, M.J., CLOUGH, R.W., MARTIN, H.C., TOPP, L.C.
"Stiffness and Deflection Analysis of Complex Structures".
J.Aero.Sci., Vol.23, No.9, (1956).

97. WALTER, A.E., REYNOLDS, A.B.
"Fast Breeder Reactors".
Pergamon Press, (1981).

98. WHITESIDES, G.E., CROSS, N.F.
"KENO-A Multigroup Monte Carlo Criticality Program".
CTC-5, Oak Ridge Computing Technology Center, (September 1969).

99. WILSON, E.L., BATHE, K.J., DOHERTY, W.P.
"Direct Solution of Large Systems of Linear Equations".
Computers & Structures, 4, 363-372, (1974).

100. WILSON, E.L.
"Solution of Sparse Stiffness Matrices for Structural Systems".
Sparse Matrix Proc. 1978, Ed.I.S. Duff and G.W. Stewart, SIAM, (1979).

101. WILSON, E.L., NICKELL, R.E.
"Application of Finite Element Method to Heat Conduction analysis".
Nuc.Engng.Des., 4, 1-11, (1966).

102. ZIENKIEWICZ, O.C.
"The Finite Element Method".
3rd Ed., McGraw-Hill, (1977).

103. ZIENKIEWICZ, O.C., CHEUNG, Y.K.
"Finite Elements in the Solution of Field Problems".
Engineer, Vol.220, (1965).

104. ZIVER, A.K.
Ph.D. Thesis, University of London, (1981).